VIBRATION FATIGUE ANALYSIS OF STRUCTURES INSTALLED ON AIR PLATFORMS

A THESIS SUBMITTED TO
THE GRADUATE SCHOOL OF NATURAL AND APPLIED SCIENCES
OF
MIDDLE EAST TECHNICAL UNIVERSITY

BY

YUSUF ELDOĞAN

IN PARTIAL FULFILLMENT OF THE REQUIREMENTS
FOR
THE DEGREE OF MASTER OF SCIENCE
IN
MECHANICAL ENGINEERING

FABRUARY 2012

Approval of the thesis:

VIBRATION FATIGUE ANALYSIS OF STRUCTURES INSTALLED ON AIR PLATFORMS

Submitted by **YUSUF ELDOĞAN** in partial fulfillment of the requirements for the degree of **Master of Science in Mechanical Engineering Department, Middle East Technical University** by,

Prof. Dr. Canan Özgen _____
Dean, Graduate School of **Natural and Applied Sciences**

Prof. Dr. Suha Oral _____
Head of Department, **Mechanical Engineering**

Assist. Prof. Dr. Ender Ciğeroğlu _____
Supervisor, **Mechanical Engineering Dept., METU**

Ahmet Levent Avşar, M.Sc. _____
Co-Supervisor, **ASELSAN Inc.**

Examining Committee Members:

Prof. Dr. Suat Kadıoğlu _____
Mechanical Engineering Dept., METU

Assist. Prof. Dr. Ender Ciğeroğlu _____
Mechanical Engineering Dept., METU

Assoc. Prof. Dr. Serkan Dağ _____
Mechanical Engineering Dept., METU

Assist. Prof. Dr. Yiğit Yazıcıoğlu _____
Aerospace Engineering Dept., METU

Inst. Dr. S. Çağlar Başlamışlı _____
Mechanical Engineering Dept., Hacettepe University

Date: 06/02/2012

I hereby declare that all information in this document has been obtained and presented in accordance with academic rules and ethical conduct. I also declare that, as required by these rules and conduct, I have fully cited and referenced all material and results that are not original to this work.

Name Surname: Yusuf ELDOĞAN

Signature:

ABSTRACT

VIBRATION FATIGUE ANALYSIS OF STRUCTURES INSTALLED ON AIR PLATFORMS

Eldoğan, Yusuf

M.Sc., Department of Mechanical Engineering

Supervisor: Assist. Prof. Dr. Ender Ciğeroğlu

Co-Supervisor: Ahmet Levent Avşar, M.Sc.

February 2012, 157 pages

Although a component satisfies all operating static requirements, failures can still occur due to vibration induced fatigue. Vibration induced fatigue is a frequent phenomenon, in cases where the natural frequencies of the structures are excited by the loading. Hence, the methods which consider all dynamic characteristic of the structure should be used to obtain accurate fatigue life predictions. These methods in frequency domain are called vibration fatigue methods which give accurate, reliable and fast results.

In this thesis, a numerical code is developed in order to predict fatigue life of structures and it is used for a bracket that is installed on an air platform. However, for verification of the numerical code, a cantilever beam is used as a case study at the beginning. First, finite element model of the cantilever beam is constructed and experimental analyses are performed to verify the finite element model.

Then fatigue life is calculated using the numerical code and it is verified comparing the results obtained by both commercial software and performed fatigue tests. For predicting fatigue life of the bracket, flight test is performed in order to obtain acceleration loading. Finite element modeling of bracket and verification of it by experimental analyses are performed and finally, accelerated fatigue life of the bracket is obtained by the developed numerical code, commercial software and fatigue test. It is concluded that the results obtained from the fatigue analyses and fatigue test are considerably close enough to justify that the analysis is significantly accurate.

Keyword: Vibration Induced Fatigue, Finite Element Method, Rainflow Cycle Counting

ÖZ

HAVA PLATFORMLARINA YERLEŞTİRİLEN PARÇALARIN TİTREŞİM KAYNAKLI YORULMA ANALİZLERİ

Eldoğan, Yusuf

Yüksek Lisans, Makine Mühendisliği Bölümü

Tez Yöneticisi: Yrd. Doç. Dr. Ender Ciğeroğlu

Ortak Tez Yöneticisi: Ahmet Levent Avşar, M.Sc.

Şubat 2012, 157 pages

Bir mekanik parça istenilen bütün statik isterleri sağlasa bile titreşimden kaynaklanan yorulamadan dolayı parçada tahribatlar meydana gelebilir. Titreşimden kaynaklanan yorulma eğer bir parçanın doğal frekansları mağruz kaldığı yükler tarafından uyarılırsa çok sık görülen bir durumdur. Bu nedenle parçanın bütün dinamik özelliklerini gözeten yöntemlerle yorulma analizini yapmak gerekmektedir. Frekans alanındaki bu metodlar titreşimden kaynaklanan yorulma metodları diye adlandırılır ve doğru, güvenilir ve hızlı sonuçlar vermektedirler.

Bu tezde mekanik parçaların yorulma ömüerlerini hesaplamak için numerik bir kod geliştirilmiştir ve hava platformuna takılan bir parçanın yorulma ömrünü bulmak için kullanılmıştır. Fakat geliştirilen kodu doğrulamak için geometrisi ve sınır koşulları basit olan bir çubuk üzerinde çalışmalar yapılmıştır. İlk olarak çubuğun sonlu elemenlar modeli oluşturulmuştur ve ardından bu modeli doğrulamak için testler yapılmıştır.

Model doğrulandıktan sonra çubuğun yorulma ömrü geliştirilen kod ile bulunmuştur ve bu sonuç yaygın olarak kullanılan başka bir yorulma analizi yazılımından elde edilen sonuç ve testlerden elde edilen sonuçlar ile karşılaştırılmıltır ve geliştirilen numerik kod doğrulanmıştır .

Hava platformuna takılan parçanın yorulma analizine başlamadan önce ilk olarak uçuş testleri yapılarak bu parçanın maruz kaldığı ivme yükleri elde edilmiştir. Ardından hava platformu parçasının da sonlu elemanlar modeli oluşturulmuştur ve ve testler ile doğrulanmıştır. Son olarak geliştirilen numerik kod ve piyasa da kullanılan başka bir yorulma analizi yazılımı ile yorulma ömürleri bulunup yine bulunan sonucu doğrulamak için bir test yapılmıştır. Sonuç olarak bulunan sonuçların birbirine ciddi ölçüde yakın olduğu değerlendirilmiştir ve yapılan analizlerin doğru olduğu değerlendirmesi yapılmıştır.

Anahtar Kelimeler: Titreşimden Kaynaklanan Yorulma, Sonlu Elemanlar Metodu, Yağmur Akışı Döngü Sayımı

To My Family

ACKNOWLEDGEMENTS

I am grateful to my thesis supervisor Assist. Prof. Dr. Ender CİĞEROĞLU and my co-supervisor M.Sc. Ahmet Levent AVŞAR for their valuable guidance, technical support and suggestions in order to complete this study.

I would like to thank my colleagues, Sabri ÖZER, Güvenç CANBALOĞLU, Aytekin ALTUNTAŞ and Ahmet DALDAL for their support at ASELSAN.

I am also grateful to my friend F. Çağrı DEMİR for his help.

I would like to thank ASELSAN Inc. for using its facilities during my thesis.

Finally, I am very thankful to all my friends who supported me during the preparation of my thesis.

TABLE OF CONTENTS

LIST OF TABLES

TABLES

LIST OF FIGURES

FIGURES

LIST OF SYMBOLS

S	:Stress
S_a	: Alternating Stress Amplitude
S_r	: Stress Range
S_m	: Mean stress
$S_{\max}$	: Maximum Stress Amplitude
$S_{\min}$	: Minimum Stress Amplitude
R	: Stress Ratio $\frac{S_{\min}}{S_{\max}} S$:
b	:Basquin exponent
C	:Material Constant
K_t	:Geometric Stress Concentration
K_f	:Fatigue Strength Concentration
q	:Notch Sensitivity
k_a	: Surface condition modification factor
k_b	: Size modification factor
k_c	: Load modification factor
k_d	: Temperature modification factor
k_e	: Reliability factor
k_f	: Miscellaneous-effects modification factor
S_e	: Laboratory test specimen endurance limit
$S_e^{'}$	: Endurance limit at the critical location of a machine part in the geometry and condition of use
S_a	: Equivalent alternating stress
$S_a^{'}$	: Alternating stress
S_m	: Mean stress

S_{ut}	: Ultimate tensile strength
S_{yt}	: Tensile yield strength
σ_1	:Maximum Principal Stress
σ_3	:Minimum Principal Stress
σ_{AMP}	:Maximum Absolute Principal Stress
n	:The number of stress cycles applied at a fixed stress amplitude
N	:The number of cycles the material can withstand at applied fixed stress amplitude
$E[D]$	:Expected Damage
R(f)	:FFT of the response of the system
$H_{TF}(f)$	:Transfer function of the system in frequency domain
$I_{load}(f)$	:FFT of the input load applied to system
$G(f)_{response\_PSD}$	: Response PSD
$G(f)_{input\_PSD}$	: Input PSD
$\mathrm{H_{TF}(f)^*}$	: Complex conjugate of the transfer function
$\lvert H_{TF}(f)\rvert^2$	: Modulus squared of transfer function
$\mathrm{I_{load}(f)^*}$	: Complex conjugate of the FFT of the input load
$p(s)$	:Probability density function (PDF) of rainflow stress ranges
m_n	:The nth spectral moment of the PSD of stress
$E[0]$	:Expected number of upward zero crossings per seconds
$E[P]$	:Expected number of peaks per second
γ	:Irregularity factor
T	: Fatigue life in seconds
S_{eq}	: Equivalent Stress

CHAPTER 1

INTRODUCTION

1.1 Metal Fatigue Damage

In military environments, if a structure is designed considering only static requirements, generally failure occurs due to dynamic characteristic of environment that the structure is subjected to. Hence, dynamic characteristic of environment and structure should be considered in order to avoid from failures. Such failures usually occur if the loading is cyclic even though stresses caused by these cyclic loadings are smaller than yield or ultimate strength of material. These kinds of failures caused by cyclic loading are called Fatigue which usually occurs in a localized portion of the structure.

1.2 History of Fatigue

Over the last century, different techniques for fatigue analysis of structures are developed at a great rate. In summary, the development can be explained as follows [1];

In 1837, Wilhelm Albert published the first article on fatigue of conveyor chains. In order to predict life of conveyor chains used in the Clausthal mines, he designed a test machine.

In 1839, metals are described as materials which can be tired by Jean-Victor Poncelet. In 1842, the stress concentration effect is discussed by William John Macquorn Rankine.

In 1843, fatigue of axle on locomotive tender is recognized by Joseph Glynn. In 1848, Railway Inspectorate reported probably a fatigue failure due to a rivet hole in tread of railway carriage wheel.

In, 1849, Eaton Hodgkinson made an experiment in order to understand the behavior of iron structures that are subjected to changing amplitudes of loads. In 1854, Braithwaite gave a report about fatigue failures and introduced the term fatigue. In 1860, fatigue testing is done systematically by Sir William Fairbairn and August Wöhler. In 1870, endurance limit concept is introduced by Wöhler and he discussed that peak stress is not as important as cyclic stress on fatigue failure. In 1903, fatigue failure in microscopic cracks is shown (Figure 1.1) by Sir James Alfred Ewing.

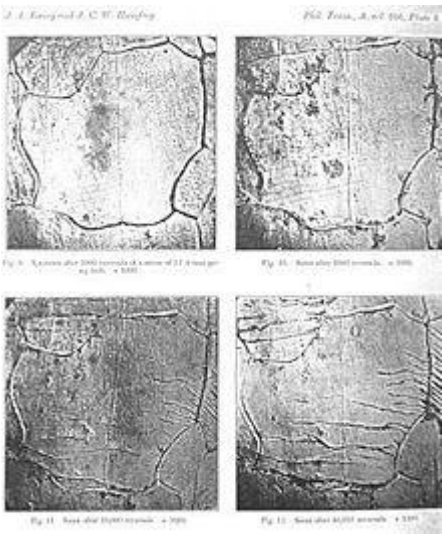

Figure 1.1: Micrographs showing how surface fatigue cracks grow as materials are further cycled. From Ewing & Humfrey (1903) [1]

In 1910, by using Wöhler's fatigue test data, a log-log relationship for S/N curves is given by O. H. Basquin. In 1924, A. Palmgren's proposed a linear damage hypothesis and in 1945, A. M. Miner popularized that hypothesis as a practical design tool.

In 1954, L. F. Coffin and S. S. Manson discussed the effects of plastic strain in the fatigue crack-growth. In 1961, P. C. Paris proposed methods for predicting the rate of growth of individual fatigue cracks against the initial skepticism and popular defense of Miner's phenomenological approach. In 1968, Tatsuo Endo and M. Matsuishi developed the rainflow-counting algorithm and they applied Miner’s rule to results obtained using rainflow counting algorithm for random loadings. In 1970, W. Elber explained the mechanisms and importance of crack closure [1].

1.3 Scope of the Thesis

In today's delicate and advanced mechanical engineering applications, consideration of fatigue is a fatal issue for all mechanical design engineers who especially work on military environments.

In practical engineering applications, if the loading is harmonic, using the maximum and minimum stress values of the structure, fatigue life of the structure can be calculated from the S/N curve. In order to predict the fatigue life of a structure, a reliable and accurate stress history is needed for the most critical point of the structure. However, since the structures which are subjected to such design efforts are usually intricate, an analytical calculation of stress is not possible.

Hence finite element method (FEM) is used in order to predict the stress history. For this reason, most engineering companies have finite element analysis (FEA) package software with many licensed copies. However, having a reliable and accurate stress history obtained from FEA software may not be sufficient if the load doesn't excite the structure harmonically because these programs are typically limited to giving the output as the maximum and minimum stress values caused by the harmonic excitation.

Especially on air platforms load history is generally composed of random data, hence, in order to predict fatigue life of a structure, empirical methods are used. For this reason, an engineer should also have a commercial Non-FEM fatigue life prediction tool in order to predict the fatigue life of a structure.

Most engineers are familiar with only using FEA software in order to see whether the structure is suitable for the design criteria or not after designing a component However, getting many licenses of the Non-FEM fatigue life prediction tools is a big deal which can cost a great deal of money for companies. In addition, learning how to use these tools is a serious challenge and requires considerable effort for the engineers.

Hence it is decided to develop a simple and user friendly numerical code that all engineers can use simultaneously which does not require much effort and time. This numerical code will be used for fatigue life calculations in both time and frequency domains.

Moreover, the numerical code will be used in order to predict the fatigue life of the real structure: Bracket that is installed on an air platform.

CHAPTER 2

FATIGUE THEORY

2.1 Literature Survey

In most of today's random vibration theory methods, spectral moments of the power spectral density are used in order to find upward mean crossings peaks and peaks per seconds. This relationship between peaks and spectral moments are firstly proposed by S.O. Rice [2].

Using the derivations developed by Rice [2], Bendat [3] presented Narrow–Band solution that is first used in frequency domain fatigue calculations. This expression is consisting of spectral moments up to fourth degree of moments. However, as might have been expected, narrow band solution method gives reasonable results only for narrow band time histories. If it is used in wide band time histories, it gives too conservative results.

In order to correct this conservatism, many methods have been developed. Generally, these methods are derived by obtaining sample time histories that are obtained from power spectral density (PSDs) in order to get Rainflow cycle count using Inverse Fourier Transform. The solutions of Wirsching et al. [4], Chaudhury and Dover [5], Tunna [6], Kam and Dover [7] and Hancock [7] were all derived using the above indicated method.

They all use spectral moments of PSD up to fourth degree. In addition to these methods, Steinberg [8] released a solution based on Gaussian distribution that simply assumes that there are no stress cycles within the ranges greater than 6 RMS values. Dirlik [9] derived an empirical closed form expression using computer simulations and Monte Carlo technique. The probability density function of Rainflow ranges is obtained using this expression.

Bishop [10] analyzed all techniques based on time and frequency domain calculations and concluded that methods based on the random vibration theory give the most accurate results. Hence, vibration fatigue theory can be used in order to avoid massively time consuming and sometimes practically impossible time domain applications. In the study, results of transient and vibration analyses results are compared and it is declared that if the structure is subjected to mean stress, vibration fatigue analysis results can give inaccurate results.

Petrucci et al. [11] proposed general problems that occur when fatigue cycle distribution is obtained directly from PSD by means of closed-form expressions instead of using digital simulations of the stress process. It is shown that the methods proposed in literature give accurate results only in some particular cases. For broad band case solutions, a close-form solution is derived from processes of narrow-band and it is proposed that this solution gives more accurate results for the fatigue cycle distribution.

Petrucci et al. [12] gave a method that allows the user to predict the fatigue life of a structure directly from stress PSD by avoiding simulations in time domain. The method can be used with any shape of stress PSD and it is proposed that it gives the most accurate fatigue life predictions according to frequency domain methods proposed in literature.

Tovo [13] proposed a new method for evaluating rainflow damage. For both broad and narrow-band Gaussian loadings, fatigue damage can be obtained accurately by using this approximation. It is based on the theory that combines peaks and valleys in Gaussian loading.

Benasciutti [14] analyzed fatigue damage due to wide-band Gaussian loading. Spectral moments are obtained from any shaped PSD and dependency between these spectral moments, rainflow cycle counting and linear cumulative fatigue damage is established. By using narrow band approximation of Rychlik [15], counting damage intensity approximation of Madsen et al. [16] and weighted factor approximation of Tovo [13], a new approach is proposed in order to improve the accuracy of the results and a simple application is given as an example.

Liou et al. [17] studied about the differences between fatigue damage analysis results while using Morrow's plastic work interaction rule and Miner's rule if a structure is subjected to variable amplitude loading. The purpose of the study was to develop a ready-to use set of formulas for prediction of fatigue life of structures Also the results of the analyses are compared with a series of fatigue tests in order to verify the derived formulas.

Wu et al. [18] reached a conclusion that Morrow's plastic work interaction damage rule gives more accurate results than Palmgren-Miner rule after studying with specimens made of AL 7075-T651. Considering random loading, fatigue damage is found for indicated materials using narrow band vibration fatigue theory and has been verified by experiments.

Pitoiset et al. [19] presented a study about efficient frequency domain methods for the estimation of high-cycle fatigue if a structure is subjected to random multiaxial loading. It was shown in this study that multiaxial rainflow method used in time domain can be applied in frequency domain by a similar way. Finally, the accuracy of results was checked and it is concluded that frequency domain calculations save time and correlate well with time domain calculations.

Aykan [20] analyzed a Helicopters Self-Defensive System's Chaff/Flare Dispenser Bracket by using vibration fatigue method. Acceleration power spectral density is obtained from operational flight tests. Finite element model of bracket is constituted in order to get stress PSD's. Experiment analyses are performed and finite element model is verified by obtained results.

After finite element model is verified stress transfer functions are obtained and by using PSD load and these transfer functions, stress PSD's are figured out. Then fatigue analysis is performed and results are compared with uniaxial shaker test result.

Kocer [21] developed a new method that obtains a modified input loading with zero mean value in order to get approximately equivalent fatigue damage due to a non-zero mean value loading. Also this method is applied for multiaxial loading applications and the accuracy of the method is discussed by performing several fatigue tests.

2.2 Damage Theories

There are three main life prediction methods listed as Stress Life, Strain Life and Crack Propagation approaches. Stress life and strain life methods predict the life of a structure until crack initiates and crack propagation analyzes the crack growth time until fracture is occurred.

When the loading is applied, if a structure stands in the elastic region, i.e. if stress levels are lower than yield stress, stress life approach is the most suitable method for the fatigue analysis. However, if plastic deformation occurs when the loading is applied, i.e. if stress levels are above the yield stress, then stress life approach cannot be used. For these situations strain life approach is the best way for fatigue analysis.

Stress life approach and strain life approach are both used for calculation of crack initiation time; however crack propagation method is used if the fatigue life of the crack after initiation is needed.

For this method crack size and its shape should be well known before the analysis. In this thesis, since stress levels are under yield stress and plastic deformation is not acceptable for the components by initial design assumption, stress life approach is analyzed in detail. Whereas, the main concepts of Strain Life approach and Crack propagation method will also be discussed.

2.2.1 Stress Life Approach

Ratio of maximum stress to minimum stress is considered in Stress-life approach. This ratio can be categorized in two ways as given in Figure 2.1.

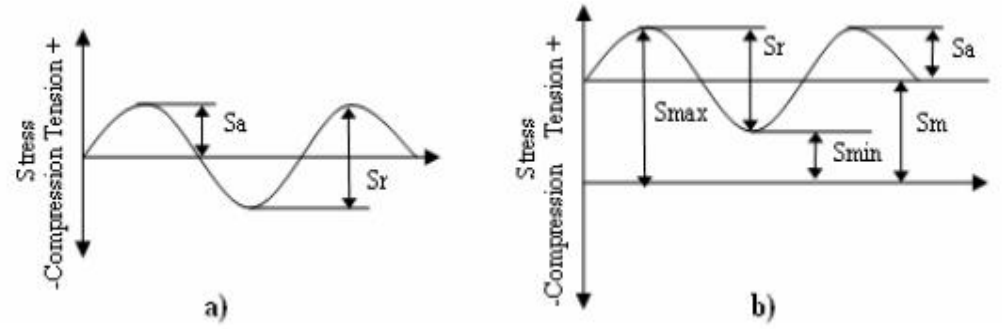

Figure 2.1 Stress Cycles a) fully reversed, b) offset [10]

where, S_a , S_r and S_m are the alternating stress amplitude, stress range and mean stress, respectively. In addition, $S_{\max}$, $S_{\min}$ and R can be defined maximum stress amplitude, minimum stress amplitude and stress ratio ($S_{\min} / S_{\max}$), respectively.

In Figure 2.1 a), a fully reversed stress cycle with a sinusoidal form is shown. This ideal loading condition is usually found for rotating shafts while they are operating at constant speed and load.

The most important property of fully reversed cycles is that he magnitudes of maximum and minimum stresses are equal but opposite in sign. Positive stress means that stress is tensile whereas negative stress means that stress is compressive. Figure 2.1 b) indicates the situation that the magnitudes of maximum and minimum stresses are not equal, which generally is the encountered case. Since both signs of the maximum and minimum stresses are positive, they are tensile stresses.

A cylinder with very small changes of cross-section and with a polished surface where the crack initiates was the most common test specimen for bending in the past. However, this type of test, called Wohler test, has limitations. Nowadays, axial loaded cylinder in tension with no sudden cross section changes and with a polished surface where crack initiates is the more preferable test specimen. Many specimens with the same specifications are tested and the needed number of cycles for total separation is accepted as N. During the test, load is kept constant. From elastic formula, nominal stress, S is calculated for each specimen and the results are plotted as the un-notched $S-N$ curve which is a basic material property. N in the logarithmic scale is plotted on the X axis while S can be plotted in linear or logarithmic scale [10]. However, using the logarithmic scale is becoming the norm.

The mean line in the finite-life region (10^4 - 10^7 cycles) is usually straight. This straight line shown in Figure 2.2 can be formulated as given in Equation (2.1) [10].

$$N = C \times S^{-b} \tag{2.1}$$

In Equation (2.1), b indicates the inverse of the line called as Basquin exponent and C is related to the intercept on the Y axis.

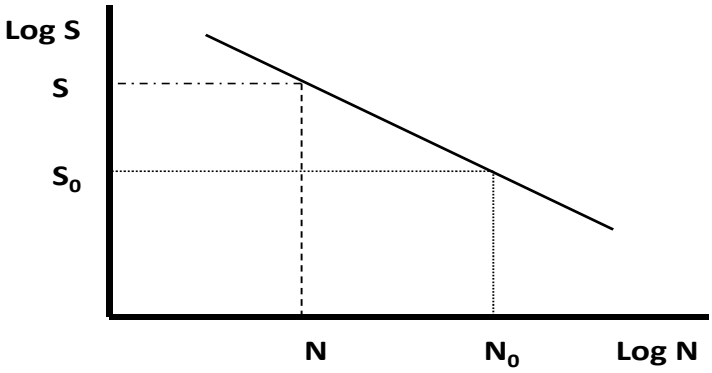

Figure 2.2 $S-N$ Data of Steel [10]

$S-N$ curve of the low alloy steels is usually composed of two lines one of which is usually horizontal and this shows the material has a fatigue limit, S_0, which is important when the infinite life is aimed. If a clear fatigue limit cannot be seen for materials, then S value that is specified at between 10^7 and 10^8 cycles can defined as endurance limit, S_e. The endurance limit and fatigue limit examples are given in Figure 2.3[10].

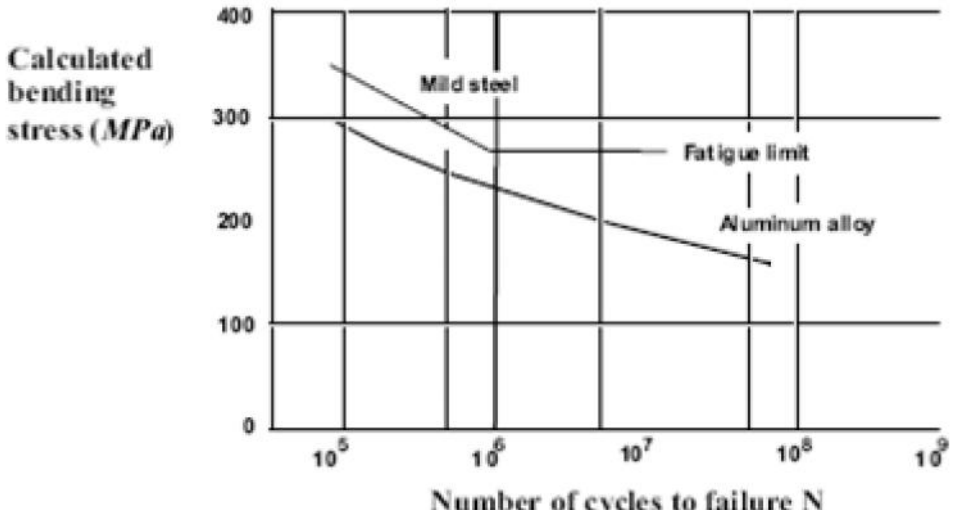

Figure 2.3 S / N Curves for Ferrous and Non-Ferrous Metals [10]

2.2.1.1 Stress Concentration and Notch Sensitivity

Equation (2.1) indicates that fatigue is very sensitive to stress. While performing fatigue analysis, this behavior is very critical because, stress concentration zones (notches, holes etc), encountered in real life designs, create huge problems during the design life of a mechanical component. Stress concentration factor called K_t is used to consider these stress concentration effects. K_t can be defined as follows [10]:

$$K_t = \frac{\text{Maximum Stress in the region of the notch}}{\text{Nominal Stress away from the notch}} \tag{2.2}$$

K_t can be defined as stress concentration due to geometrical discontinuities. However, it should be considered that there is a relationship between stress concentration and material properties. As previously mentioned the fatigue test specimens do not have sudden changes in geometry like notches.

However it is known that if the geometry has a notch then the obtained $S-N$ curve could be different. At this point K_f called stress reduction factor should be taken into account. K_f can be defined as follows:

$$K_f = \frac{\text{Stress needed to cause failure in an un-notched specimen}}{\text{Stress needed to cause failure in a notched specimen}} \tag{2.3}$$

In order to obtain K_f from K_t the notch sensitivity factor, q, is used. This notch sensitivity factor is related with material properties and determines the sensitivity of material to geometrical notch sensitivity, K_t.

$$q = \frac{K_f - 1}{K_t - 1} \tag{2.4}$$

Multiplying K_f by nominal reversing stress, modified reversing stress can be derived or dividing the un-notched specimen endurance limit by K_f, the notched specimen endurance limit can be obtained in order to be used in fatigue calculations.

2.2.1.2 Endurance Limit Modifying Factors

$S-N$ curves of materials obtained in laboratory conditions cannot be used in real life cases due to many different real life environmental effects that materials are subjected to.

Since it is not feasible to test a material with every case that the material can be exposed to in real life, modifying factors are developed in order to get modified endurance limit from endurance limit obtained in laboratory environment. Considering all effects, Marin [22] investigated the Equation (2.5) for modifying endurance limit according to real life cases as given below:

$$\mathrm{S_e} = k_a \cdot k_b \cdot k_c \cdot k_d \cdot k_e \cdot k_f \cdot S_e^{'}, \tag{2.5}$$

where, k_a, k_b, k_c, k_d, k_e and k_f can be defined as surface condition factor, size modification factor, load modification factor, temperature modification factor, reliability factor and miscellaneous-effects modification factor, respectively. In addition, S_e and $S_e^{'}$ are called laboratory test specimen endurance limit and endurance limit at the critical location of a machine part in the geometry and condition of use, respectively.

2.2.1.3 Mean Stress Effect

Fatigue life depends mainly on the stress amplitude that occurs in the component, but if there exists a mean stress on the component, changing of the global stress is unavoidable. Usually some forms of loads such as gravitation or pre-tension are carried by components before the operational stresses are applied or the input loading can have a mean value. For a given life, the allowable amplitude of fatigue stress gets smaller if the mean stress is more tensile and gets larger if the mean stress is more compressive. The main assumption is that mean stress affects the allowable applied stress in a linear way [10].

The line representing fatigue life can be obtained if fatigue strength at any mean stress is known. Goodman's Rule is the most known and used method for deriving modified alternating stress according to mean stress.

There are also other mean stress approaches, like Gerber and Soderberg's Rules. Soderberg's model is the most conservative method. In addition there is one more method that is called Modified Goodman's Rule. The graphical representations of all mean stress correction methods are illustrated in Figure 2.4.

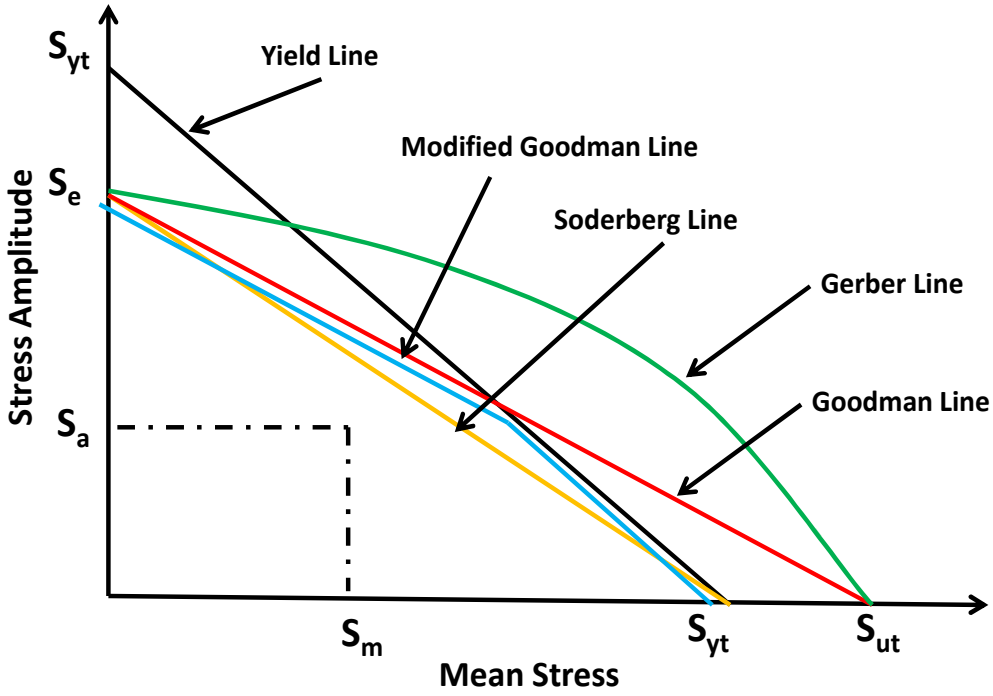

Figure 2.4 Mean Stress Modification Methods

The formulations, used in order to get the lines indicated in Figure 2.4, are as follows:

$$\text{Goodman's model: } \frac{S_a}{S_a^{'}} + \frac{S_m}{S_u} = 1, \tag{2.6}$$

$$\text{Gerber's model: } \frac{S_a}{S_a^{'}} + \left(\frac{S_m}{S_u}\right)^2 = 1, \tag{2.7}$$

$$\text{Soderberg's model: } \frac{S_a}{S_a^{'}} + \frac{S_m}{S_y} = 1, \tag{2.8}$$

where, S_a , $S_a^{'}$, S_m , S_{ut} and S_{yt} can be defined as equivalent alternating stress, alternating stress, mean stress, ultimate tensile strength and tensile yield strength, respectively.

2.2.1.4 Type of the Stress Amplitude

Cracks usually occur by a dominant stress perpendicular to the crack direction. Hence, the most sensible indication of the driving force may be accepted as Absolute Maximum Principal Stress.

The range of the maximum principal stress to the minimum principal stress is called Absolute Maximum Stress range and growing of cracks depends on this range. The meaning of the "Absolute Maximum Principal" stress can be easily observed from the following example shown in Table 2.1.

Table 2.1 Illustration of Absolute Maximum Principal Stress Range

Time	0	1	2	3	4	**Max Range**
Max Principal (MPa)	100	-100	200	-200	500	700
Min Principal (MPa)	50	-150	-500	-250	-10	550
Abs Max Principal (MPa)	100	-150	-500	-250	500	1000

It can be easily observed that keeping the signs of stresses as are basis, firstly larger stress range is obtained and then signs of the stresses are left [10]. The method used in order to obtain Absolute Maximum Stress is given by Equation (2.9).

$$\sigma_{AMP} = \sigma_3 \text{ if } |\sigma_3| \geq |\sigma_1| \quad , \quad otherwise\ \sigma_{AMP} = \sigma_1 \tag{2.9}$$

where, σ_1 , σ_3 and σ_{AMP} are maximum principal stress, minimum principal stress and maximum absolute principal stress, respectively.

2.2.1.5 Variable Amplitude Loading That Cause to Fatigue Damage

The variable amplitude loading is more common in real life applications. The changes of the amplitude of the sine waves from time to time are the simplest extension of the constant amplitude case shown in Figure 2.5.

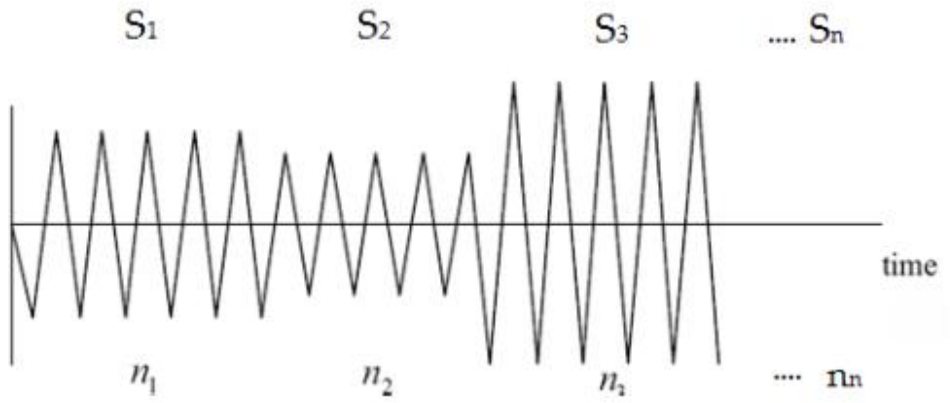

Figure 2.5 Block Loading Sequence [10]

The history shown in Figure 2.5 contains n_1 cycles of amplitude S_1, n_2 cycles of amplitude S_2, n_3 cycles of amplitude S_3 and so on. In real life cases it is observed that usually a small number of S values called S_n repeat itself. The sequence up to S_n is called block and estimating how many of these blocks can be applied before failure occurs is the target. The general used rule is Miner or Palgren-Miner [10].

Considering first n_1 cycles of S_1, the number of cycles of S_1 which would cause failure if no other stresses were present can be obtained from S-N data. If these numbers of cycles are called N_1 then the assumption is for n_1 cycles of S_1 use up a fraction n_1 / N_1 of the whole fatigue life.

Similar calculations can be done for all other stress levels and summing all the results gives the total damage for one block. This equation, which is based on linear damage sum, is given as below [10];

$$\sum \frac{n}{N} = 1, \tag{2.10}$$

where, n and N are the number of stress cycles applied at a fixed stress amplitude and the number of cycles the material can withstand at applied fixed stress amplitude, respectively.

This is the general formulation of the Miner's Rule. Although Miner's rule gives the most acceptable results for fatigue damage, the main three assumptions should be carefully examined.

- The damage of all the cycles of a given amplitude is the same whether they occur early or late in the life.
- The damage caused by S_1 is not affected by the presence of the S_2 etc.
- The rule governing the damage caused by both S_1 and S_2 is the same.

The formulation of obtaining the total damage caused by so many different cycles for given amplitudes is given below [10];

$$E[D] = \sum \frac{n}{N}, \tag{2.11}$$

where, $E[D]$ can be defined as expected damage.

There are some other cumulative damage rules that consider material plasticity, stress history effects etc. Shanley's theory, Marco-Starkey theory, Corten and Dolan theory [23] and Morrow's plastic work interaction theory [17] are some of the theories found in literature. Although Palmgren-Miner's rule sometimes gives conservative results ([10, 12]) Palmgren-Miner rule is still used widely in the applications of the fatigue life estimates.

2.2.1.6 Counting Methods Used For Vibration Fatigue Analysis

If the stress history is random, obtaining the loading cycle occurrences, amplitudes and mean values in a time history is very difficult.

There are many ways to identify these values like Rainflow counting, Peak counting, Level Crossing counting and Range counting procedures [24]. Rainflow counting is the most reasonable and widely used method proposed by Tatsuo Endo and M. Matsuiski in 1968 [25].

There are some commonly used procedures in order to obtain Rainflow cycles [10], however the most practical one is as follows [24];

Let X represents range under consideration; Y, previous range adjacent to X; and S, starting point in the history.

1. Read next peak or valley. If out of data, go to Step 6.
2. If there are less than three points, go to Step 1. Form ranges X and Y using the three most recent peaks and valleys that have not been discarded.
3. Compare the absolute values of ranges X and Y.
   a) If $X < Y$, go to Step 1.
   b) If $Y < X$, go to Step 4.
4) If range Y contains the starting point S, go to step 5; otherwise, count range Y as one cycle; discard the peak and valley of Y; and go to Step 2.

5) Count range Y as one-half cycle; discard the first point (peak or valley) in range Y; move the starting point to the second point in range Y; go to Step 2.
6) Count each range that has not been previously counted as one-half cycle

Figure 2.6 is used to illustrate the process. Details of the cycle counting are as follows [24];

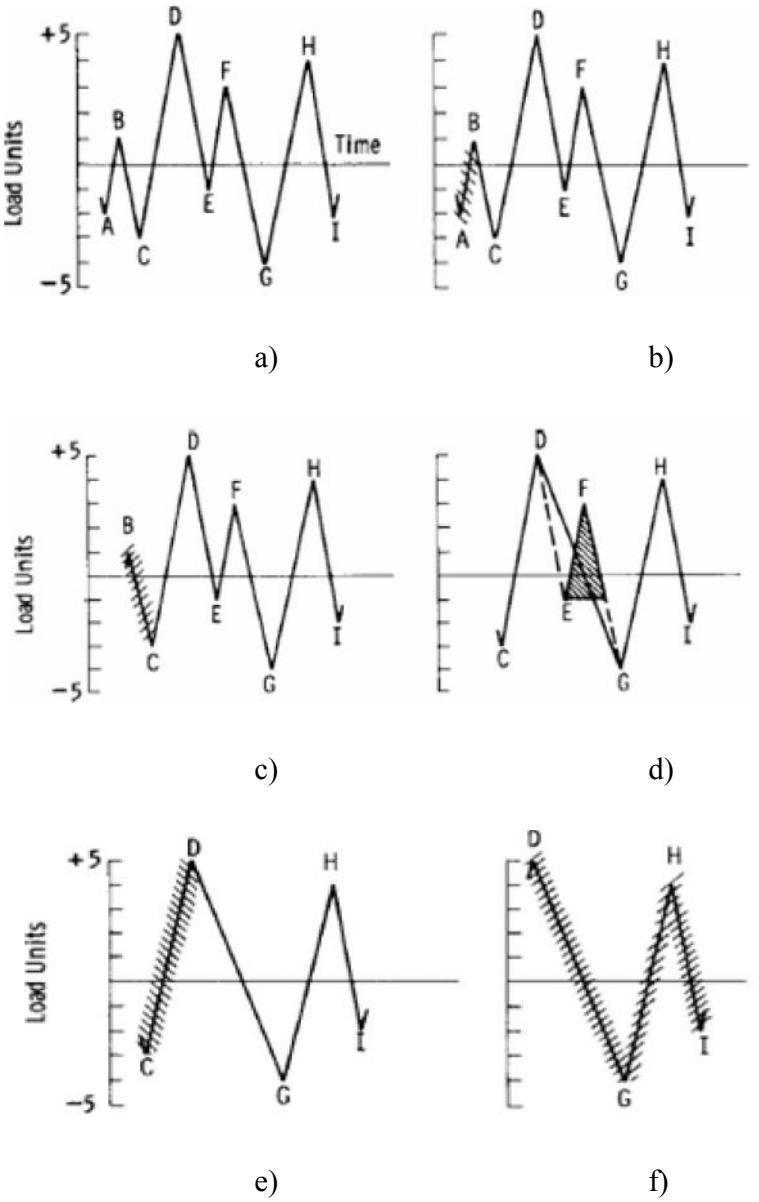

Figure 2.6 Illustration of Rainflow Cycle Counting Method [24]

1. $S = A$; $Y = |A - B|$; $X = |B - C|$; $X > Y$. Y contains S, that is, point A. Count $|A - B|$ as one-half cycle and discard point A; $S = B$.
2. $Y = |B - C|$; $X = |C - D|$; $X > Y$. Y contains S, that is, point B. Count $|B - C|$ as one half-cycle and discard point B; $S = C$. (Figure 2.6 c))
3. $Y = |C - D|$; $X = |D - E|$; $Y > X$.
4. $Y = |D - E|$; $X = |E - F|$; $Y > X$.
5. $Y = |E - F|$; $X = |F - G|$; $X > Y$. Count $|E - F|$ as one cycle and discard points E and F. (Figure 2.6 d). (A cycle is formed by pairing range $E - F$ and a portion of range $F - G$)
6. $Y = |C - D|$; $X = |D - G|$; $X > Y$. Y contains S , that is, point C. Count $|C - D|$ as one-half cycle and discard point C. $S = D$. (Figure 2.6 e))
7. $Y = |D - G|$; $X = |G - H|$; $Y > X$.
8. $Y = |G - H|$; $X = |H - I|$; $Y > X$. End of data.
9. Count $|D - G|$ as one-half cycle, $|G - H|$ as one-half cycle, and $|H - I|$ as one half cycle. (Figure 2.6 f))
10. End of the Counting.

Results of Rainflow Cycle Counting Method for the example shown in Figure 2.6 are given in Table 2.2.

Table 2.2 Results of Rainflow Cycle Counting Method for Example Shown in Figure 2.6 [24]

RANGE UNITS	CYCLE	EVENTS
1	0	
2	0	
3	0.5	A-B
4	1.5	B-C, E-F
5	0	
6	0.5	H-I
7	0	
8	1	C-D, G-H
9	0.5	D-G
10	0	

2.2.2 Strain Life Approach

If the cyclic loads are relatively large, plastic deformation can occur and that leads to very short life of the structure compared to design specification. If plastic deformation occurs in a component, Strain-Cycle curve should be used rather than $S-N$ curve to obtain fatigue life [21].

2.2.3 Crack Propagation Approach

Both Stress Life and Strain Life approaches are valid until the crack initiates. After crack is initiated, considerable time should pass for the propagation of the crack and the fracture. The calculation of this time is done by means of Linear Elastic Fracture Mechanics theory.

2.3 Vibration Fatigue Approach

In frequency domain, vibration fatigue approach is used to determine fatigue life of a component, if the input loading or stress history collected from that component is random. PSD obtained from random time histories is the best expression and used as the input for calculation of fatigue in frequency domain [20].

In order to transform random time data to PSD, Fast Fourier Transform (FFT) is required. By using FFT, sine wave functions with unique amplitude, frequency and phase are obtained. These obtained sine waves can be determined at any point in time. (Figure 2.7)

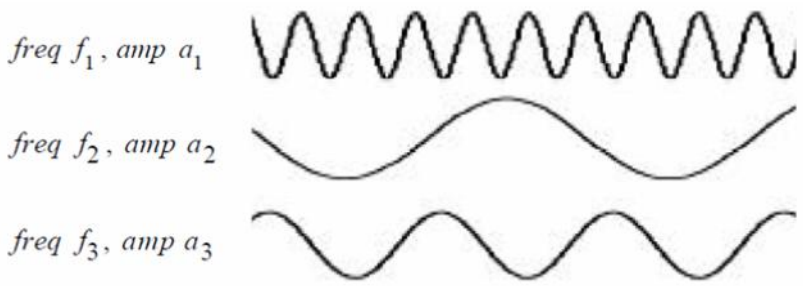

Figure 2.7 Deterministic Processes [10]

The sine waves shown in Figure 2.7 are still in time domain as seen. If Fast Fourier Transform is extended, random time data finally can be transformed to frequency domain as shown in Figure 2.8.

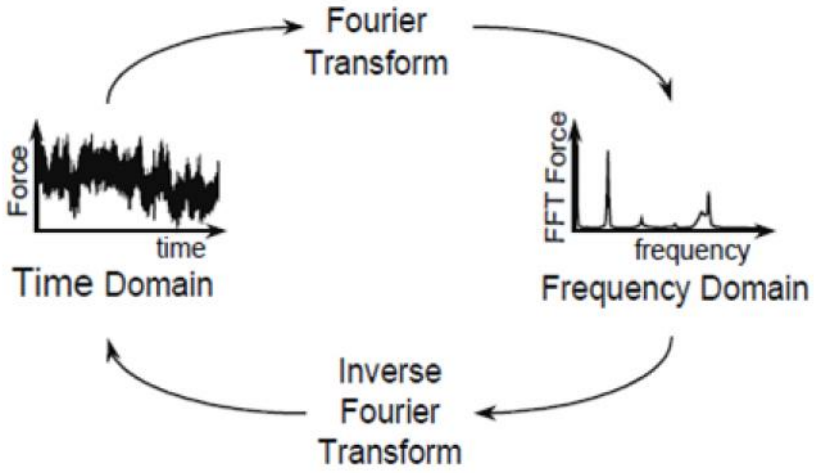

Figure 2.8 Frequency Domain Data Obtained From Random Time Data Using Fourier Transform [26]

PSD is obtained by taking the modulus squared of FFT. While obtaining PSD, phase information is lost, however, frequency and amplitude of each sine wave is retained. (Figure 2.9)

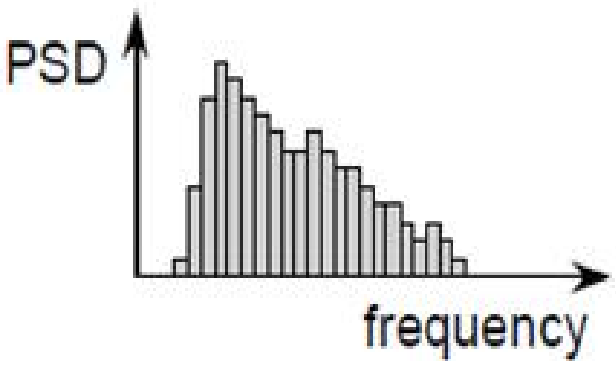

Figure 2.9 PSD By Taking Modulus Squared of Fast Fourier Transform [26]

In Figure 2.10, there are some general examples that show PSD's of different forms of random time histories.

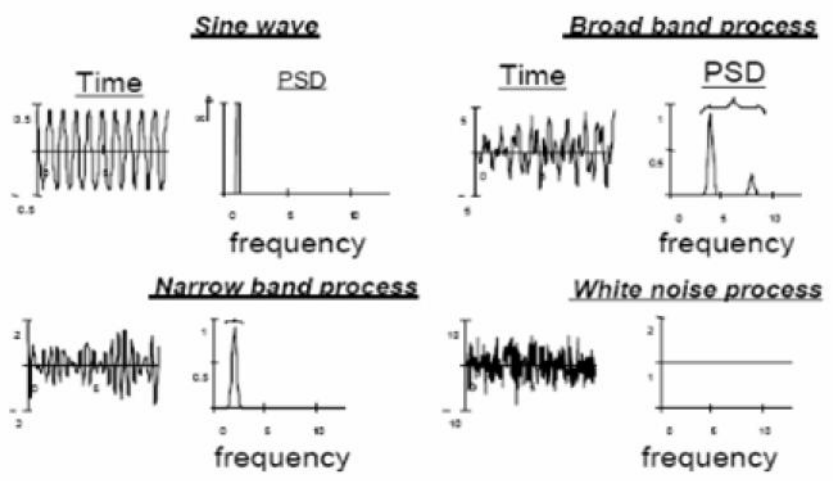

Figure 2.10 Time Histories and Their PSD's [10]

For frequency domain fatigue life calculations transfer function is needed. If the system is linear, by multiplying the PSD input with transfer function, response of the system can be obtained.

In frequency domain, in order to obtain output response of a linear system, the Equation (2.12) can be used.

$$\mathrm{R}(f) = H_{TF}(f) \cdot I_{load}(f), \tag{2.12}$$

where, $\mathrm{R}(f)$, $H_{TF}(f)$, $I_{load}(f)$ and f can be defined as FFT of the response of the system, transfer function of the system in the frequency domain, FFT of the input load applied to system and frequency, respectively.

As indicated above, the response PSD can be obtained by taking modulus squared of response FFT. The formulation of obtaining response PSD is given as follow:

$$G(f)_{response\_PSD} = \frac{1}{2 \cdot T}(H_{TF}(f) \cdot I_{load}(f) \cdot H_{TF}(f)^{*} \cdot I_{load}(f)^{*}), \tag{2.13}$$

$$G(f)_{response\_PSD} = (H_{TF}(f) \cdot H_{TF}(f)^{*} \cdot G(f)_{input\_PSD}), \tag{2.14}$$

$$G(f)_{response\_PSD} = \left|H_{TF}(f)\right|^{2} \cdot G(f)_{input\_PSD}, \tag{2.15}$$

where, $G(f)_{response\_PSD}$, $G(f)_{input\_PSD}$, $\mathrm{H_{TF}(f)^*}$, $|H_{TF}(f)|^2$, $\mathrm{I_{load}(f)^*}$ and T are response PSD, input PSD, complex conjugate of the transfer function, modulus squared of transfer function, complex conjugate of the FFT of the input load and period of function, respectively.

In order to obtain stress PSD from a structure exposed to input PSD, Equation (2.15) can be used if the transfer function is linear.

Detailed work is performed in order to verify this Equation (2.15) whether it works or not by considering a two degree of-freedom system given in ANSYS Mechanical APDL Help as VM68. Calculations and verification are given in Appendix A.

In order to calculate expected fatigue damage, $E[D]$, firstly Probability Density Function (PDF) of rainflow stress ranges , $p(S)$, should be determined. Mathematically, storing histories in the form of PDF is the best way. A typical PDF is shown in Figure 2.11 [26].

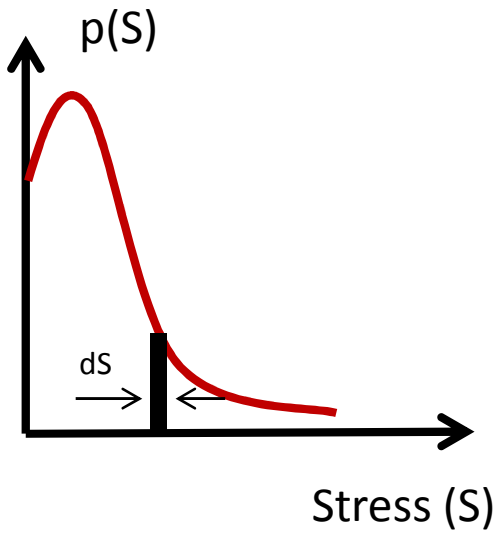

Figure 2.11 Probability Density Function (PDF) [26]

The bin widths, dS and total number of cycles in the histogram, S_t are required in order to obtain PDF from a stress range histogram. The opposite work can also be performed using PDF. $p(S)\cdot dS$ gives the probability of stress ranges between $S_i - \frac{dS}{2}$ and $S_i + \frac{dS}{2}$.

Finally, multiplying the probability of stress ranges ($p(S)\cdot dS$) with the total number of cycles (S_t) in the histogram, the number of total cycles, $n(S)$, for a given stress level , S, can be obtained. The formulation for $n(S)$ is given by Equation (2.16) [26] as follows;

$$n(S) = p(S)\cdot dS \cdot S_t \tag{2.16}$$

In order to use Equation(2.11), $n(S)$ is obtained from PDF. For a given stress level, S, total number of cycles, $N(S)$, which cause failure, will be found according to Wohler curve formulation given in Equation (2.1).

Finally, by substituting Equation (2.16) and Equation (2.1) into Equation (2.11), Expected damage, $E[D]$, can be found as.

$$E[D] = \sum_i \frac{n_i(S)}{N(S_i)} = \frac{S_t}{C}\int_0^\infty S^b \cdot p(S)\cdot dS \tag{2.17}$$

In frequency domain, there are many different techniques that determine the PDF. Although they appear to be complicated, they are only functions of four spectral moments of the PSD (m_0, m_1, m_2, m_4).

Before determining indicated techniques, brief information will be given about spectral moments and terms developed from these spectral moments. These spectral moments of the PSD shown in Figure 2.12 and expressed by Equation (2.18) can be obtained if $G(f)$ is defined.

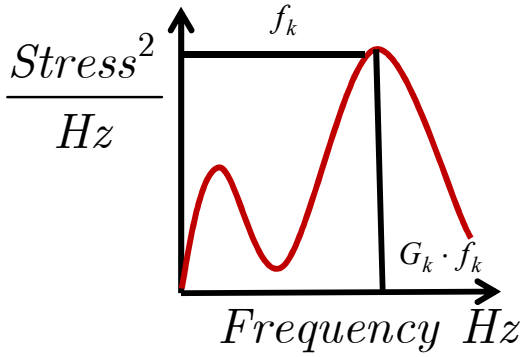

Figure 2.12 Spectral Moments of PSD

$$m_n = \int_0^\infty G(f) \times df = \sum_{k=1}^{m} f^n{}_k \times G_k\left(f_k\right) \times \delta f\,, \tag{2.18}$$

where, δf can be defined as frequency increment.

For a random signal, S.O Rice [2] developed a very important relationship for the number of upward mean crossings per second, $E[0]$, and peaks per second, $E[P]$, expressed in terms of spectral moments as given below.

$$E[P] = \sqrt{\frac{m_4}{m_2}}, E[0] = \sqrt{\frac{m_2}{m_0}} \tag{2.19}$$

By using Equation (2.19), another factor called irregularity factor can be obtained as;

$$\gamma = \frac{E[0]}{E[P]} = \sqrt{\frac{{m_2}^2}{m_0 \cdot m_4}} \tag{2.20}$$

Theoretically, this factor can only take a value in the range of 0 to 1. If the value is 1, the process is narrow band and if the value is closer to 0 that shows process tends to be white noise. Expected number of zeros, peaks and the irregularity factor is shown in Figure 2.13.

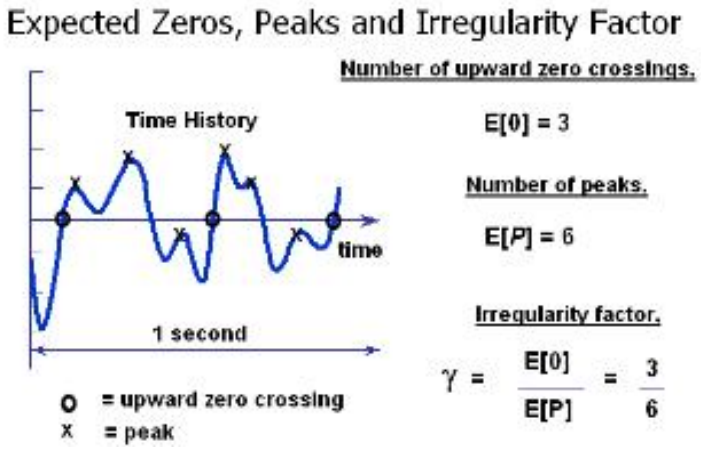

Figure 2.13 Expected Zeros, Peaks and Irregularity Factor [10]

Also note that;

$$E[P] \cdot T = S_t, \tag{2.21}$$

where, T is fatigue life in seconds.

By substituting Equation (2.21) into Equation (2.17), expected damage formulation given in Equation (2.22) is obtained to be used in frequency domain applications.

$$E[D] = \sum_i \frac{n_i(S)}{N(S_i)} = \frac{E[P] \cdot T}{C} \int_0^\infty S^b \cdot p(S) \cdot dS \tag{2.22}$$

By setting $E[D]$ equal to 1, fatigue life, T, can be found in seconds. While calculating fatigue damage by using Equation (2.22), an appropriate cut-off value should be used for the upper limit of integration.

Root Mean Square (RMS) value of stress is used and is normally set to 3 RMS (for amplitude) or 6 RMS (for range). However, to be conservative, 4.5 RMS can be selected as upper limit of integration in order to avoid unexpected failures [10].

In order to calculate expected damage by using Equation (2.22), $p(S)$ should be found as indicated above. Bendat [3] first proposed frequency domain solution which gives conservative results due to the fact that it substitutes the peaks of Rayleigh PDF with stress ranges. Hence, for wide-band calculations it overestimates the fatigue life, Bendat's solution is called Narrow-Band. The formulation of Narrow-Band that contains $p(S)$ (Equation (2.23)) is given in Equation (2.24).

$$p(S) = \frac{S}{4 \cdot m_0} e^{\frac{-S^2}{8 \cdot m_0}} \tag{2.23}$$

$$E[D]=\sum_i \frac{n_i(S)}{N(S_i)}=\frac{E[P]\cdot T}{C}\int_0^{\infty} S^b\cdot\frac{S}{4\cdot m_0}e^{\frac{-S^2}{8\cdot m_0}}\cdot dS \tag{2.24}$$

In order to avoid from the conservative results obtained from narrow-band solutions, many expressions are investigated as mentioned above.

Generally the data is transformed to time domain from frequency domain using Inverse Fourier Transform in order to get a sample time data. Then, rainflow counting of this sample data is performed.

The first expression developed by Wirsching [4],

$$E[D]=E[D]_{NB}\left(a+(1-a)(1-\varepsilon)^c\right) \tag{2.25}$$

where,

$$a=0.926-0.033b \tag{2.26}$$

$$c=1.587b-2.323 \tag{2.27}$$

$$\varepsilon=\sqrt{1-\gamma^2} \tag{2.28}$$

Tunna [6] changed expression of $p(S)$ given in narrow-band solution as,

$$p(S)=\frac{S}{4\cdot\gamma\cdot m_0}e^{\frac{-S^2}{8\cdot\gamma\cdot m_0}} \tag{2.29}$$

Hancock [7] proposed equivalent stress method,

$$\left(S_{eq}\right)_{Hancock} = \left(2\cdot\sqrt{2\cdot m_0}\right)\left[\gamma\cdot\Gamma\left(\frac{b}{2}+1\right)\right]^{\frac{1}{b}} \tag{2.30}$$

Chaudhuery and Dover [5] used another expression for equivalent stress;

$$\left(S_{eq}\right)_{CandD} = \left(2\cdot\sqrt{2\cdot m_0}\right)\left[\frac{\varepsilon^{b+2}}{2\cdot\sqrt{\pi}}\cdot\Gamma\left(\frac{b}{2}+1\right)+\frac{\gamma}{2}\cdot\Gamma\left(\frac{b}{2}+2\right)+erf\left(\gamma\right)\cdot\frac{\gamma}{2}\cdot\Gamma\left(\frac{b}{2}+2\right)\right]^{\frac{1}{b}} \tag{2.31}$$

The simplest form of equivalent stress is given by Steinberg [8],

$$\left(S_{eq}\right)_{Steinberg} = \left[0.683\left(2\cdot\sqrt{m_0}\right)^{b}+0.271\cdot\left(4\cdot\sqrt{m_0}\right)^{b}+0.043\left(6\cdot\sqrt{m_0}\right)^{b}\right]^{\frac{1}{b}} \tag{2.32}$$

By substituting S_{eq} into general fatigue damage $E[D]$, rule, the formulation given in Equation(2.33) can be obtained. Using this equation fatigue damage can be found.

$$E[D] = \frac{E[P]\cdot T}{C}\cdot S_{eq} \tag{2.33}$$

The best correlation in order to find $p(S)$ is proposed by Dirlik [9] and it is given in Equation(2.34). Dirlik investigated this method without using narrow-band solution. This empirical closed form of PDF is obtained by using computer simulations based on Monte Carlo technique [10].

$$p(S)=\frac{\frac{D_1}{Q}\cdot e^{\frac{-Z}{Q}}+\frac{D_2\cdot Z}{R^2}\cdot e^{\frac{-Z^2}{2\cdot R^2}}+D_3\cdot Z\cdot e^{\frac{-Z^2}{2}}}{2\cdot\sqrt{m_0}} \tag{2.34}$$

where,

$$D_1=\frac{2\cdot(x_m-\gamma^2)}{1+\gamma^2},D_2=\frac{1-\gamma-D_1+D_1^{\,2}}{1-R},D_3=\frac{1-D_1+D_2}{1-R}$$

$$Q=\frac{1.25\cdot(\gamma-D_3-D_2\cdot R)}{D_1},R=\frac{\gamma-x_m-D_1^{\,2}}{1-\gamma-D_1+D_1^{\,2}},Z_i=\frac{S}{2\cdot\sqrt{m_0}},x_m=\frac{m_1}{m_0}\cdot\sqrt{\frac{m_2}{m_0}}$$

CHAPTER 3

FINITE ELEMENTANALYSIS OF CANTILEVER BEAM AND BRACKET

Verification is needed for the developed numerical code before performing fatigue analysis of the bracket that is installed on an air platform. Hence, a cantilever beam is selected as a case study for verification. It is known that in order to predict fatigue life of a structure, stress histories of the most critical points in the structure should be obtained correctly. For obtaining these correct stress histories, structures should be modeled in finite element environment accurately. Before importing the structures to finite element environment, 3D models are designed by a CAD (Pro Engineer 4.0) program. (Figure 3.1)

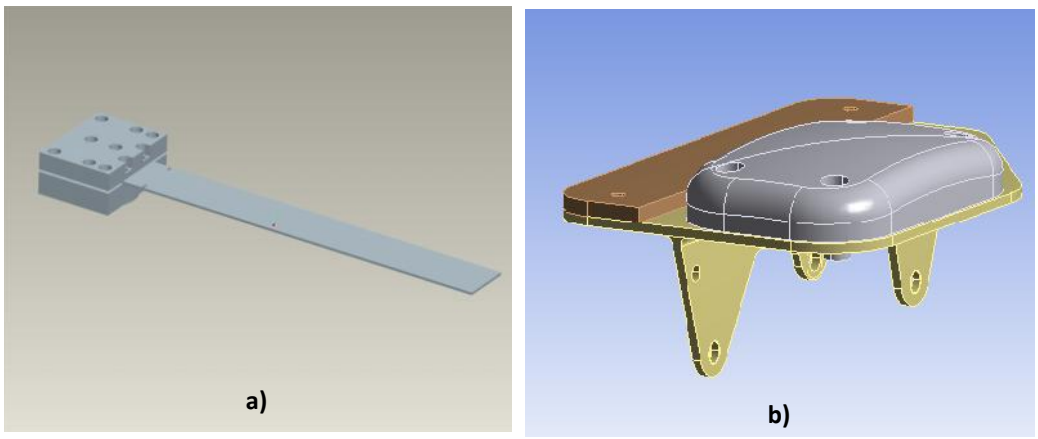

Figure 3.1 a) 3D Model of the Test Fixture for Shaker Table and Beam b) Bracket

There are two sided symmetric notches on the beam for accelerating the fatigue test and the other dimensions are shown in Figure 3.2.

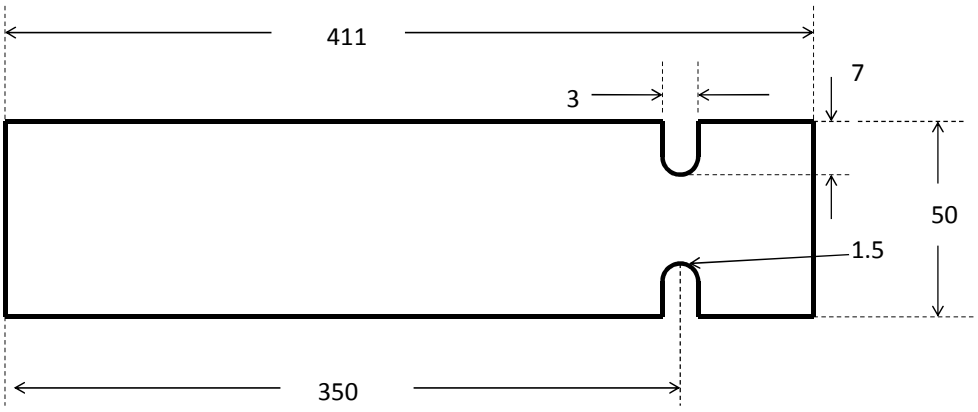

Figure 3.2 Dimension of the Cantilever Beam

3.1 Modal Analysis of Cantilever Beam and Bracket

After 3D models of structures are obtained, they are imported to finite element environment (ANSYS Workbench). For meshing, ANSYS Workbench uses SOLID 186 element as default. SOLID 186 is a higher order 3D solid element that exhibits quadratic displacement behavior and has 20 nodes [27]. Shape of the element chosen is hexahedral because tetrahedral elements tend to have artificial stress concentrations due to their shape.

Especially if the mesh is coarse, the triangular faces of the tetrahedral element causes stress concentrations in the structure. Hence hexahedral elements are used in order to have less number of elements and better stress result without stress concentrations due to mesh [10]. Although the hexahedral element is used, an appropriate element size should be chosen for accurate stress and fatigue results. This means, mesh sensitivity is an important factor for getting the accurate stress results.

Coarse mesh may not give the actual stress; however, fine mesh size may be inessential to obtain the actual stress level. It should be noted that very fine mesh size means large storage capability and increase in calculation time. Therefore, in order to choose an appropriate element size, several static analyses with different mesh densities are performed and the optimal mesh size is selected for the dynamic analyses used in fatigue life calculations.

In the area of that maximum stress occurs, a small area is selected and, the element size in that area is iterated until stress converges to an appropriate value. The global and local mesh sizes and results for them are given in Table 3.1 and Table 3.2 for both cantilever bam and the bracket respectively.

Table 3.1 Mesh Sensitivity Analysis Results for Cantilever Beam

Iteration Number	**Global Mesh Size (mm)**	**Area of Maximum Stress**	**Max Principal Stress Result (MPa)**
1	6	6	12.832
2	5	5	14.936
3	4	4	15.612
4	3	3	16.547
5	2	1	16.830

Table 3.2 Mesh Sensitivity Analysis Results for the Bracket

Iteration Number	**Global Mesh Size (mm)**	**Area of Maximum Stress**	**Max Principal Stress Result (MPa)**
1	3	3	2.19
2	3	2	2.03
3	3	1	1.96
4	3	0.7	1.94

For cantilever beam, globally 2 mm and on the notched area 1 mm mesh size is selected. 14028 SOLID186 elements and 62312 nodes are obtained. For Bracket, globally 3 mm and on the critical area 0.7 mm mesh size is selected. 21909 SOLID186 elements and 70021 nodes are obtained. Meshed models of cantilever beam and Bracket are given in Figure 3.3 and Figure 3.4, respectively.

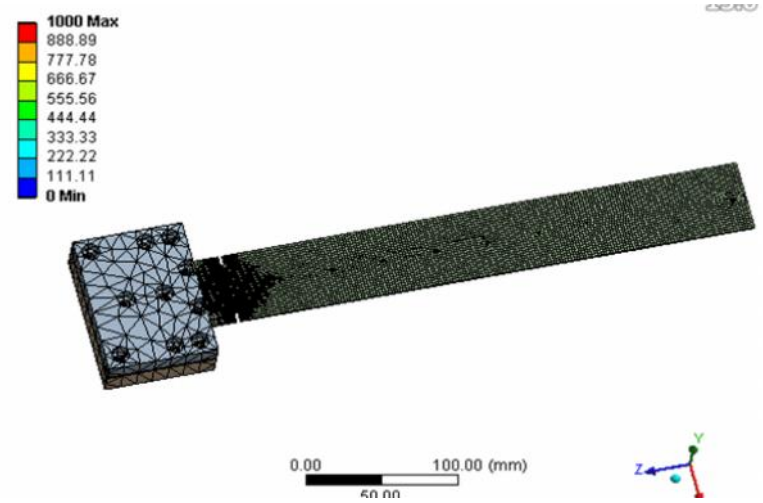

Figure 3.3 Meshed Model of the Test Fixture for Shaker Table and Beam

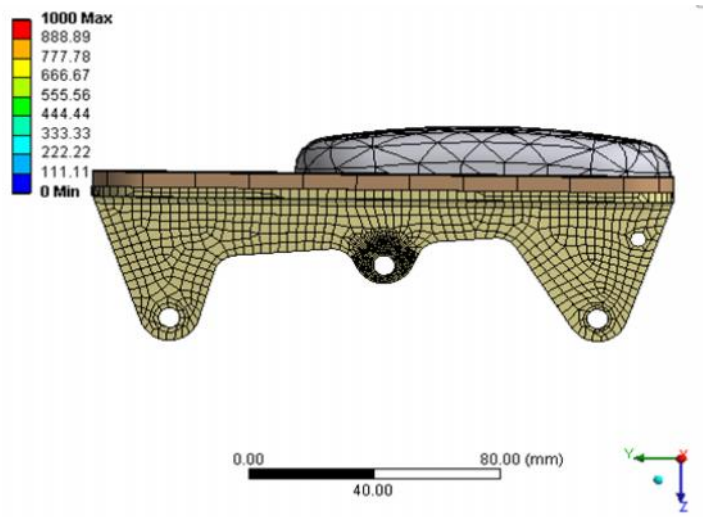

Figure 3.4 Meshed Model of the Bracket

For modeling contacts, only linear types of contacts are used. Bonded contact is a linearly solved type of contact which is supported by ANSYS. Hence, while performing the modal analysis, neglecting the all bolts from the model can be an acceptable assumption and for all contacts of bolts, bonded contacts are used.

In fact, the cantilever beam fixture is fixed to shaker table by five bolts and Bracket is fixed to fixture by three bolts. However, it is assumed that the connecting surfaces which are fixed by bolts do not move relative to each other or separate, hence, fixed boundary conditions are applied to the blue surfaces given in Figure 3.5 and Figure 3.6.

In addition, the information about the materials that the components are made of and properties of these materials are shown in Table 3.3.

Table 3.3 Material Properties of the Structures

Part Names	Modulus Of Elasticity (MPa)	Density (kg/m^3)	Poisson's ratio
Beam (AL 6061 T6)	68946	2849	0.33
Bracket (AL 7075 T7351)	71700	2810	0.33

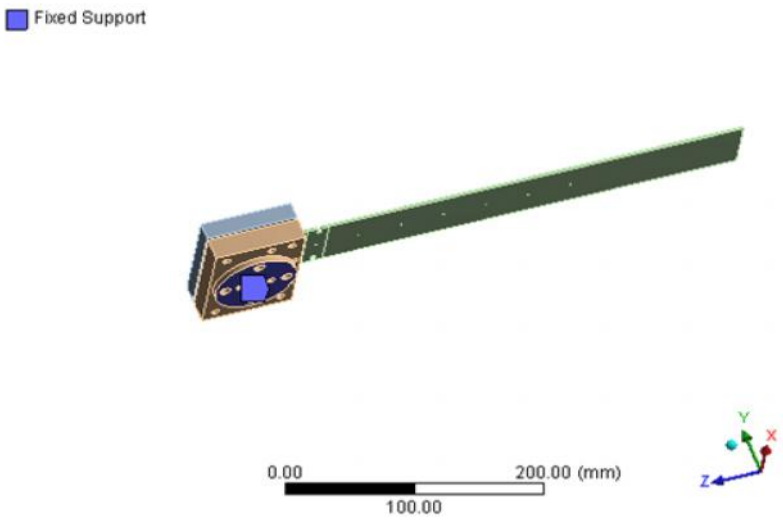

Figure 3.5 Fixed Boundary Condition for Cantilever Beam

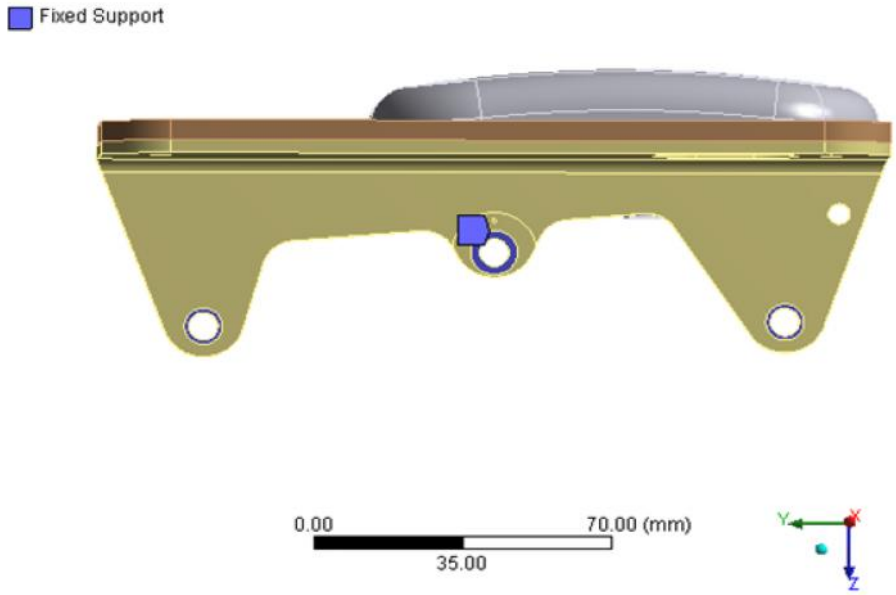

Figure 3.6 Fixed Boundary Condition for the Bracket

It is assumed that these models represent the real structure however; experimental analyses are needed for verification. Hence after numerical analyses are performed, experimental analyses that are given in Chapter 4 are carried out and results will be compared.

Since it is assumed that there is proportional damping associated with the structures, there is no need to use damping ratio for modal analyses. If the structure has proportional damping ratio, the mode shapes and natural frequencies do not change according to damping ratio therefore damping ratio is not a parameter for modal analysis.

PCG Lanczos solver is used for modal analyses. Modal analysis of the cantilever beam is performed up to 1500 Hz, which will be sufficient to determine the stress history in the range of 0-500 Hz, and it is assumed that modes higher than 1500 Hz do not have significant contribution to the stress history.

Moreover, it should be taken into account that experimental analyses will be performed using an accelerometer positioned on the structures.

Although accelerometer does not have a large mass, it may affect the natural frequencies of the structure because of the dynamic mass effect.

Hence, considering mass effect of the accelerometer, one more modal analysis is performed just for accurate comparison and verification of the finite element model of the structures versus manufactured models. Since, experimental analysis of cantilever beam will be performed the transverse direction of the cantilever beam (on the Direction of Y axis shown in Figure 3.13), only the bending modes due to this excitation direction are considered. These bending mode shapes (0-500 Hz range) for both without and with accelerometer configurations are shown in Figure 3.8 and Figure 3.9.

Similarly, since experimental analysis of Bracket will be performed for the Direction of X axis (Figure 3.21), bending mode shapes of Bracket are considered and they are shown in Figure 3.11 and Figure 3.12.

Also the locations of the accelerometers on the cantilever beam and Bracket are shown in Figure 3.7 and Figure 3.10 respectively.

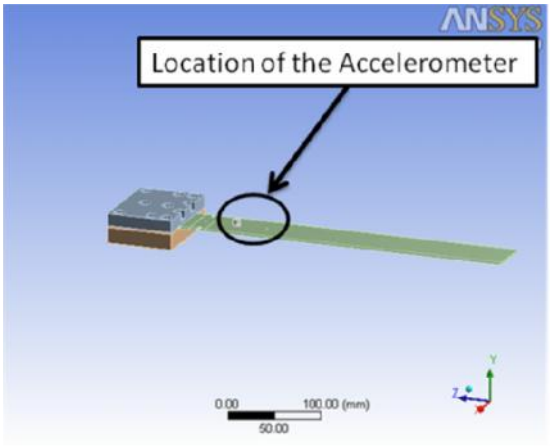

Figure 3.7 Location of the Accelerometer

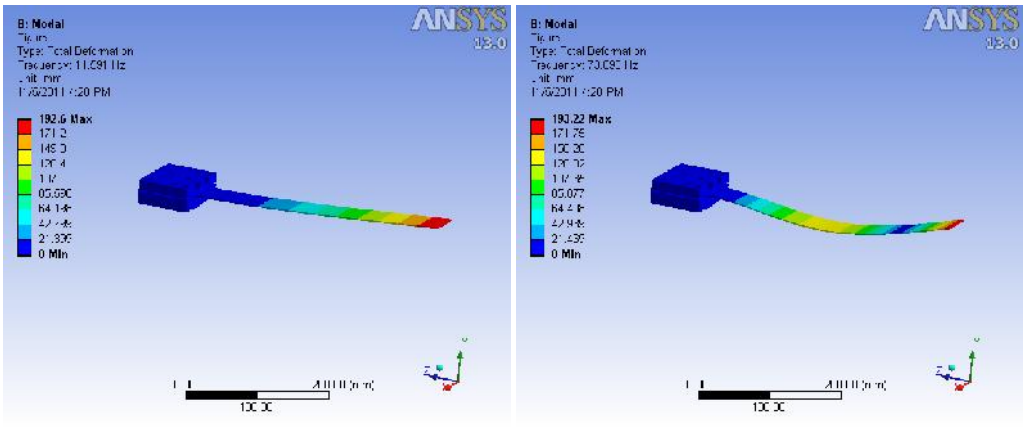

First Bending Mode, 11.591 HZ Second Bending Mode 72.098 Hz

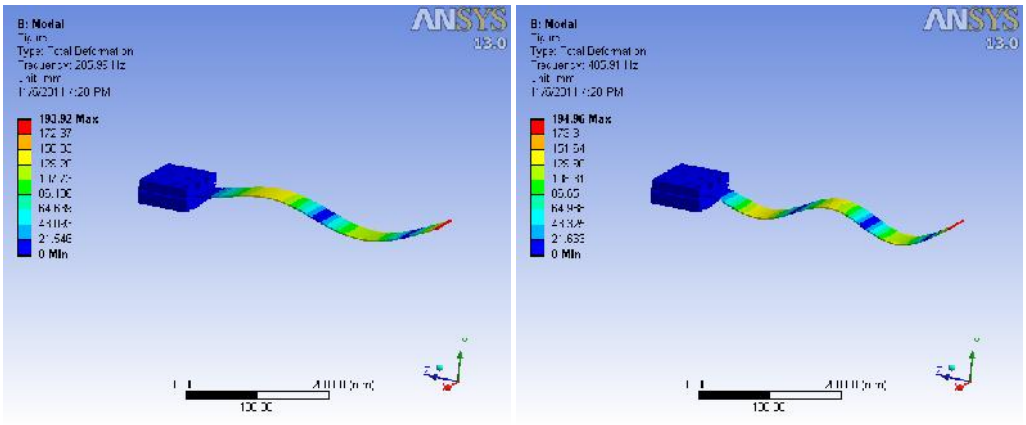

Third Bending Mode, 205.99 HZ Fourth Bending Mode, 405.91 HZ

Figure 3.8 First Four Bending Modes of the Cantilever Beam without Accelerometer

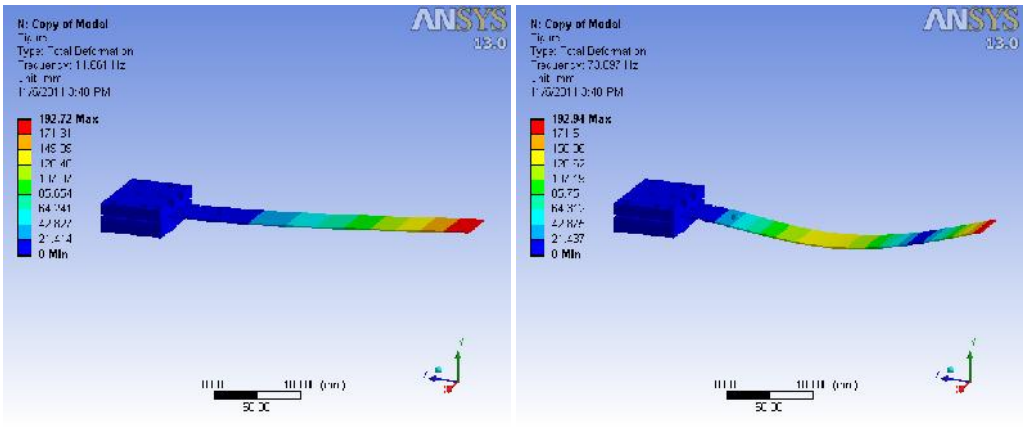

First Bending Mode, 11.661 HZ Second Bending Mode, 73.097 Hz

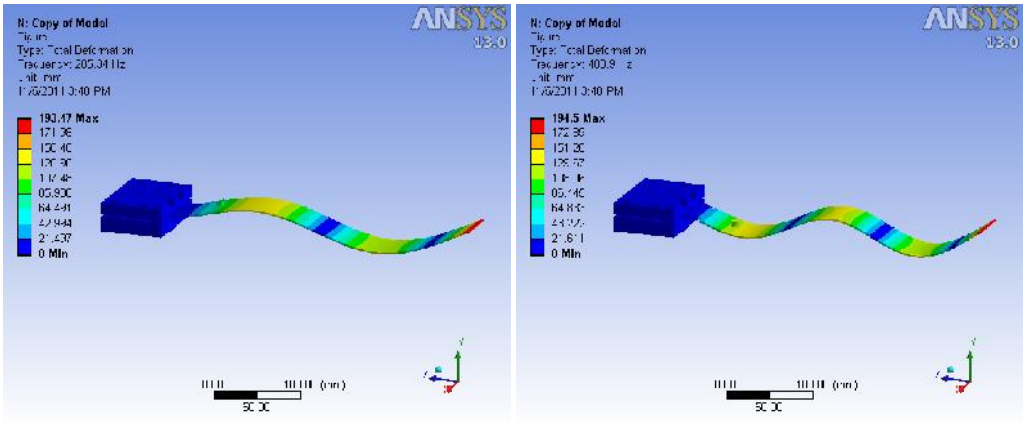

Third Bending Mode, 205.34 HZ Fourth Bending Mode, 403.9 HZ

Figure 3.9 First Four Bending Modes of the Cantilever Beam with Accelerometer

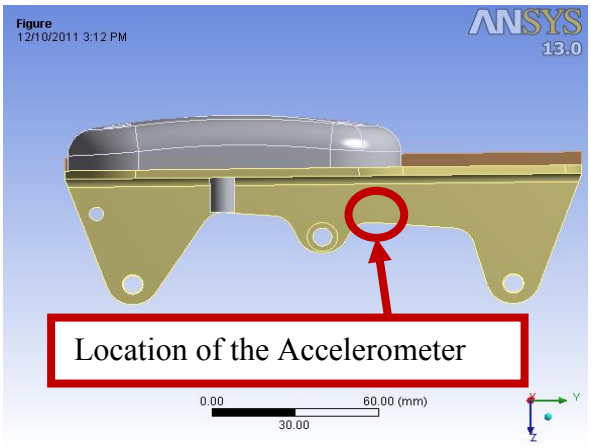

Figure 3.10 Location of the Accelerometer

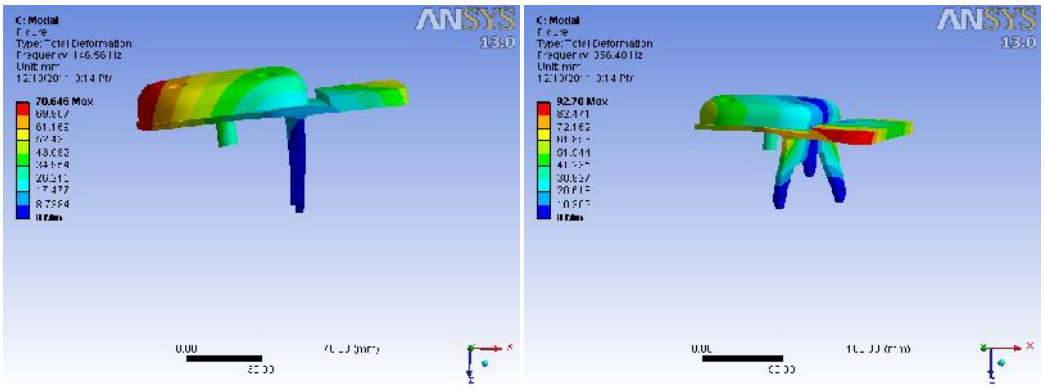

First Mode, 146.56 HZ Second Mode, 356.48 Hz

Figure 3.11 Mode Shapes of the Bracket without Accelerometer

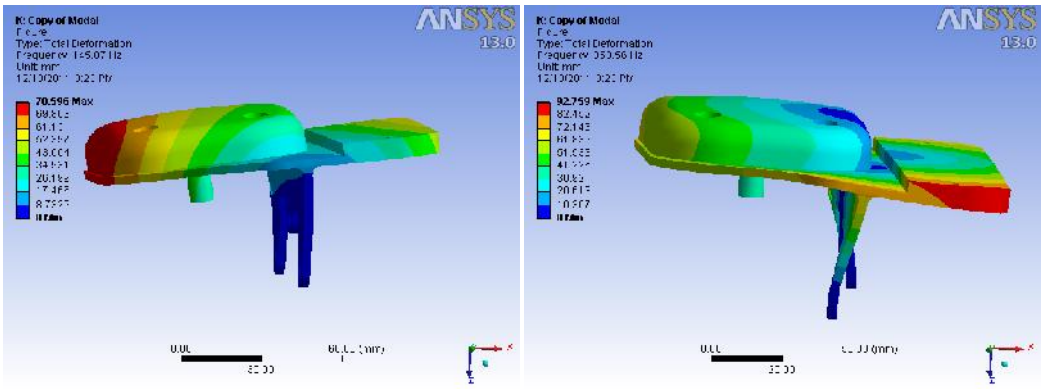

First Mode, 145.87 Hz Second Mode, 353.56 Hz

Figure 3.12 Mode Shapes of the Bracket with Accelerometer

The differences between with and without accelerometer natural frequencies of both cantilever beam and Bracket are listed in Table 3.4 and Table 3.5. Also, the modes and natural frequencies of the bracket and cantilever beam up to 1500 Hz are listed in Table 3.6 and Table 3.7, respectively. It should be noted that since the range of input is 0-500 Hz, while performing fatigue analyses the modes up to 500 Hz are used. However while calculating stress values for the range of 0-500 Hz, contributions of all modes up to 1500 Hz are considered.

Table 3.4 Difference Between with and without Accelerometer Natural Frequencies of the Cantilever Beam

Mode Number	Natural Frequency (Hz) (with accelerometer)	Natural Frequency (Hz) (without accelerometer)	Difference %
1	11.66	11.59	0.60
2	73.10	72.10	1.39
3	205.34	205.99	0.32
4	403.90	405.91	0.50

Table 3.5 Difference Between with and without Accelerometer Natural Frequencies of the Bracket

Mode Number	Natural Frequency (Hz) (with accelerometer)	Natural Frequency (Hz) (without accelerometer)	Difference %
1	145.87	146.56	0.47
2	353.56	356.48	0.82

Table 3.6 Natural Frequencies of Bracket Up to 1500 Hz

Mode Number	Natural Frequency (Hz) (without accelerometer)
1	146.56
2	356.48
3	800.59
4	1071.3
5	1478.5

Table 3.7 Natural Frequencies of Cantilever Beam Up to 1500 Hz

Mode Number	**Natural Frequency (Hz) (without accelerometer)**
1	11.59
2	72.1
3	166.85
4	205.99
5	254.53
6	405.91
7	505.76
8	675.31
9	860.15
10	1012.5
11	1238.6
12	1417.4

After modal analyses are carried out, in order to verify the finite element models with real structures, random vibration and harmonic analyses are performed. By performing random vibration analyses, acceleration and stress responses are obtained and harmonic analysis is performed in order to get FRF for cantilever beam.

3.2 Random Vibration Analysis for Cantilever Beam and Bracket

For all cantilever beam random vibration analyses, the direction of base excitation is Y axis as shown in Figure 3.13. In order to get acceleration response PSD of transverse (Y axis) direction (Figure 3.14), random vibration analysis is performed for the base excitation PSD input given in Figure 3.15.

Random vibration analysis is performed for the 5-500 Hz frequency range and measured damping ratios given in Table 4.4 are used as input to ANSYS.

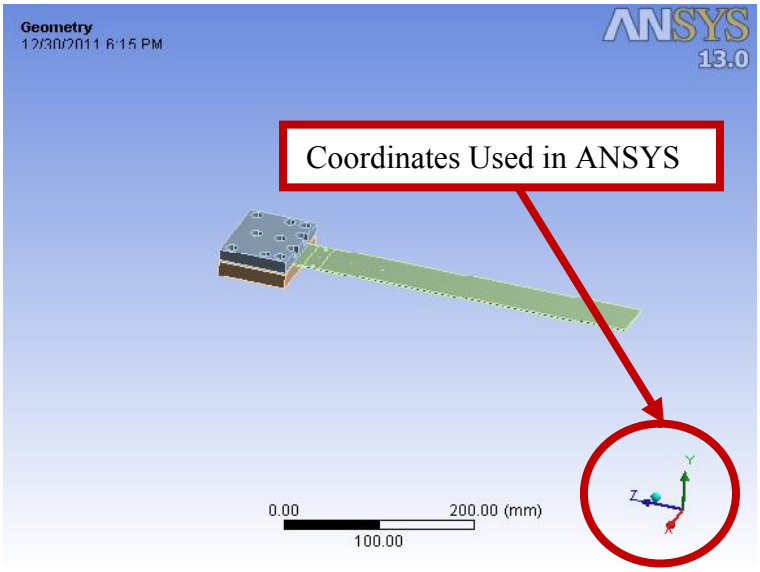

Figure 3.13 Coordinates Used in ANSYS

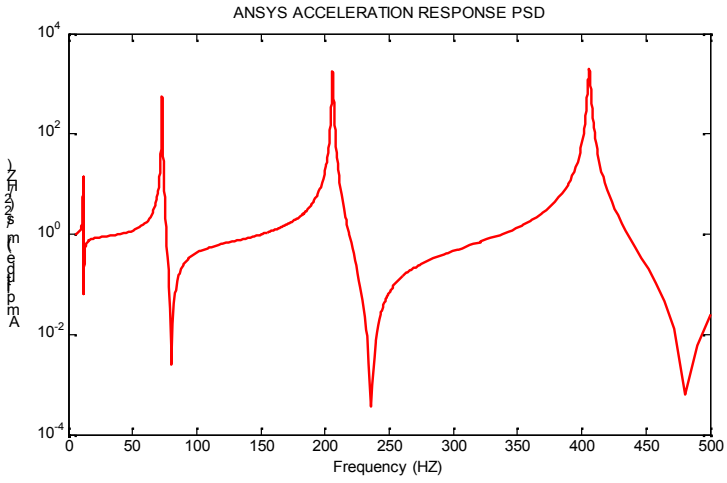

Figure 3.14 ANSYS Acceleration PSD Result for 0.01 g^2/Hz White Noise PSD Input (Cantilever Beam)

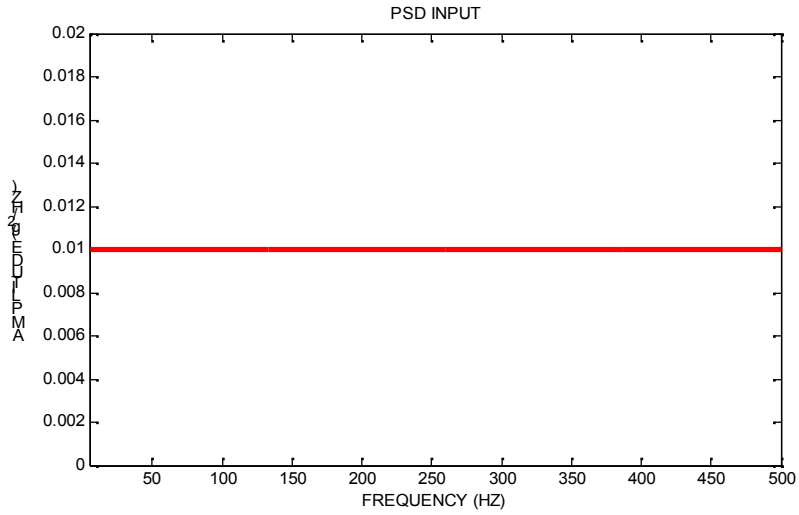

Figure 3.15 0.01 g^2/Hz Amplitude White Noise PSD

Then, in order to get normal Z stress PSD (Figure 3.16), another random vibration analysis is performed for base excitation PSD input given in Figure 3.17.

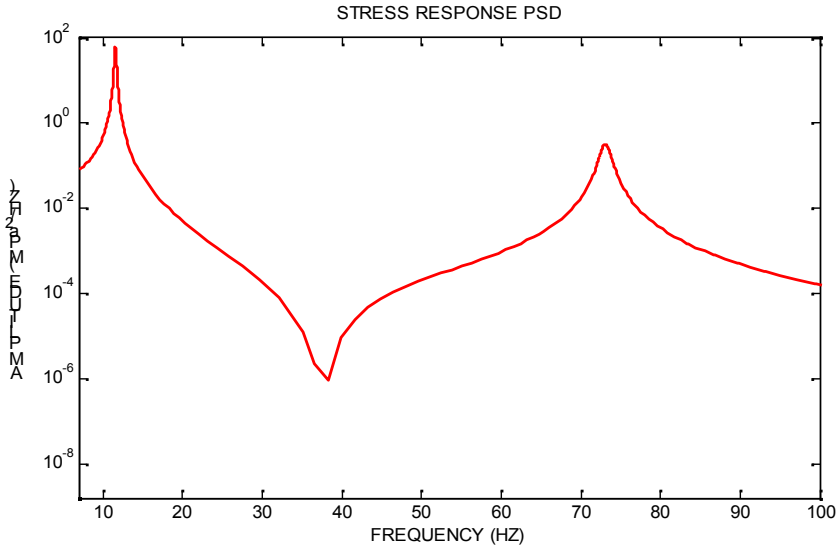

Figure 3.16 ANSYS Stress PSD Result for 0.001 g^2/Hz White Noise PSD Input (Cantilever Beam)

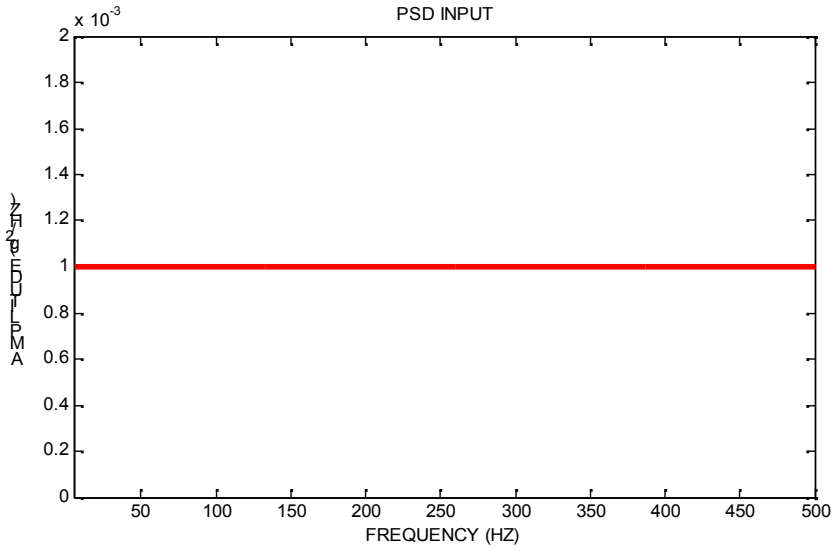

Figure 3.17 0.001 g^2/Hz Amplitude White Noise PSD

The locations of the points from where acceleration and stress response PSD's are obtained for cantilever beam are given in Figure 3.18.

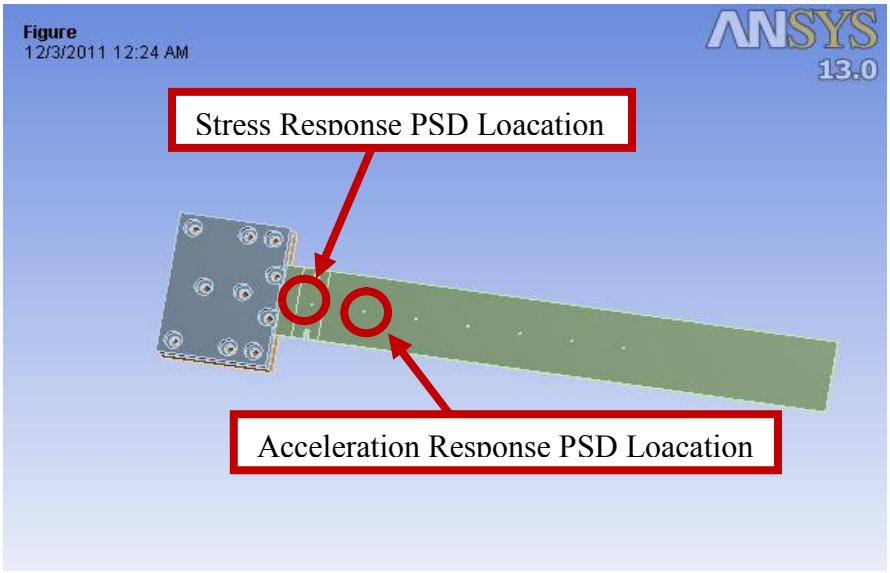

Figure 3.18 The Locations from where Acceleration and Stress Response PSD's are Obtained

In order to verify the normal Z stress response PSD's of the Bracket for given output location, random analyses are performed for base excitation (on the Direction of X axis) with PSD inputs given in Figure 3.15 and Figure 3.17. Random vibration analyses are performed for the 5-500 Hz frequency range and measured damping ratios given in Table 4.6 are used as input to ANSYS. These identified stress response PSD results are shown in Figure 3.19 and Figure 3.20. The coordinates used in ANSYS for Bracket is given in Figure 3.21.

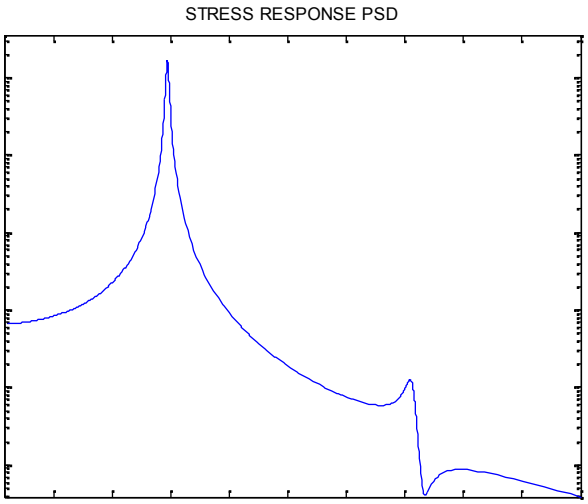

Figure 3.19 ANSYS Stress PSD Result for 0.001 g^2/Hz White Noise PSD Input (Bracket)

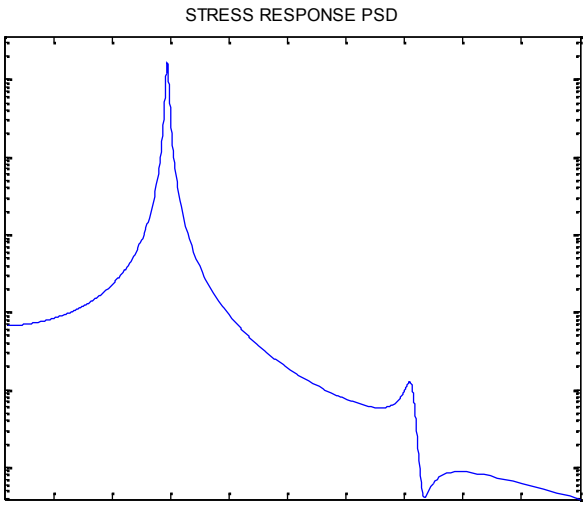

Figure 3.20 ANSYS Stress PSD Result for 0.01 g^2/Hz White Noise PSD Input (Bracket)

The location of the point from where stress response PSD's are obtained on the Bracket is given in Figure 3.21.

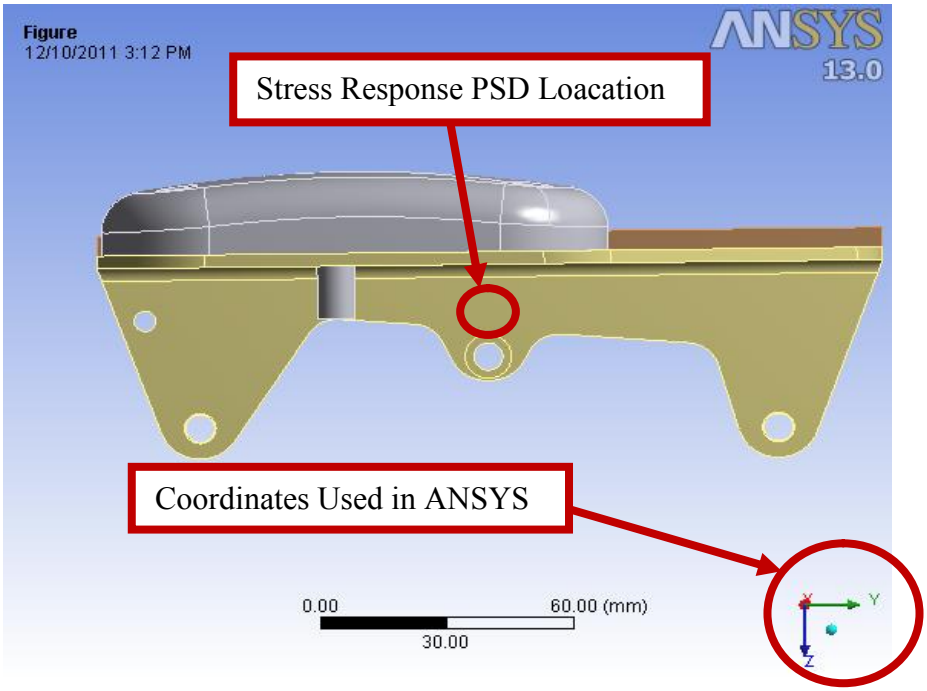

Figure 3.21 The Locations from where Stress Response PSD's are Obtained

3.3 Harmonic Analysis of Cantilever Beam and Bracket

In order to obtain FRF of cantilever beam for indicated force and output locations in Figure 3.22, a harmonic analysis is performed and the cross FRF shown in Figure 3.23 is obtained. 1 N Force is applied to cantilever beam on the Direction of Y axis for 5-500 Hz frequency range and measured values given in Table 4.4 are used as damping ratios in ANSYS.

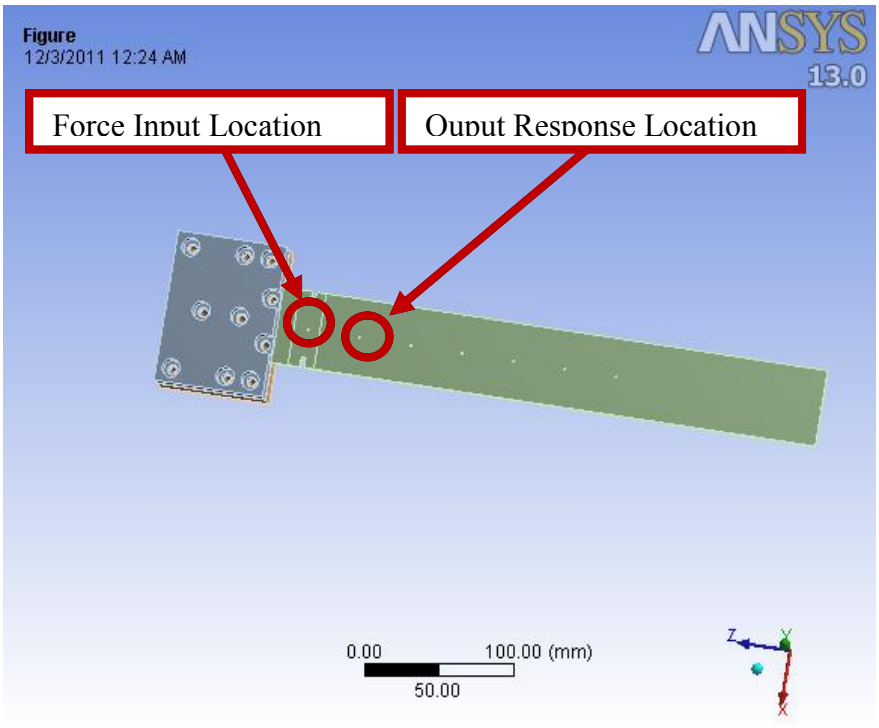

Figure 3.22 Input and Output Locations for the Frequency Response Function of Cantilever Beam

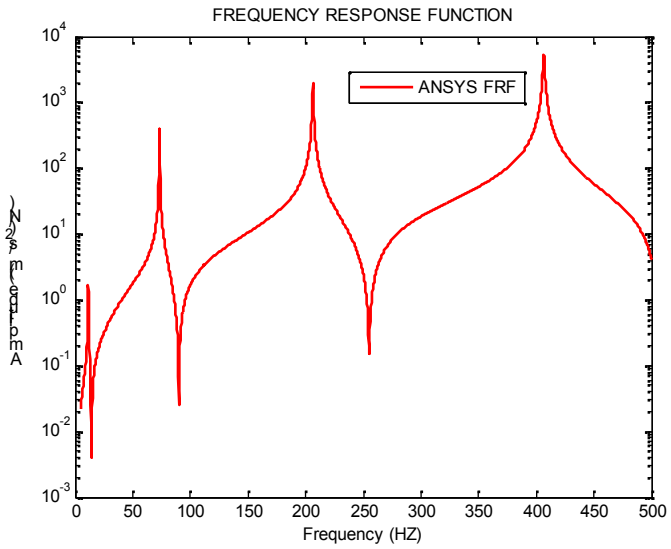

Figure 3.23 Cross FRF for the Cantilever Beam

All analyses performed up until now will be used for verification of finite element models of cantilever beam and Bracket with experiment results that are obtained using real structures. The detailed information about verification will be given in Chapter 4. However, in order to perform a fatigue analysis, harmonic analysis with unit amplitude (9810 mm/s^2, unit g) sinusoidal wave acceleration input is needed. Frequency range of the harmonic analysis is defined as 0-500 Hz for both cantilever beam and Bracket. The stress results in this range are found by using modes up to 1500 Hz calculated in modal analysis (Mode Superposition method). As mentioned above fatigue analysis of cantilever beam will be performed for PSD input in the transverse direction of the cantilever beam (on the Direction of Y axis shown in Figure 3.13). Hence, performing one harmonic analysis that has unit g amplitude on the Direction of Y axis (Figure 3.13) is enough for getting the needed stress history. However, fatigue analysis of Bracket will be performed for each axis of Bracket. Therefore, three harmonic analyses are performed in order to obtain stress histories of the most critical nodes on each axis. According to harmonic analyses results it is observed that, for cantilever there is one critical node and for Bracket there are three critical nodes. The detailed information for selecting the critical nodes is given Appendix C.

The locations of the most critical points of the cantilever beam and Bracket are given in Figure 3.24 and Figure 3.25 respectively.

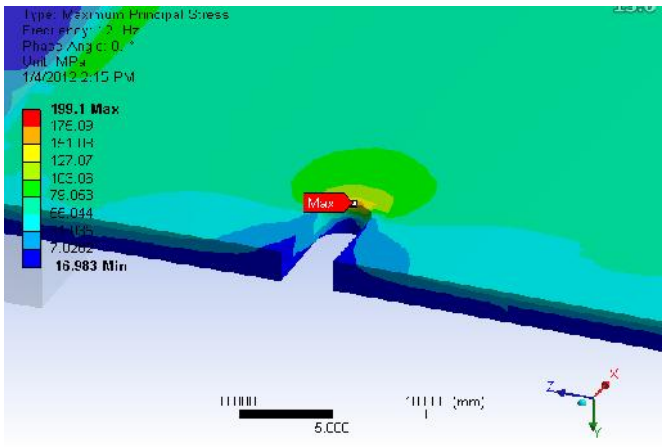

Figure 3.24 Most Critical Location of Cantilever Beam

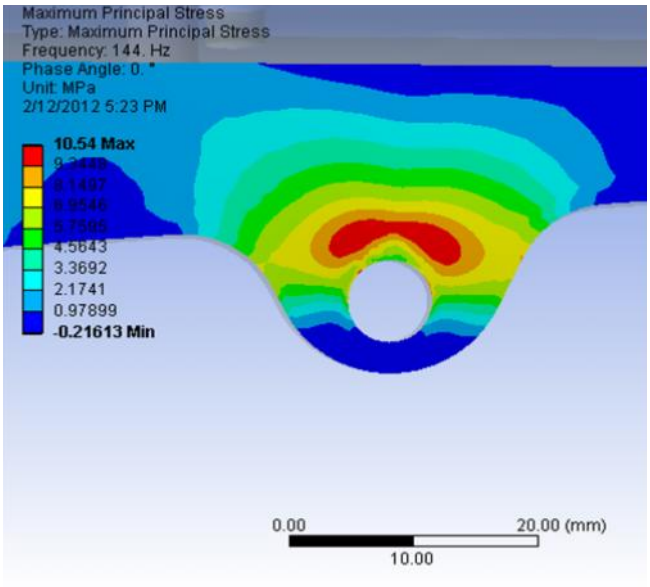

Figure 3.25 Most Critical Locations of Bracket

After the most critical nodes are identified, the transfer functions for the maximum and the minimum principal stress histories of these nodes of both structures are obtained and will be used while deriving the transfer function that is used in order to find stress PSD.

CHAPTER 4

EXPERIMENTAL ANALYSIS OF STRUCTURES AND VERIFICATION OF FINITE ELEMENT MODELS

After final geometry of the cantilever beam and fixture components are obtained, they are manufactured according to 3D CAD models. The beam is manufactured from standard sheet metal in order to avoid the problems that may possibly be caused by manufacturing. Also the radius and the surface of the notches are manufactured carefully and smoothly in order to keep up with the CAD model for determination of the fatigue life accurately. The manufactured beam and shaker fixture are shown in Figure 4.1.

Figure 4.1 Manufactured Beam and Shaker Fixture

Bracket was manufactured before performing fatigue analysis therefore shaker fixture components are designed and manufactured according to 3D CAD model. Bracket and shaker fixture components are shown in Figure 4.2.

Figure 4.2 Manufactured Bracket and Shaker Fixture

While performing vibration tests for verification of finite element model, several tools are needed, such as a force transducer, an accelerometer, data acquisition system and signal processing software. The properties of used instruments and software are given in Table 4.1.Transducer properties are given in Table 4.2.

Table 4.1 Software and Instrumentation of Vibration Setup

Instrumentation and Software	
Accelerometer	Bruel & Kjaer 4507 biax PCB 356A01
Impact Hummer	Bruel & Kjaer 8200+2646
Analyzer	Pulse Front-End 3560C
Software	Pulse 11.0

Table 4.2 Transducer Properties

Transducer Type	**Nom. Sensitivity**	**External Gain**	**Input Sensitivity**
Force	1 mV/N	1 V/V	1 mV/N
Accelerometer	10 mV/m/s^2	1 V/V	10 mV/m/s^2

Moreover, strain gage tests are performed for verification of finite element model. The properties of data acquisition system and strain gage used in experiments are given in Table 4.3.

Table 4.3 Properties of Data Acquisition System and Strain Gage Used in Experiments

Data Aquisition	Dewtron Dewe-501
Strain Gage Model	HBM k-ly4-1-07-120-0

4.1 Experimental Analysis of Cantilever Beam for Verification

In order to verify the finite element model, three different tests are performed. The first test is impact hammer test in order to get cross FRF shown in Figure 3.23 experimentally. The locations of the input and output points for cross FRF are shown in Figure 4.3 and the cross FRF is shown in Figure 4.4.

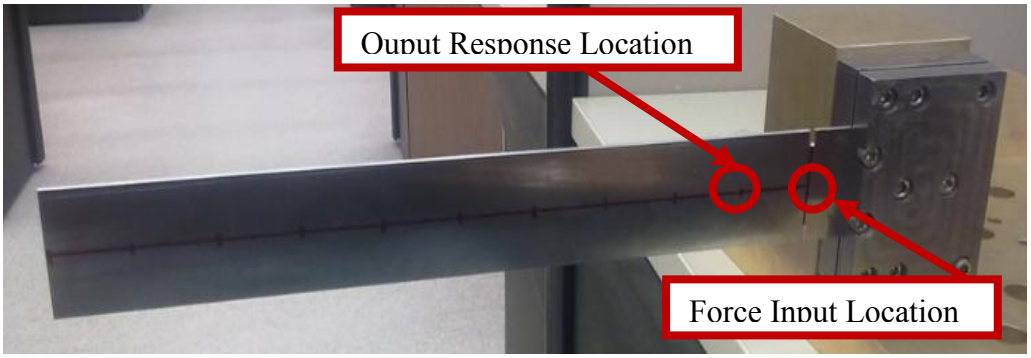

Figure 4.3 Input and Output Locations for the Frequency Response Function

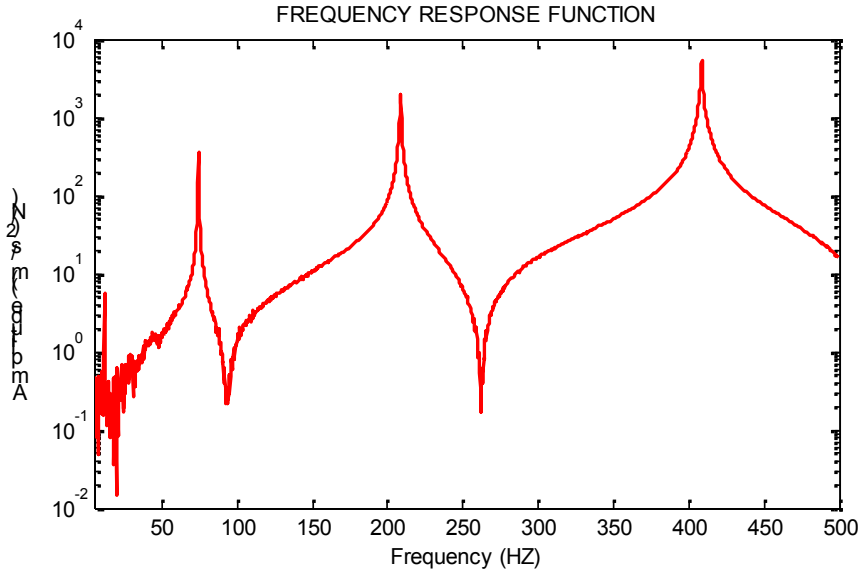

Figure 4.4 Experimental Cross FRF for the Cantilever Beam

The other two tests are performed by the vibration test equipment shown in Figure 4.5. The second test is performed by giving a white noise PSD shown in Figure 3.15 to electromagnetic vibration shaker and obtaining the output PSD (Figure 4.7) by accelerometer located on beam shown in Figure 4.6.

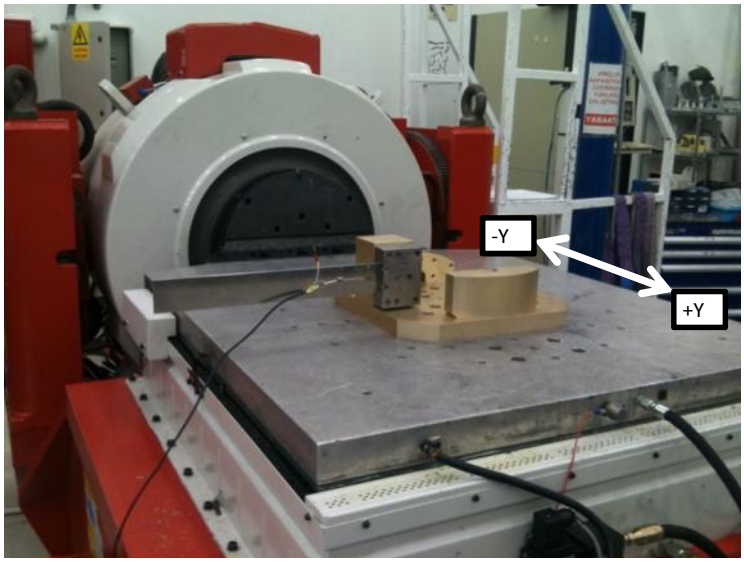

Figure 4.5 A View of Electromagnetic Vibration Test Equipment

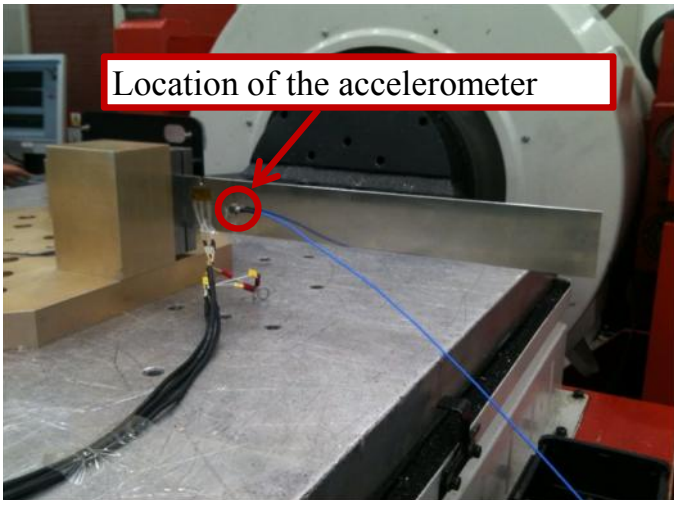

Figure 4.6 Location of Accelerometer

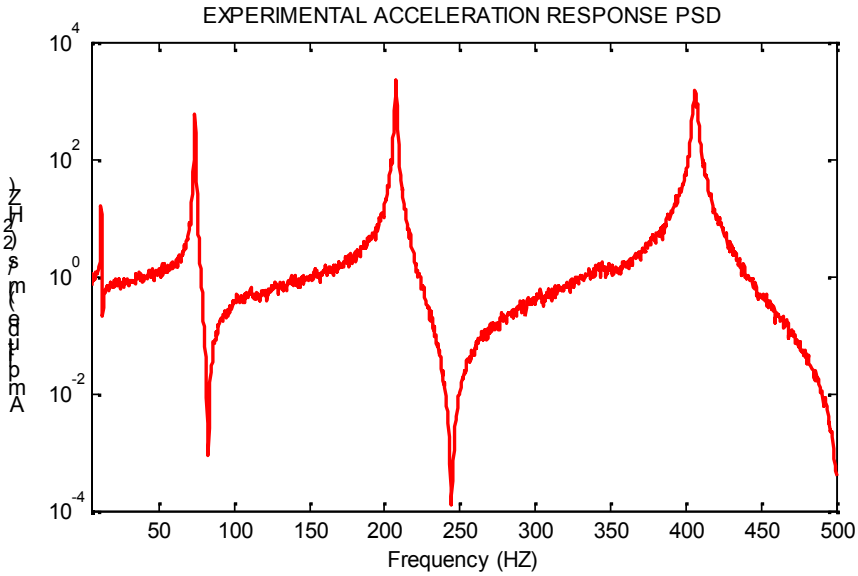

Figure 4.7 Experimental Acceleration Response PSD Result for 0.01 g^2/Hz White Noise PSD Input

The third test is performed by giving the white noise PSD shown in Figure 3.17 to electromagnetic vibration shaker and getting the output strain data by uniaxial strain gage located on beam shown in Figure 4.8.

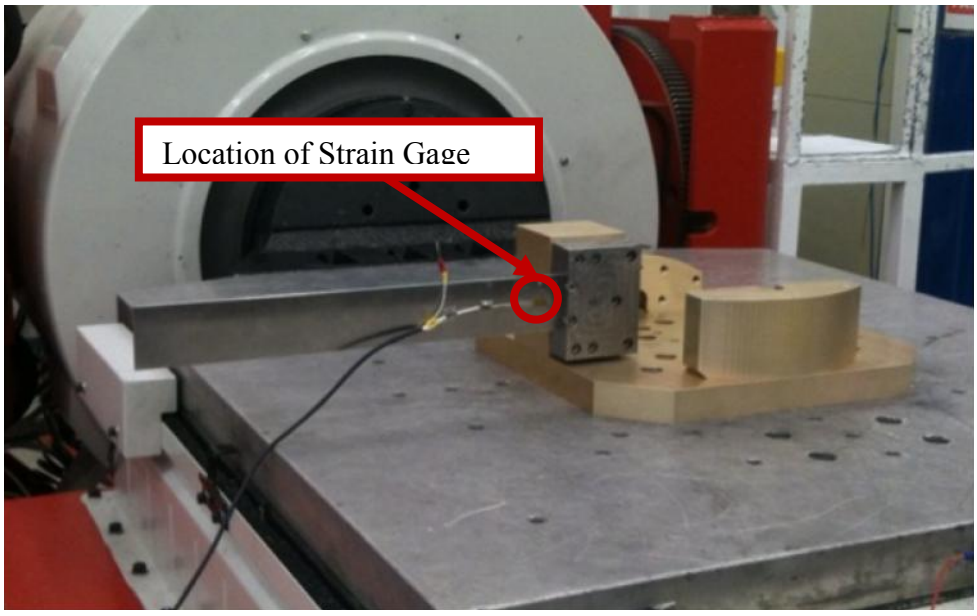

Figure 4.8 Location of Strain Gage

Sampling frequency is chosen to be 200 Hz. The strain-time data is collected and it is converted to stress-time data by multiplying the obtained strain with E (Modulus of Elasticity) of the cantilever. The duration of the collected stress data shown in Figure 4.9 is 60 seconds. In order to compare experimental stress results with FEA stress results, the data is transformed from time domain to frequency domain by using Pwelch method. Since the sampling frequency is 200 Hz, PSD is obtained up to 100 Hz due to Nyquist frequency. The resolution of the PSD is chosen as 0.3125 Hz. The obtained PSD data is shown in Figure 4.10.

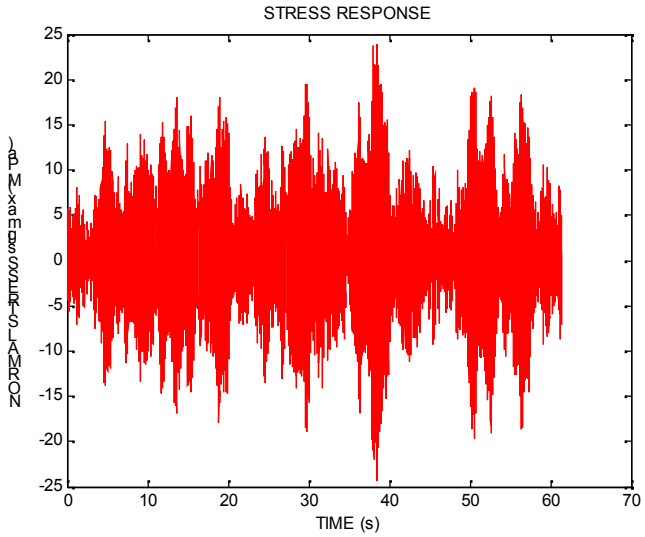

Figure 4.9 Collected Stress Data for 0.001 g^2/Hz White Noise PSD Input

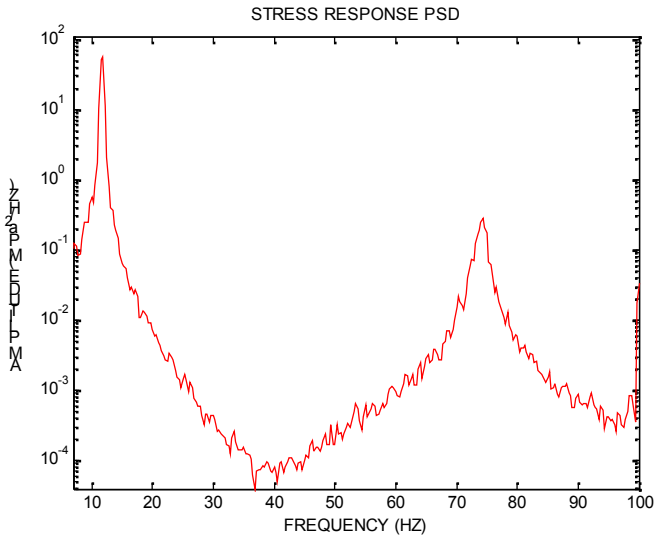

Figure 4.10 Collected Stress PSD Result for 0.001 g^2/Hz White Noise PSD Input

Analyzing the collected FRF data given in Figure 4.4 and acceleration response data given in Figure 4.7, it is clearly seen that there are four bending modes of the cantilever beam up to 500 Hz. Also from the indicated FRF data, natural frequencies and damping ratios are obtained (Table 4.4).

Table 4.4 Natural Frequencies and Damping Ratios Obtained from FRF Tests

Mode	Natural	Damping
1	11.75	1.0
2	74.5	0.3
3	209	0.2
4	409.5	0.1

4.1.1 Verification of Finite Element Model of Cantilever Beam

Natural frequencies, obtained from finite element analysis and experiment, are compared in Table 4.5.

Table 4.5 Comparison of the Experimental and ANSYS Natural Frequencies

Mode Number	Natural Frequency ANSYS (Hz)	Natural Frequency Experiment (Hz)	Difference %
1	11.66	11.75	0.76
2	73.10	74.50	1.88
3	205.34	209.00	1.75
4	403.90	409.50	1.37

It can be easily observed that natural frequencies are very close to each other. This means that finite element model of the structure is accurately constructed, however; comparing the natural frequencies is not enough for the verification of finite element model alone. Hence acceleration FRF and acceleration and stress response PSD results are compared as shown in Figure 4.11 to and Figure 4.13.

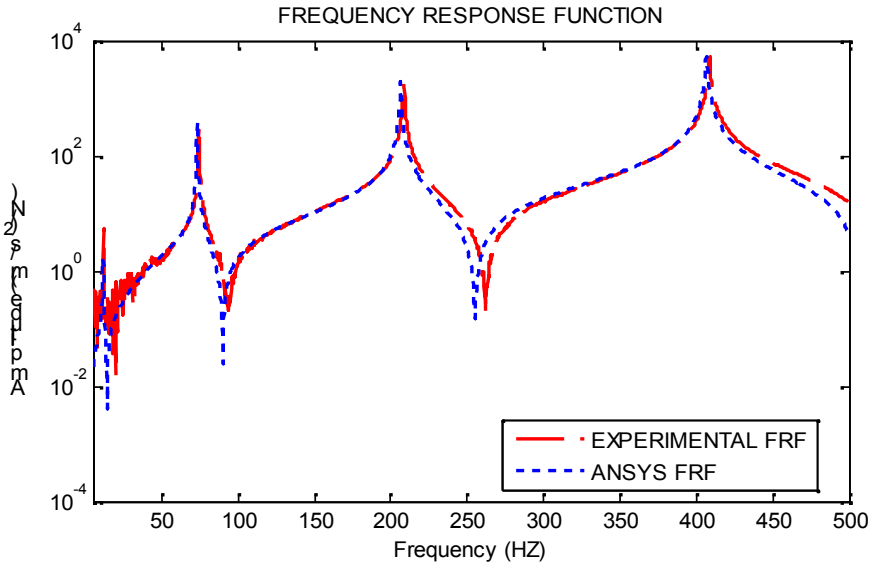

Figure 4.11 Acceleration FRF Comparison

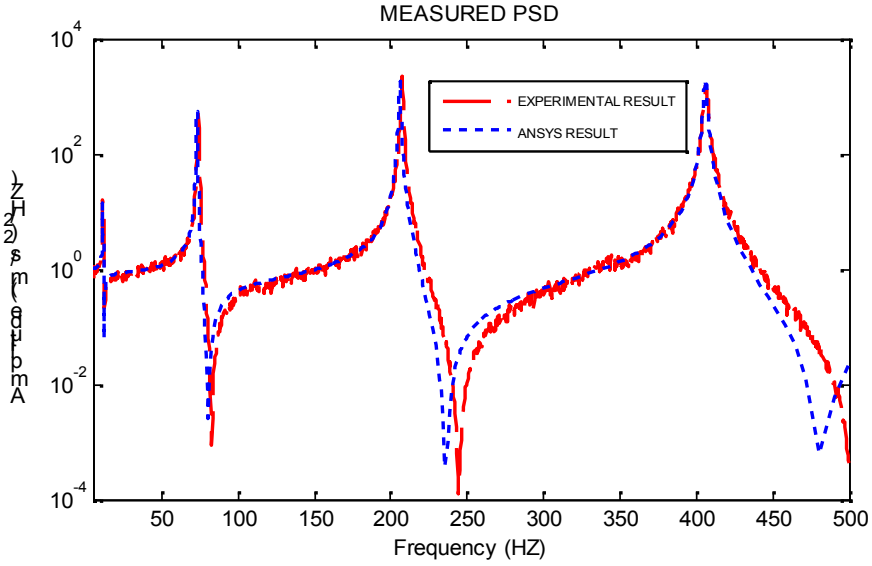

Figure 4.12 Acceleration Response PSD Comparison for 0.01 g^2/Hz White Noise PSD Input

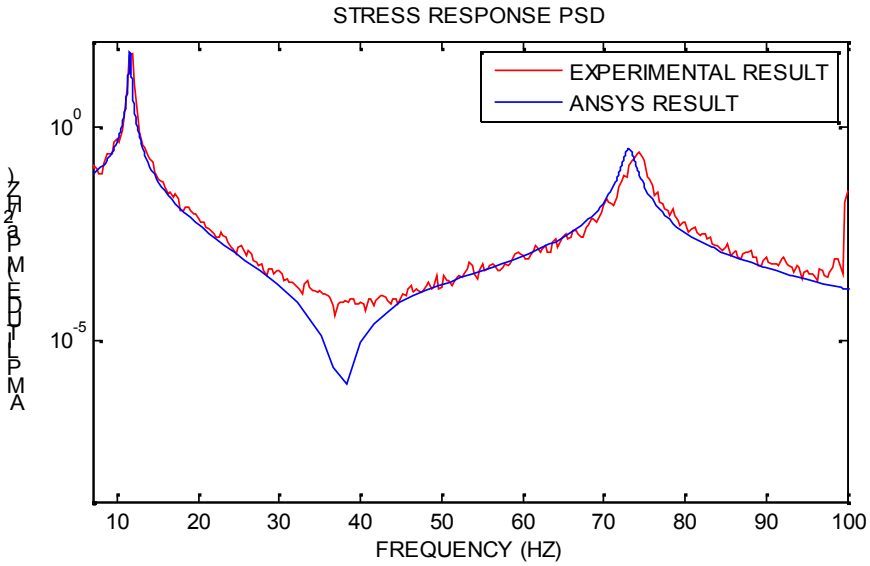

Figure 4.13 Stress Response PSD Comparison for 0.001 g^2/Hz White Noise PSD Input

As mentioned above if a structure has a proportional damping ratio, damping doesn't affect the natural frequencies. When the natural frequencies are compared it can be easily observed that the behavior of the finite element model is very close to that of the real structure. Also it can be recognized by observing acceleration FRF comparison, acceleration response PSD comparison and stress response PSD comparison. From the comparison of experimental and FEM results, it can be concluded that the real structure can be accurately represented by the FEM. The damping ratios for each mode are obtained from acceleration FRF results and fatigue analysis will be performed using these obtained real damping ratios.

In conclusion the finite element model is verified with real structure and can be used for harmonic analysis in order to predict fatigue life of the structure.

4.2 Experimental Analysis of Bracket for Verification

In order to verify the finite element model of Bracket, two different tests are performed. The tests are performed by using the vibration test equipment indicated in Figure 4.5.

The first test is performed by giving a white noise PSD shown in Figure 3.17 to electromagnetic vibration shaker and obtaining the output PSD (Figure 4.15) by accelerometer located on Bracket shown in Figure 4.14. Then, transmissibility is obtained from acceleration response PSD and it is shown in Figure 4.16.

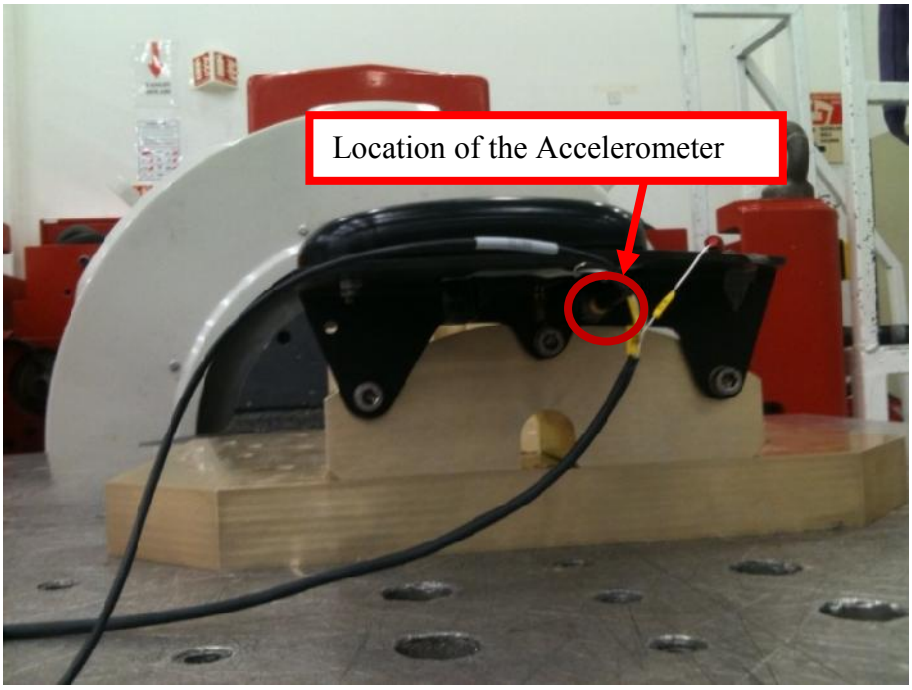

Figure 4.14 Location of the Accelerometer

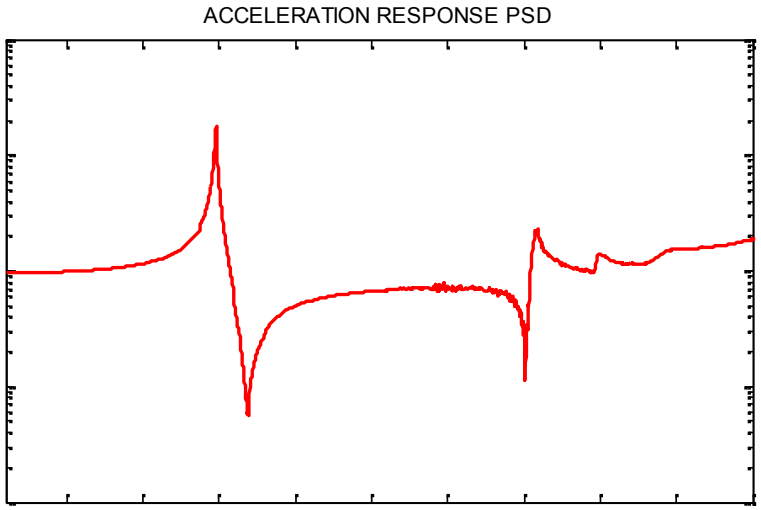

Figure 4.15 Experimental Acceleration Response PSD Result for 0.001 g^2/Hz White Noise PSD Input

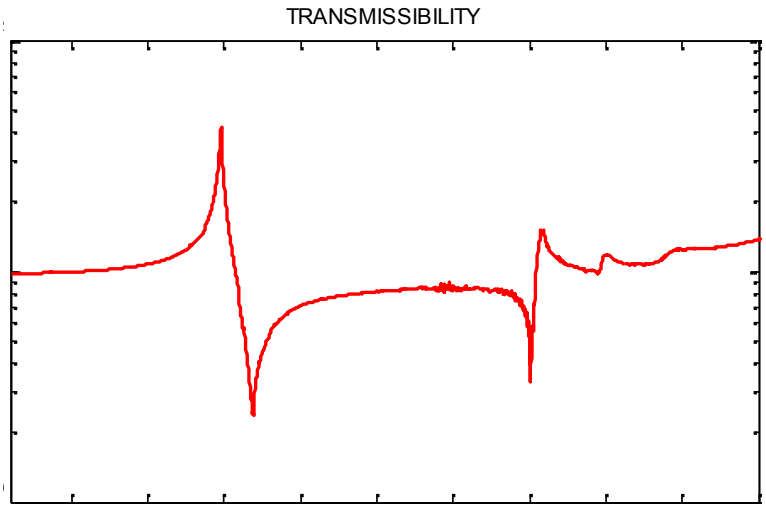

Figure 4.16 Transmissibility of the Bracket

The second test is performed by giving the white noise PSD shown in Figure 3.15 and Figure 3.17 to electromagnetic vibration shaker and obtaining the output stress data by using uniaxial strain gage located on Bracket shown in Figure 4.17

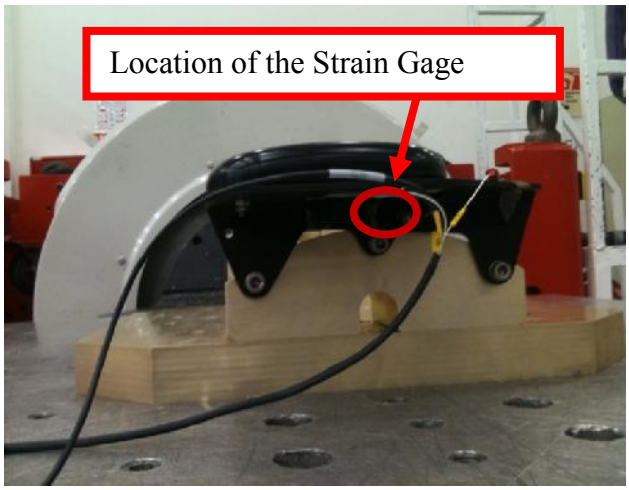

Figure 4.17 Location of the Strain Gage

Sampling frequency is chosen to be 1000 Hz. The strain-time data is collected and it is converted to stress-time data by multiplying the obtained strain with E (Modulus of Elasticity) of the Bracket. The duration of the collected stress data shown in Figure 4.18 is 45 seconds and the duration of collected stress data shown in Figure 4.19.is 32 seconds.

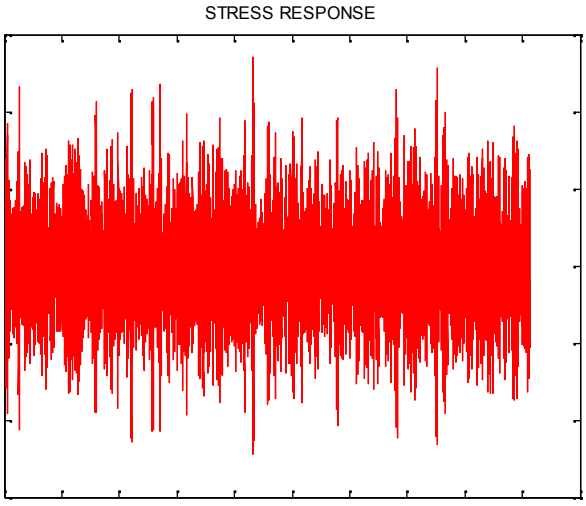

Figure 4.18 Collected Stress Data for 0.001 g^2/Hz White Noise PSD Input

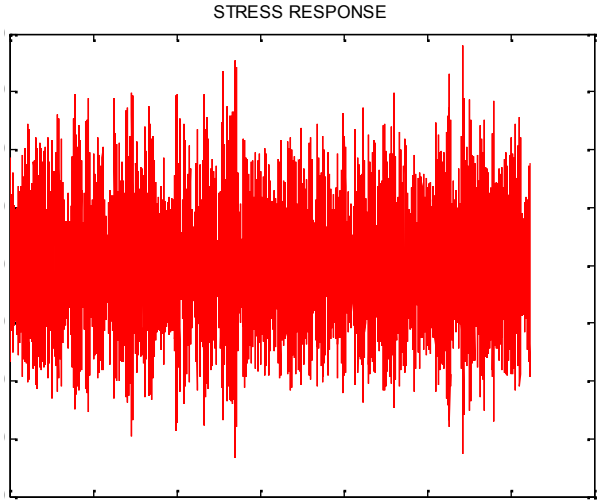

Figure 4.19 Collected Stress Data for 0.01 g^2/Hz White Noise PSD Input

In order to compare experimental stress results with FEA stress results, the data is transformed from time domain to frequency domain by using Pwelch method. Since the sampling frequency is 1000 Hz, PSD is obtained up to 500 Hz due to Nyquist frequency. The resolution of the PSD is chosen as 0.3125 Hz. Each obtained PSD data is shown in Figure 4.20 and Figure 4.21.

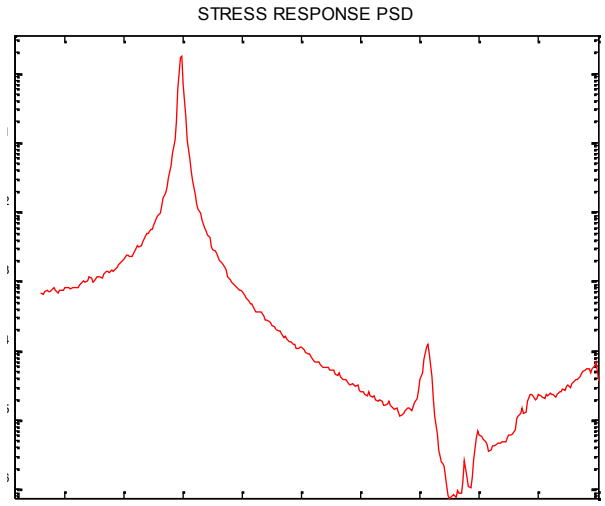

Figure 4.20 Collected Stress PSD Result for 0.001 g^2/Hz White Noise PSD Input

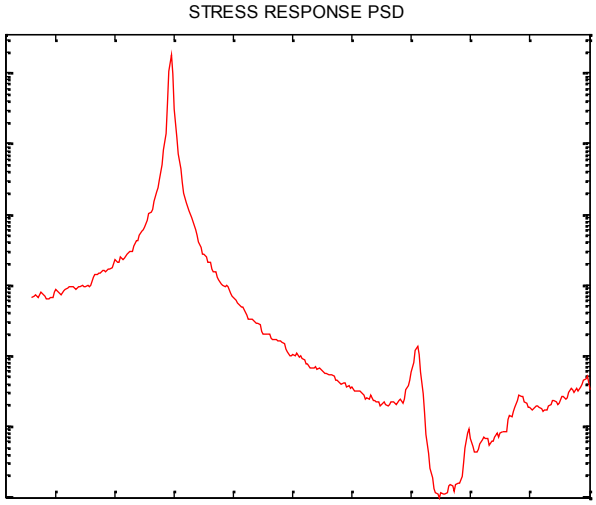

Figure 4.21 Collected Stress PSD Result for 0.01 g^2/Hz White Noise PSD Input

In addition to strain gage tests that are performed for verification of finite element model, another strain gage test is performed by giving the real PSD loading that is obtained from flight tests of air platform (Figure 4.27) to electromagnetic vibration shaker and getting the output stress data by using the same uniaxial strain gage located on Bracket shown in Figure 4.17. Sampling frequency is again chosen to be 1000 Hz. The duration of the collected stress data shown in Figure 4.22 is 90 seconds.

The reason of performing this strain gage experiment is to make a comparison of fatigue life results obtained in time and frequency domains. Hence, the data is transformed from time domain to frequency domain by using Pwelch method with the same parameters that were used in the derivation of Figure 4.20 and Figure 4.21. The obtained stress PSD is shown in Figure 4.23.

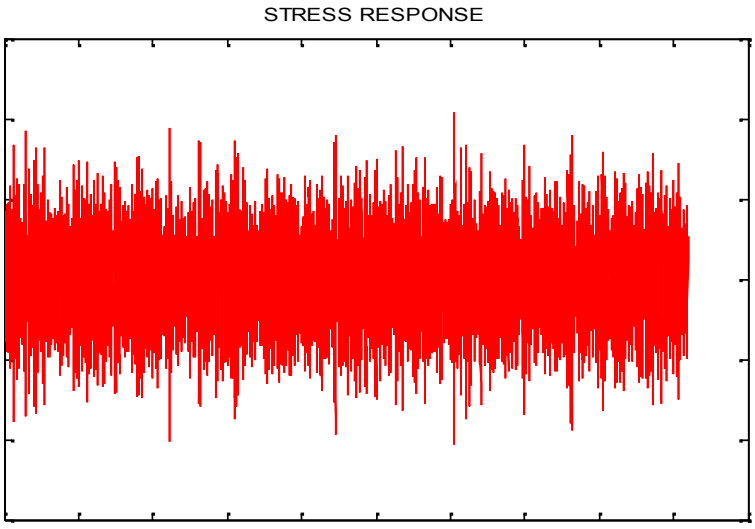

Figure 4.22 Collected Stress Data for Obtained Real PSD Input

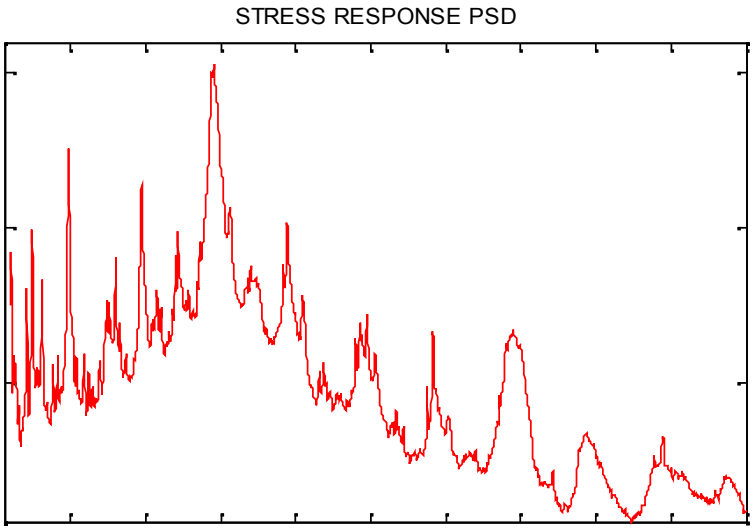

Figure 4.23 Collected Stress PSD Result for obtained real PSD Input Shown in Figure 4.27

From transmissibility function that is given in Figure 4.16, it is clearly seen that there are two modes of the Bracket up to 500 Hz. From the collected data, natural frequencies and damping ratios are obtained which are given in Table 4.6.

Table 4.6 Natural Frequencies and Damping Ratios Obtained from Transmissibility Function

Mode Number	Experimental Natural Frequency Hz	Damping Ratio %
1	147.8	1
2	357.3	1.25

4.2.1 Verification of Finite Element Model of Bracket

Firstly, natural frequencies, obtained from finite element analysis and experiment, are compared in Table 4.7.

Table 4.7 Comparison of the Experimental and ANSYS Natural Frequencies

Mode Number	Natural Frequency ANSYS (Hz)	Natural Frequency Experiment (Hz)	Difference %
1	145.87	147.80	1.31
2	353.56	357.30	1.05

It can be easily observed that natural frequencies obtained from finite element software have around 1% error which does not constitute a significant difference. This means that finite element model is accurate; however, comparing the natural frequency is not enough for verification of finite element model alone as discussed before. Hence, stress response PSD results are compared as shown in Figure 4.24 and Figure 4.25.

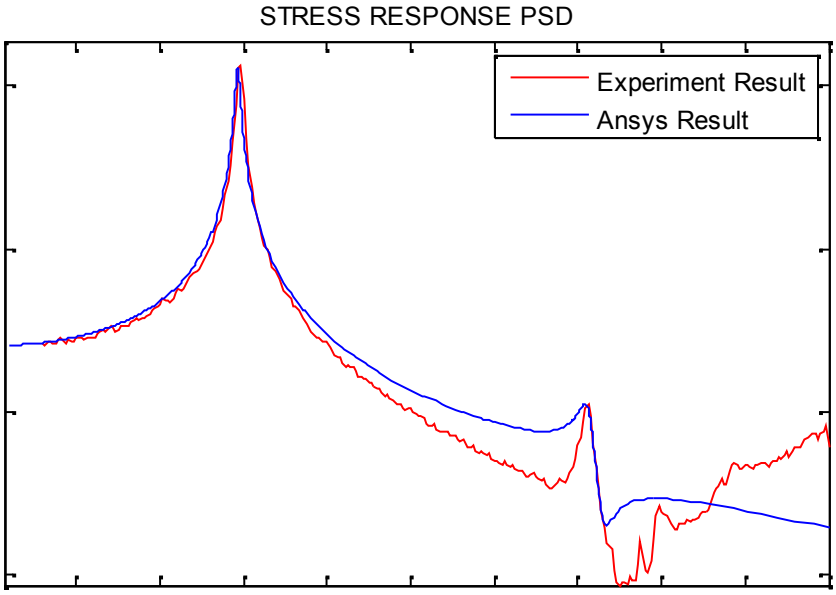

Figure 4.24 Stress Response PSD Result Comparison for 0.001 g^2/Hz White Noise PSD Input

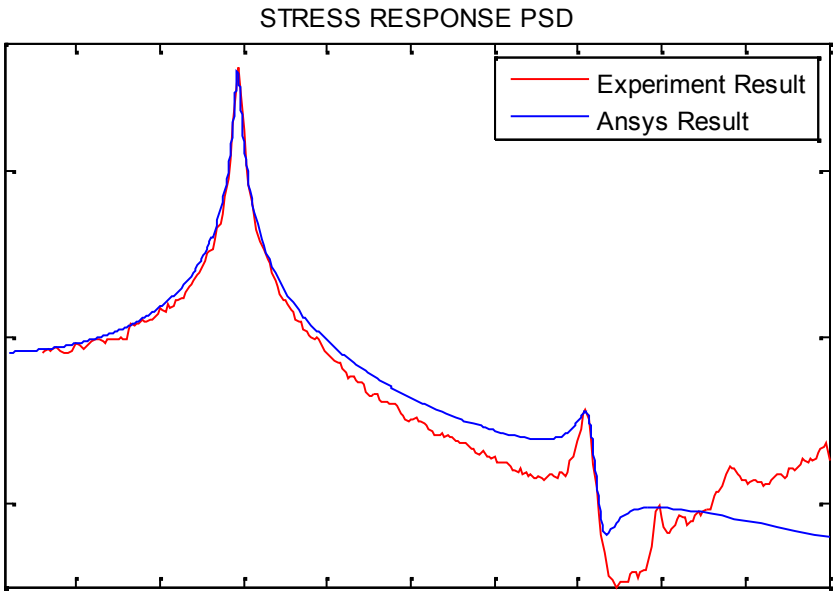

Figure 4.25 Stress Response PSD Result Comparison for 0.01 g^2/Hz White Noise PSD Input

When all the results are taken into consideration, it can be concluded the results are close to each other around the natural frequency in wide frequency range and a narrow frequency range around the second natural frequency differing with an insignificant margin.

The damping ratios for each mode are obtained from the transmissibility function result given in Figure 4.16 and fatigue analysis will be performed using these obtained real damping ratios.

4.3 Analysis of Loading That is Applied to Bracket

As mentioned above, stress histories are needed to perform a fatigue analysis. In order to get the stress information the structure can be tested with strain gages. However, before failure occurs, the critical locations on the structure couldn't generally be observed. Hence, knowing where to locate strain gages is not strictly possible. Also strain gage test results depend on geometry of the structure hence; if geometry is changed, tests should be repeated. In order to overcome such an inconvenience, finite element analyses are performed for obtaining stress histories for the most critical location of the structure.

Then, it becomes possible to calculate fatigue life. However, in such a case accurate loading information that the structure is subjected to is required.

Once the load information is obtained, since loading information doesn't depend on geometry and small changes, there is no need to repeat tests during design iterations.

As a result, if one has the finite element model of the structure and the loading information; fatigue life of the structure can easily be calculated using stress histories obtained from the finite element analysis. However, it is known that small changes in loading may result in large changes in the stress results hence that may lead to inaccurate fatigue life prediction of the structures.

This situation can be avoided by obtaining accurate loading information that structure is exposed to during its life. Hence, flight test is performed according to a flight profile that was created by the pilots simulating real flight conditions (normal flight and attack maneuvers) that air platform is subjected to during its operational life.

Tri-axial accelerometers (Bruel & Kjaer 4507 biax) are used for obtaining the load data at the position of the Bracket. 1600 Hz is set for the sampling frequency of the accelerometer. While the load data is recorded continuously, durations of all maneuvers' are saved immediately hence which leads to easily separating maneuvers load during analysis. (Table 4.8)

In the analysis, the whole flight profile data is used. During the whole flight, the acceleration versus time data for each axis is measured using accelerometers. However, in order to perform a fatigue analysis, PSD of the time data is required. Hence, using Fourier Transform method, acceleration PSD is obtained for each axis. The acceleration PSD of each axis is given in Figure 4.26, Figure 4.27 and Figure 4.28.

Table 4.8 Profile of the Flight

Maneuver No:	**Type of Maneuver**	**Duration (Minutes)**
1	Engine Running (Idling)	7
2	Engine Running (Full Capacity)	13
3	Hover	8
4	Climbing	2
5	Gliding	5
6	Climbing (Rotating)	5
7	Gliding (Rotating)	5
8	Same Level Flight (90 kts)	3
9	Same Level Flight (120 kts)	4
10	Same Level Flight (VNE)	2
11	Rotating at Same Level Flight	5
12	Pattern of Firing	5
13	Landing	16

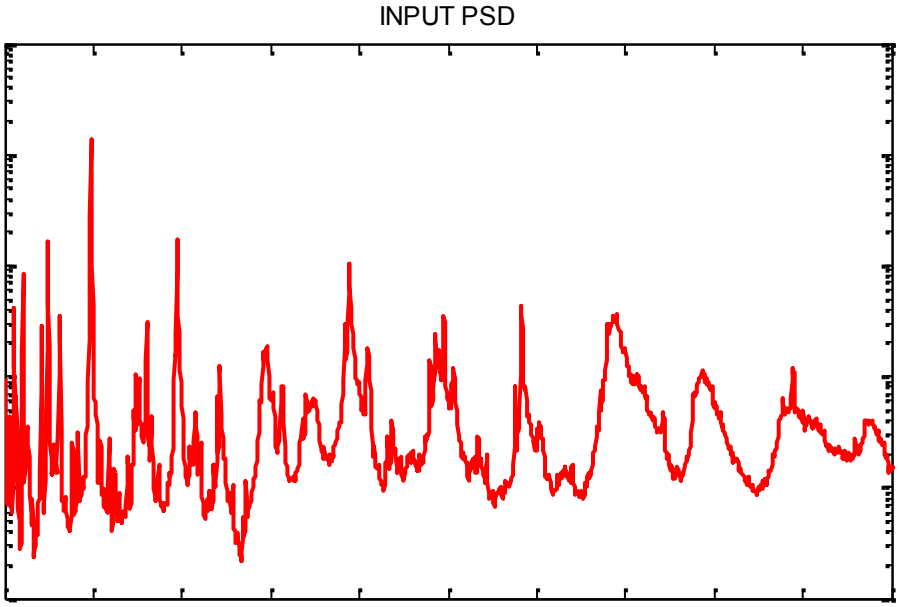

Figure 4.26 Acceleration PSD on the X -axis of Bracket

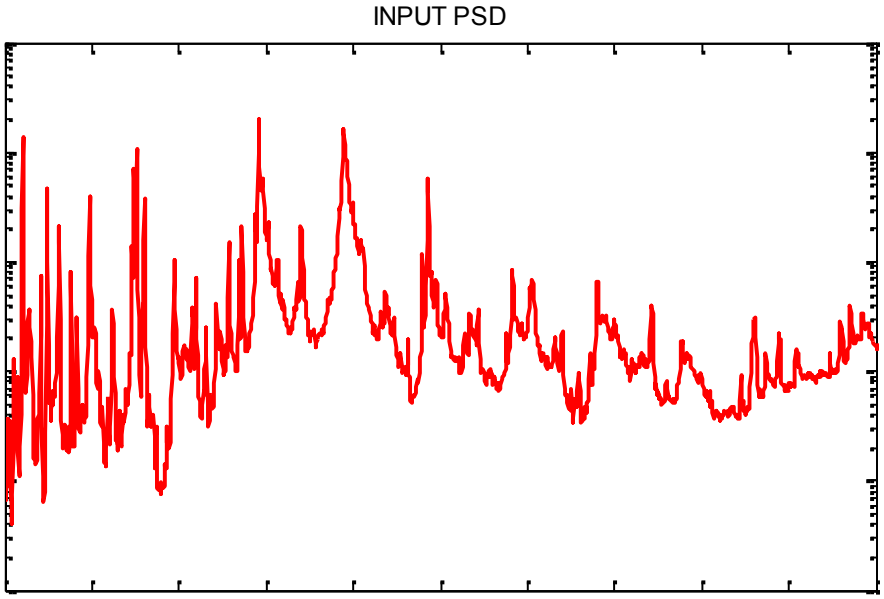

Figure 4.27 Acceleration PSD on the Y -axis of Bracket

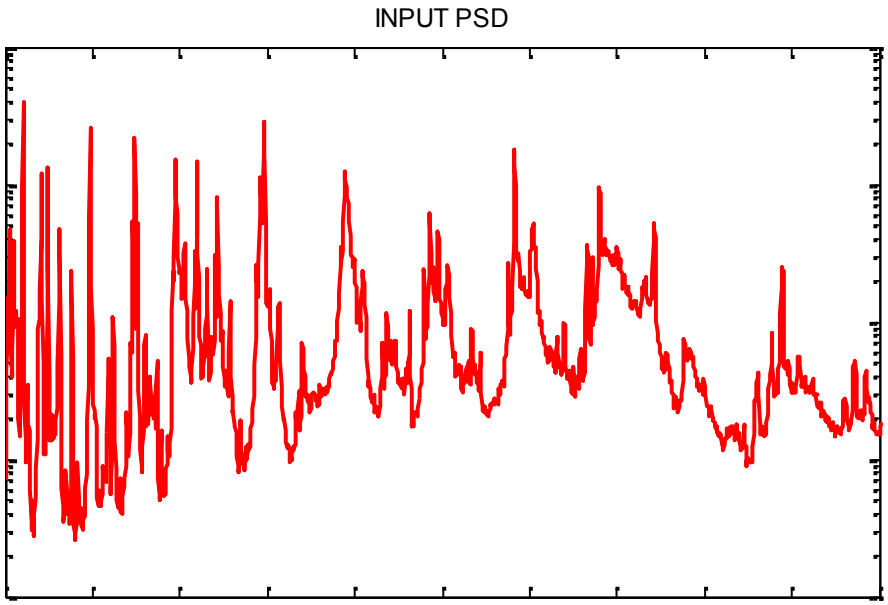

Figure 4.28 Acceleration PSD on the Z -axis of Bracket

In addition, fatigue analysis will be repeated using the PSD loading defined in "TABLE 514.5C-IV" and "FIGURE 514.5C-10" of MIL-STD-810F [28] given in Figure 4.29.

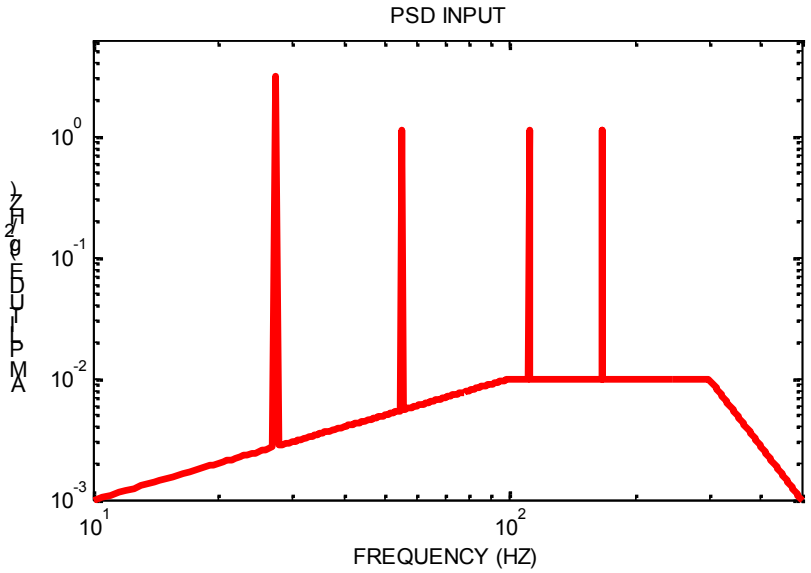

Figure 4.29 PSD Input (Air Platform Vibration Profile) [28]

Before performing the fatigue analyses, RMS values of all PSD's are obtained in order to forecast which load has the higher possibility of causing the most damage to Bracket.

Table 4.9 RMS Values PSD's in Each Direction

PSD LOADS	RMS Values (m/s^2)	RMS Values (g)
X Direction	5.8	0.6
Y Direction	4.6	0.5
Z Direction	2.3	0.2
MIL-STD-810 F	24.9	2.5

4.4 Accelerated Testing of the Bracket

While performing fatigue analysis, the operational flight loading (Figure 4.27) is applied to the Bracket. However, when the result is analyzed carefully, it is clear that performing a fatigue test with real flight loading is not feasible due to long test duration which may take years. Hence, it is required to accelerate the fatigue testing. A possible way of accelerating the testing is increasing the amplitudes of the loading. Considering the requirements defined in military standard [28], the duration of the fatigue test is accelerated to 4 hours.

Also as indicated in Chapter 5, due to insignificant damage contributions of Y (Figure 4.26) and Z (Figure 4.28) axis loadings, fatigue test is performed using only X (Figure 4.27) axis loading. The amplitude of X axis loading is increased to 26 times of that of original loading and obtained PSD loading is given in Figure 4.30. The GRMS value of the modified PSD loading is 3.

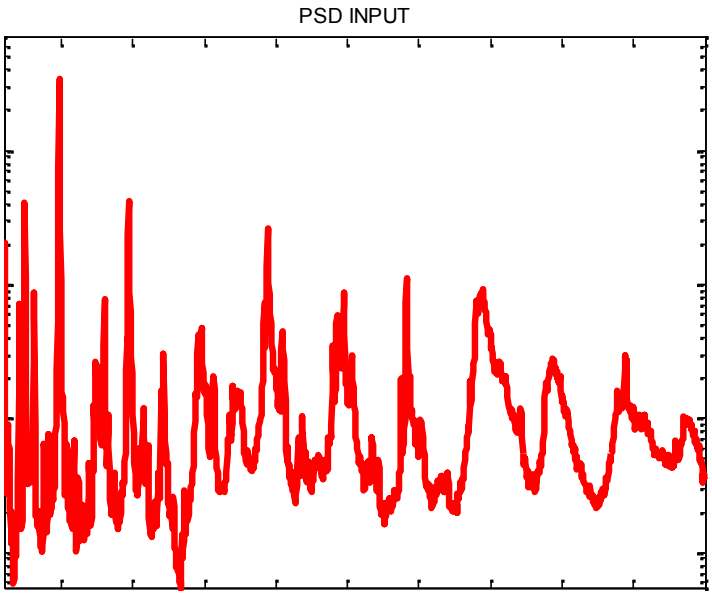

Figure 4.30 Scaled PSD Loading for Accelerated Testing

However, it has to be checked whether the system continues to be linear or not when the amplitude of loading is increased. Because, when a different Bracket (Figure 4.31) was analyzed, it was seen that the structure behaves non-linearly when it was subjected to high amplitude loading. Hence, both Brackets are checked by performing four different sine tests using shaker.

They are excited on their natural frequencies from low amplitude sine to high amplitude sine and acceleration responses are obtained from the accelerometers which are close to connection regions of both Brackets. Since the loadings are sinusoidal, the responses are expected to be sinusoidal and maximum and minimum values of the responses are expected to be same if the systems are linear. Hence, it is checked whether maximum and minimum amplitudes of the sine are similar to each other or not. For comparison, test results of a different Bracket is also given in Table 4.10 additionally, the test results of the actual Bracket are given in Table 4.11.

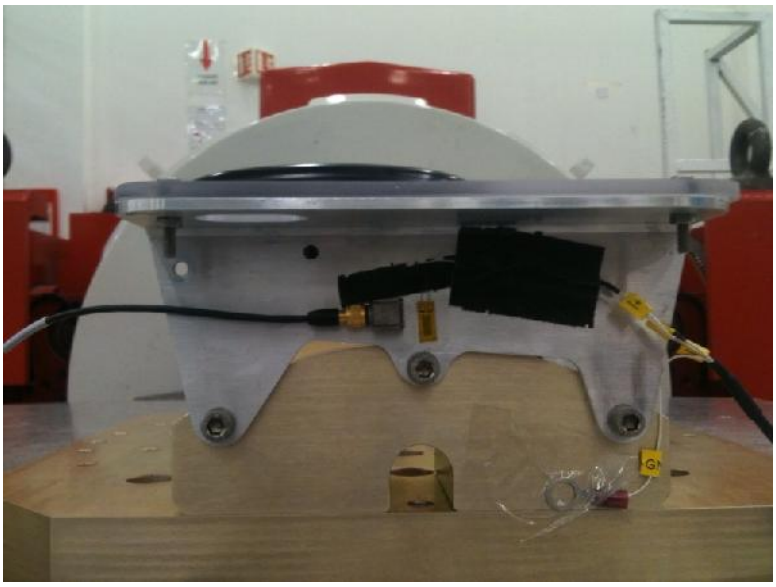

Figure 4.31 The Different Bracket

Table 4.10 Sine Test Results of the Different Bracket

Amplitude of Sine (g)	**Frequency HZ**	**Maximum Amplitude (m/s^2)**	**Minimum Amplitude (m/s^2)**	**Difference Between Maximum and Minimum Amplitude %**
0.5	94	12.64	-12.77	1.00
0.75	94	20.52	-21.14	3.04
1.5	94	39.07	-45.82	17.29
2.25	94	52.71	-61.00	15.72

Table 4.11 Sine Test Results of Bracket

Amplitude of Sine (g)	Frequency HZ	Maximum Amplitude (m/s^2)	Minimum Amplitude (m/s^2)	Difference Between Maximum and Minimum Amplitude %
0.45	147	14.08	-13.81	1.91
0.9	147	28.02	-29.51	5.33
1.35	147	42.50	-45.05	6.01
1.5	147	48.55	-51.14	5.34

Also the collected acceleration data is given in Figure 4.32 and Figure 4.33 for both Brackets.

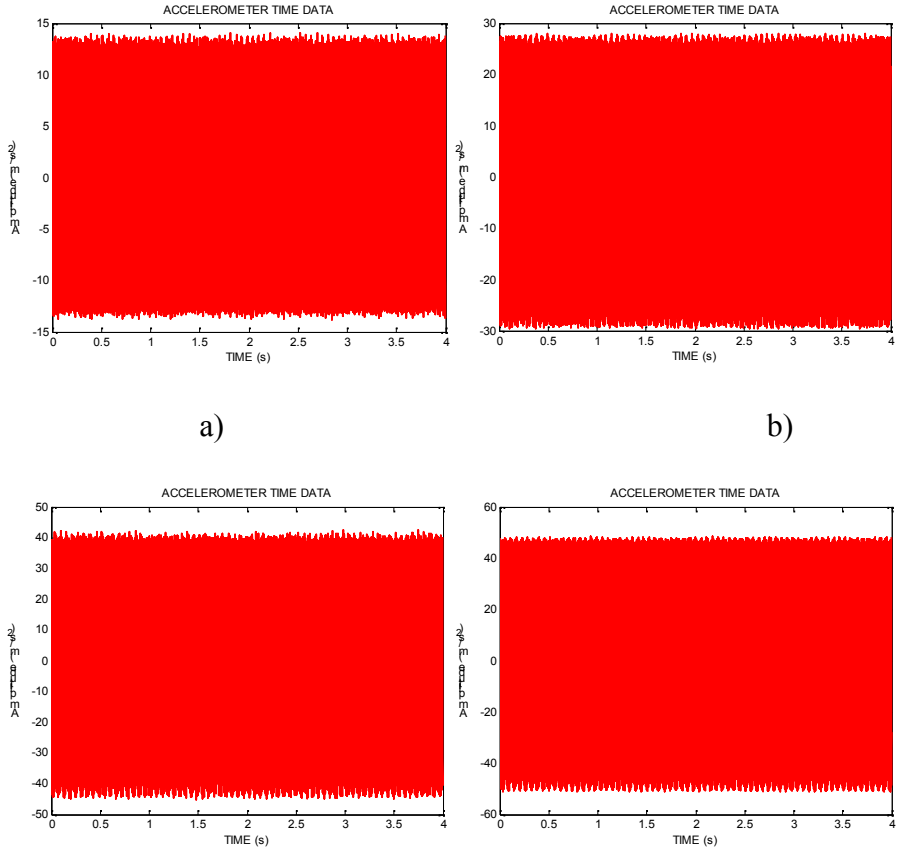

Figure 4.32 Sine Test Results for a) 0.45g b) 0.9g c)1.35g d) 1.5g of Bracket

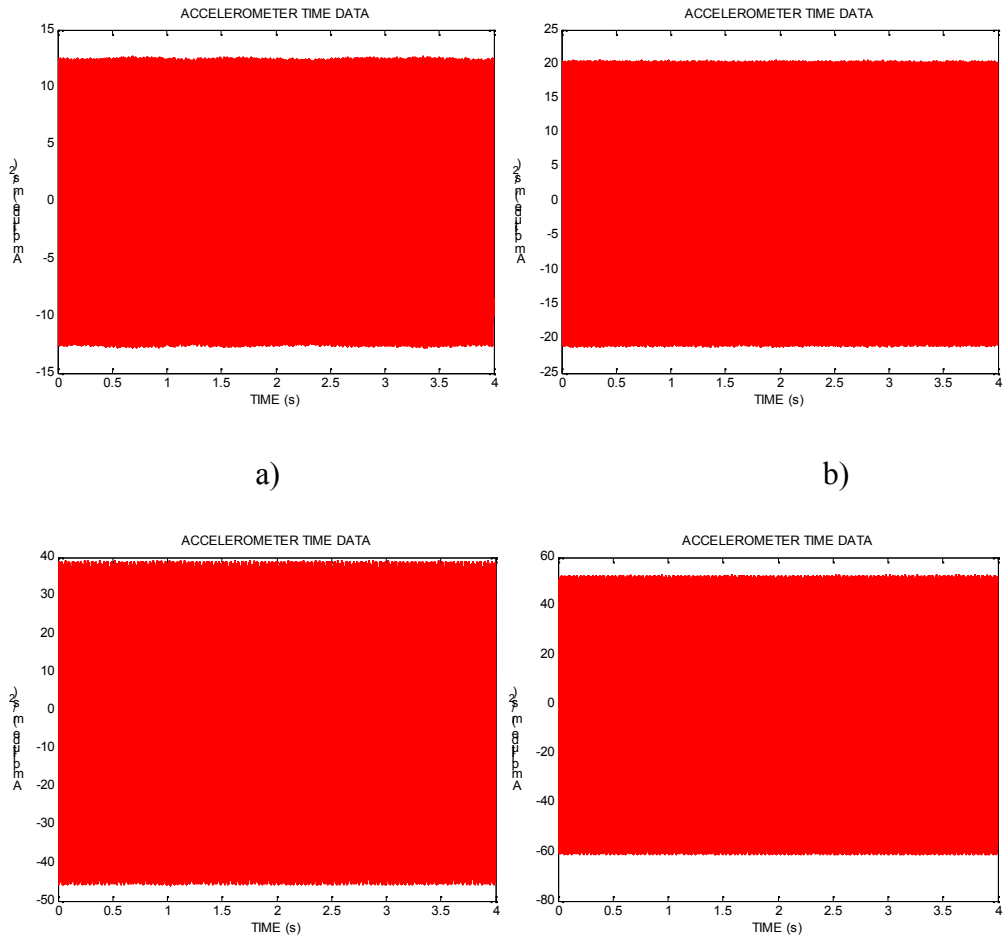

Figure 4.33 Sine Test Results for a) 0.5g b) 0.75g c)1.5g d) 2.25g of Different Bracket

Moreover, the linearity of the actual Bracket is checked by analyzing the results obtained from strain gage after real and accelerated load random vibration shaker tests. The real load acceleration PSD in the X axis (Figure 4.26) and the scaled load PSD (Figure 4.30) are applied to structures using the electromagnetic shaker and results of the tests of the bracket are given in Table 4.12 and Table 4.13.

Table 4.12 Strain Gage Results for the Bracket

AMPLITUDE (g^2/HZ) (10-500 HZ)	GRMS VALUE OF THE PSD INPUT	STRAIN GAGE DATA MAX (MPa)	STRAIN GAGE DATA MIN (MPa)	DIFFERENCE BETWEEN MAX AND MIN %
Real Load	0.59	10.36	-10.34	0.20
Accelerated Load	3.00	50.12	-49.82	0.60

Table 4.13 Strain Gage Result Comparison for the Bracket

AMPLITUDE (g^2/HZ) (10-500 HZ)	GRMS VALUE OF THE PSD INPUT	RMS VALUE OF THE STRESS PSD (MPa)
Real Load	0.59	2.62
Accelerated Load	3.00	13.63
Ratio of Accelerated Load to Real Load	5.06	5.20

It can be easily observed that when the amplitudes of the real load PSD are increased by 26 times, the GRMS value of the loading is increased by $\sqrt{26} = 5.06$ times. Hence, it is expected that the RMS stress value should be increased by the indicated ratio. When Table 4.12 and Table 4.13 are analyzed, it can be easily observed that the maximum and the minimum stress values are very close to each other and when the input loading is increased by 5.06 times, the output stress values is increased by the same ratio.

In conclusion, while the different bracket behaves non-linearly, actual bracket can be considered to behave linearly when the amplitude of the loading is increased.

CHAPTER 5

FATIGUE LIFE ANALYSIS AND TESTING OF CANTILEVER BEAM AND BRACKET

Finite element models are verified with experimental results and harmonic analyses are performed in order to predict fatigue life of cantilever beam and Bracket. In the following sections, methods and parameters used in fatigue analyses and experiments will be explained. For the cantilever beam, fatigue result obtained by numerical code will be verified by commercial software and that of experimental results. Fatigue life analyses of Bracket using real load and scaled load will be performed by the developed numerical code and commercial software will be verified using experimental results. Detailed information is given in the following sections.

5.1 Fatigue Life Analysis and Testing of Cantilever Beam

In order to perform a fatigue analysis for the cantilever beam, a white noise PSD is chosen for the loading. The PSD has 0.09 g^2/Hz amplitude between 5-500 Hz. This magnitude is chosen after many analyses are performed since fatigue failure of the cantilever beam may occur in a long time period up to several years if an appropriate loading is not chosen. The loading PSD is shown in Figure 5.1. S-N curve of the AL 6061 T6 shown in Figure 5.2 is used in fatigue analyses.

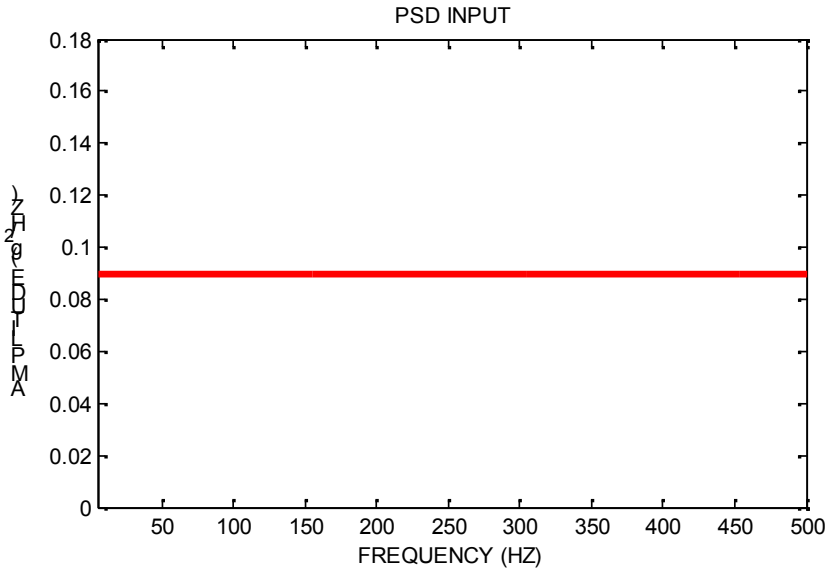

Figure 5.1 PSD Input for the Fatigue Analysis

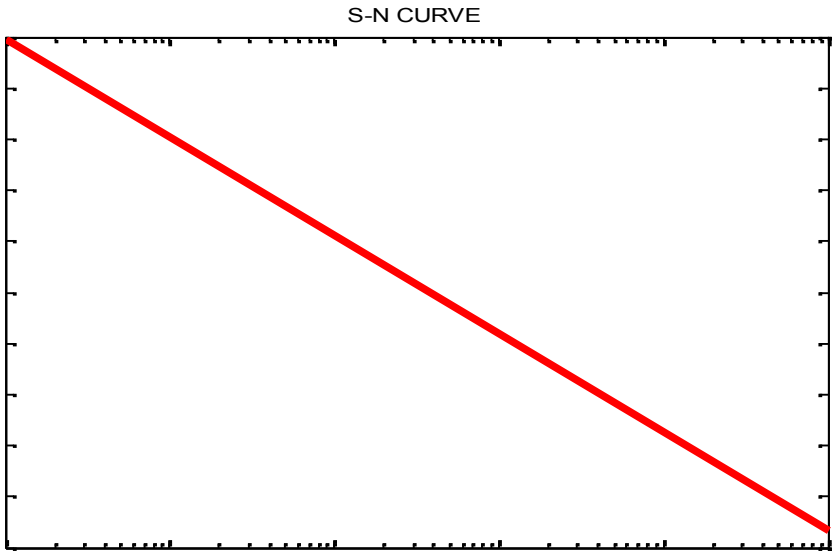

Figure 5.2 Al 6061 T6 S-N Curve

Dirlik [9] method is chosen as the fatigue life calculation method. There is no need for mean stress correction since the beam will be excited normal to the gravity direction. This means there is no stress contribution caused by the gravity.

5.1.1 Fatigue Life Analysis Using Developed Numerical Code

Before the stress PSD's are found, indicated in Chapter 3, the transfer functions are obtained from the results of harmonic analyses that are performed using ANSYS. The transfer function used in fatigue calculations is derived from maximum and minimum principal stresses according to Absolute Maximum Principal Stress theory. Comparison of the maximum and the minimum principal stresses together with the transfer function are shown in Figure 5.3. Finally, stress PSD shown in Figure 5.4 is calculated.

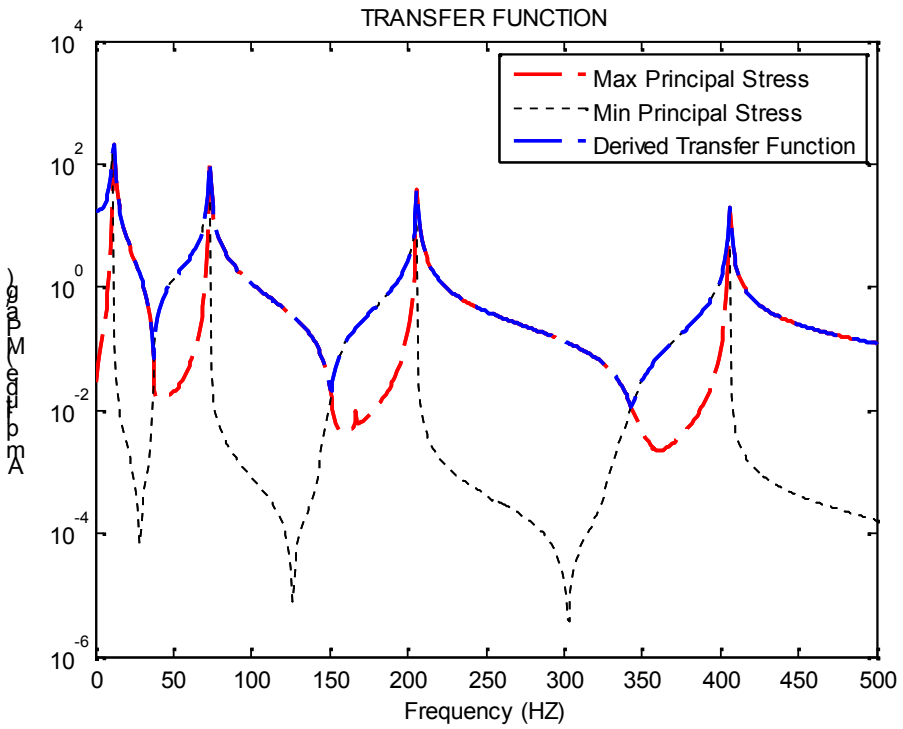

Figure 5.3 Comparison of the Maximum, Minimum Principal Stress Histories and Transfer Function

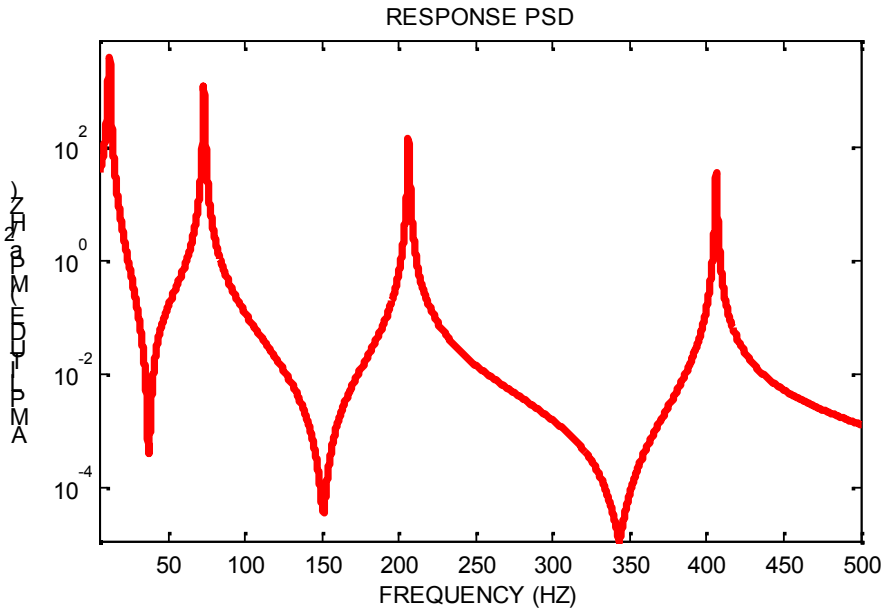

Figure 5.4 Stress PSD (Numerical Code)

By using stress PSD, all stress levels are calculated in order to find the duration after which the cantilever beam will fail due to fatigue. Finally, the fatigue life of the cantilever beam is estimated to be 983 seconds by using the developed numerical code.

5.1.2 Fatigue Life Analysis of Cantilever Beam Using Commercial Software

After harmonic analysis with unit load is performed, using the stress results and material information fatigue analysis is performed. All needed parameters mentioned above are used for commercial software too.

As a result, the stress PSD shown in Figure 5.4 is obtained together with 771 seconds of fatigue life.

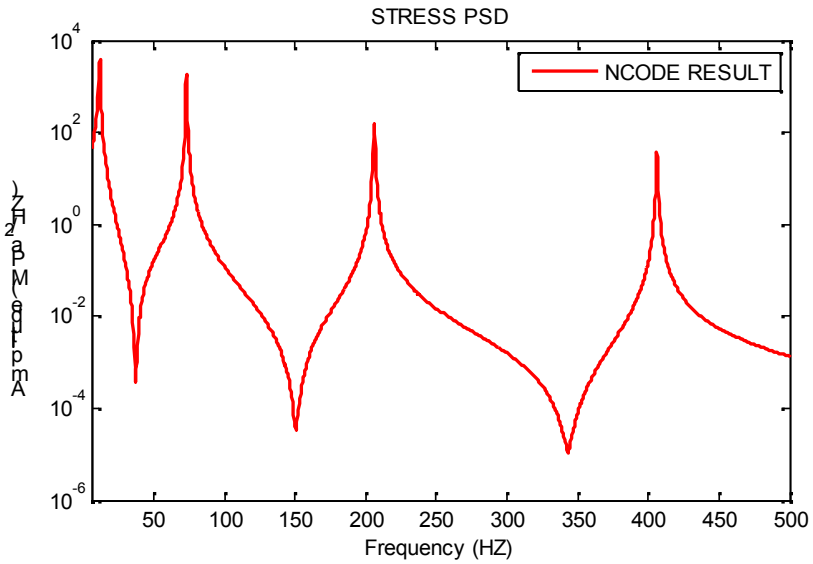

Figure 5.5 Stress PSD (Commercial Software)

5.1.3 Fatigue Life Testing of Cantilever Beam

The fixture is fixed to vibration shaker as shown in Figure 5.6. The PSD profile shown in Figure 5.1 is the input.

Figure 5.6 A View of the Cantilever Beam Fixture Fixed to Electromagnetic Vibration Test Equipment

As it can be observed, the excitation direction of the shaker is normal to the gravity direction. Hence there is no mean stress correction for the numerical calculations. When the crack is observed the test is stopped and the time from the beginning to the end of the test is accepted to be the fatigue life of the cantilever beam. Since only one fatigue test for the beam can lead to an inaccurate result, the test will be repeated seven times and the average of the results will be accepted as the fatigue life of the beam. The fatigue life results for the seven test items and average of them is listed in Table 5.1.

Table 5.1 Fatigue Life Test Results

CONDITION	**FATIGUE LIFE (s)**
TEST ITEM 1	1320
TEST ITEM 2	1260
TEST ITEM 3	1250
TEST ITEM 4	1380
TEST ITEM 5	1200
TEST ITEM 6	1400
TEST ITEM 7	1200
AVERAGE LIFE	1287

5.1.4 Fatigue Life Results Comparison of Cantilever Beam

As mentioned in the vibration fatigue theory section, PDF is calculated from stress PSD; hence the accuracy of obtained stress PSD is very important. Considering this effect, stress PSD's obtained from the numerical code and commercial software are compared which is given in Figure 5.7. Comparison of fatigue life results is performed and it is given in Table 5.2. In addition, comparison of the locations of the crack initiation for both finite element and manufactured models is given in Figure 5.8.

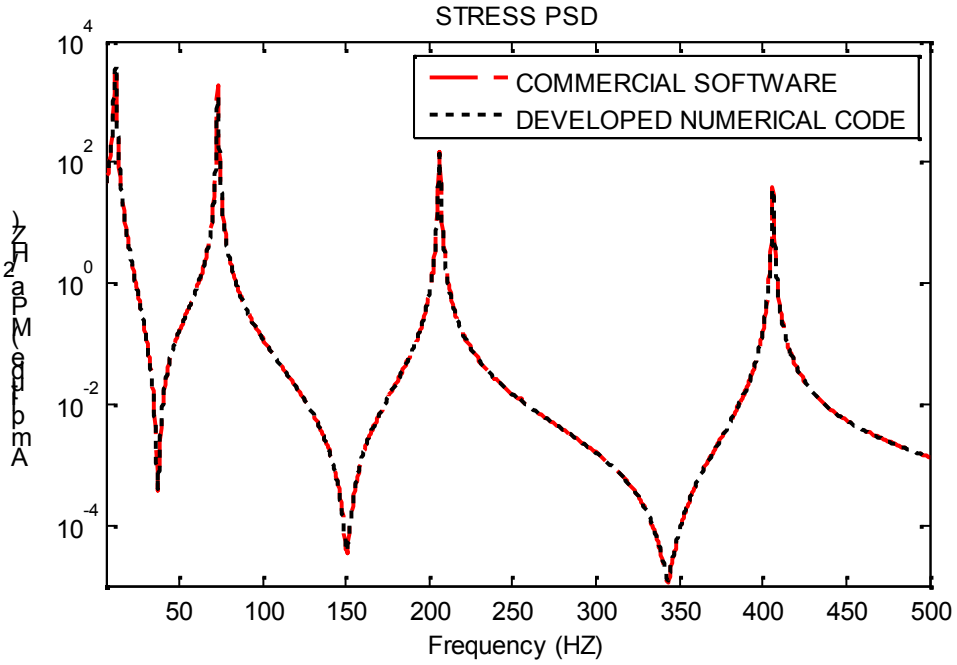

Figure 5.7 Comparison of PSD's Obtained from Numerical Code and Commercial software

Table 5.2 Fatigue Life Result Comparison

	Numerical Code Result	**Commercial software Result**	**Fatigue Test Average Life Result**
Fatigue Life (s)	983	771	1287

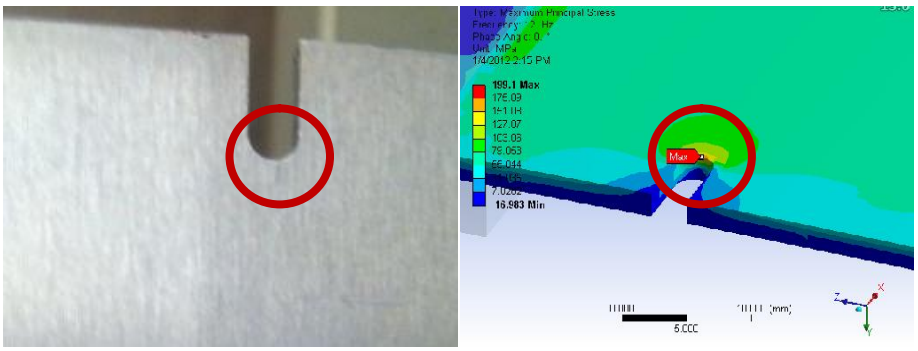

Figure 5.8 Locations of the Crack Initiation for Both Finite Element and Manufactured Models

Investigating the results, it can be concluded that there is insignificant difference in fatigue life results between commercial software and developed numerical code. Commercial software does not use the resolution of frequency of the harmonic analysis taken from ANSYS and it determines resolution of the stress PSD using its own algorithm while calculating fatigue life of the structures. This causes small differences between stress PSD's and RMS stress values calculated from them. However, as mentioned above, fatigue life is very sensitive to stress, hence, exactly the same fatigue life result cannot be obtained.

While performing fatigue analysis using developed numerical code, if the stress PSD obtained from commercial software (Figure 5.5) is used, it is recognized that calculated fatigue life result is almost the same with that of commercial software. The comparison of results is given in Table 5.3.

Table 5.3 Fatigue Life Results Comparison (Commercial software Stress PSD is Used)

	Numerical Code Result	**Commercial Software Result**
Fatigue Life (s)	733	771

5.2 Fatigue Life Analysis and Testing of Bracket

In order to perform a fatigue analyses for the Bracket, PSD loadings on each axis are obtained from flight test which was mentioned above. $S-N$ curve of the AL 7075 T7351 shown in Figure 5.2 is used to perform fatigue analysis. Dirlik [9] method is chosen as calculation method and no mean stress correction is used.

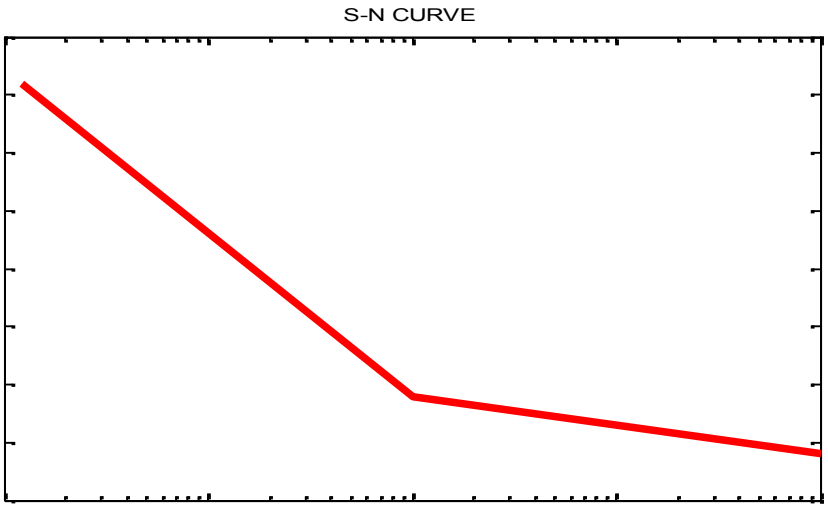

Figure 5.9 Al 7075 T7351 S-N Curve

5.2.1 Fatigue Life Analysis Using Developed Numerical Code

As mentioned above three fatigue analyses are performed on each axis of Bracket. Also the most critical nodes are observed and for each fatigue analysis, the transfer functions of each node are derived from the maximum and the minimum principal stresses according to Absolute Maximum Principal Stress theory. In addition, comparison of the maximum and the minimum principal stresses is performed together with the transfer function and then, stress PSDs are obtained. Derived transfer functions, comparison of the maximum and the minimum principal stresses and stress PSDs for all critical nodes are given between Figure 5.10 and Figure 5.27.

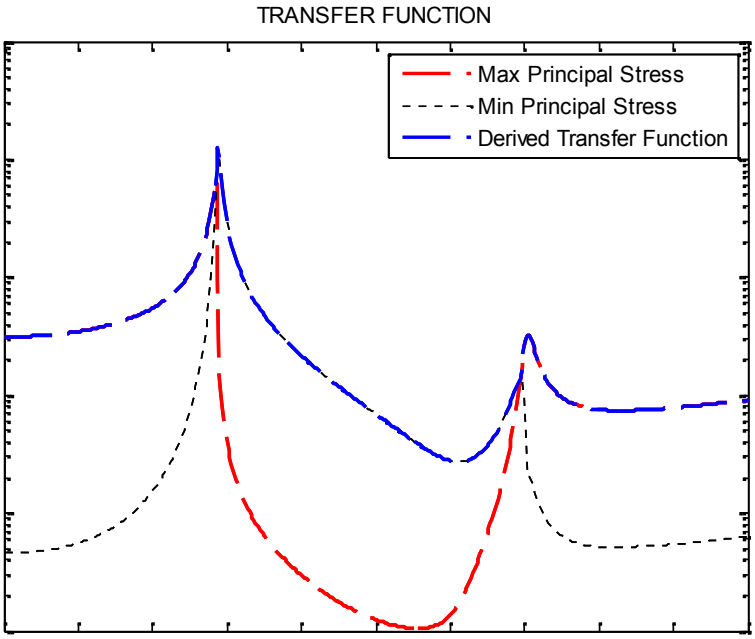

Figure 5.10 Comparison of the Maximum, Minimum Principal Stress Histories and Transfer Function for Node 23811 (The Load Is Applied on the Direction of X Axis)

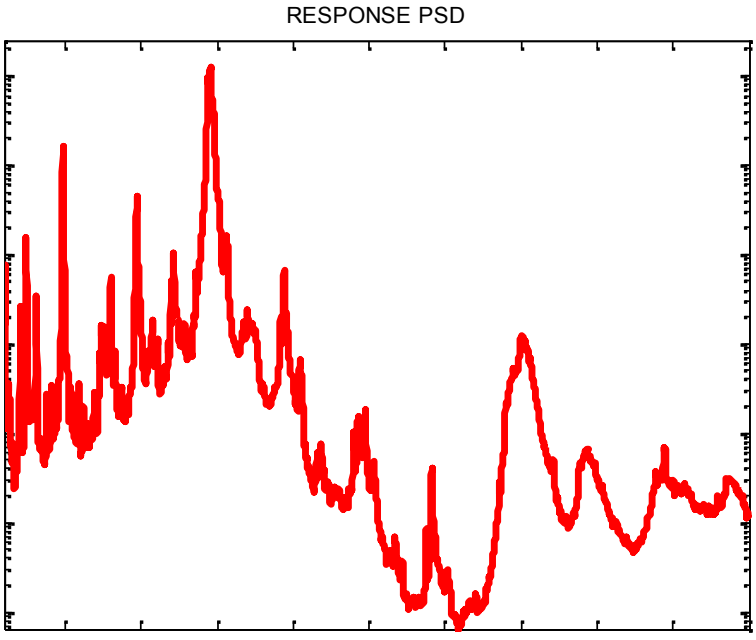

Figure 5.11 Stress PSD for Node 23811 (The Load Is Applied on the Direction of X Axis)

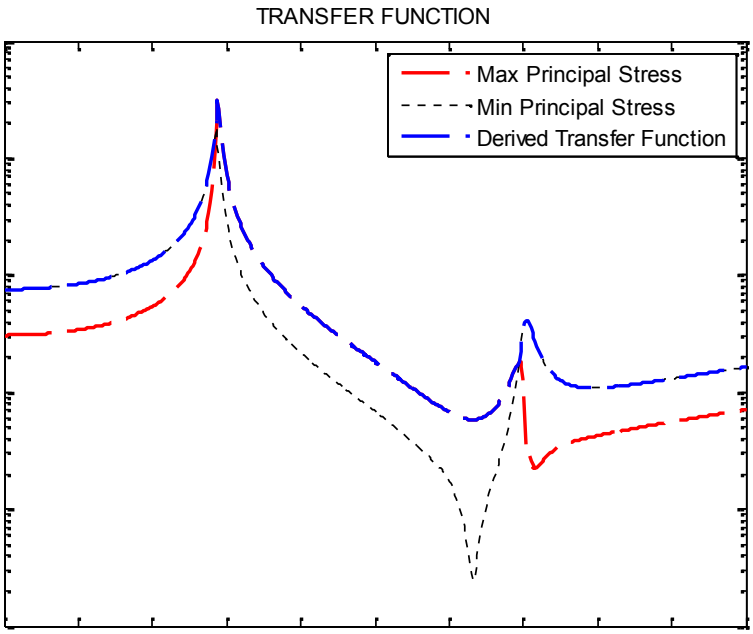

Figure 5.12 Comparison of the Maximum, Minimum Principal Stress Histories and Transfer Function for Node 29206 (The Load Is Applied on the Direction of X Axis)

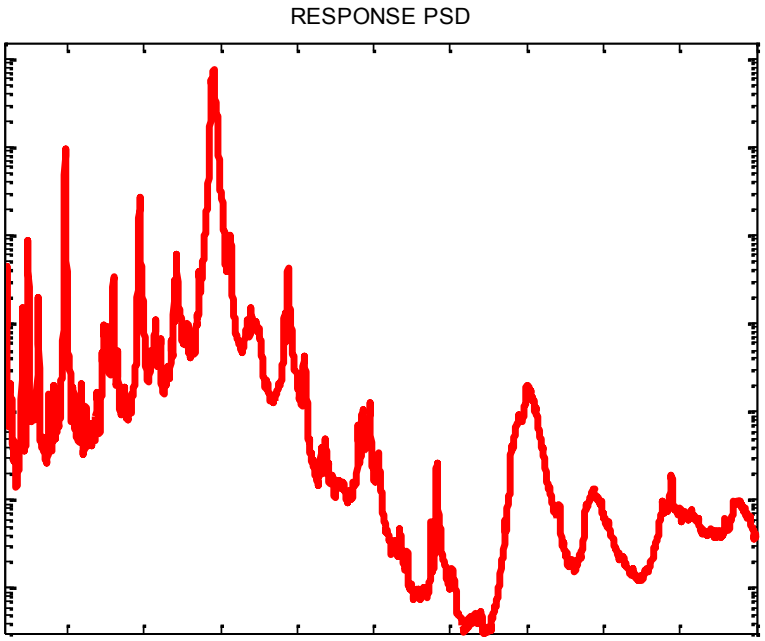

Figure 5.13 Stress PSD for Node 29206 (The Load Is Applied on the Direction of X Axis)

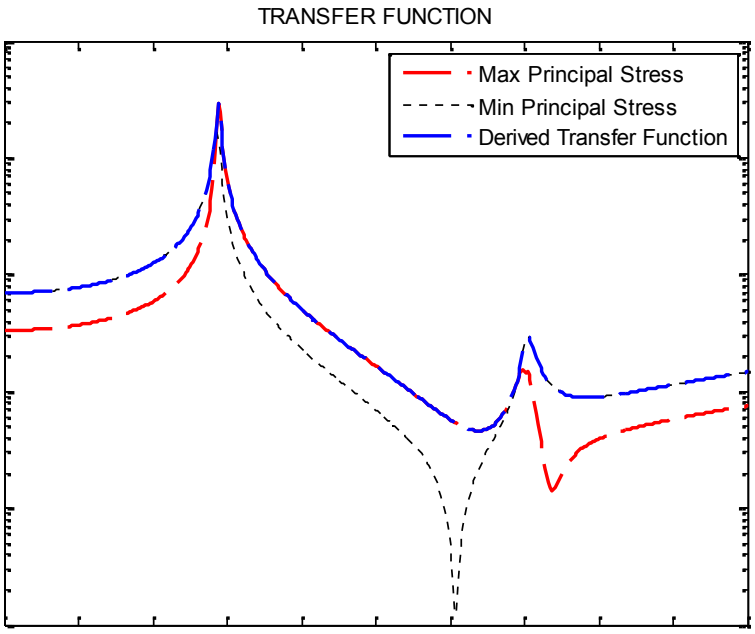

Figure 5.14 Comparison of the Maximum, Minimum Principal Stress Histories and Transfer Function for Node 29217 (The Load Is Applied on the Direction of X Axis)

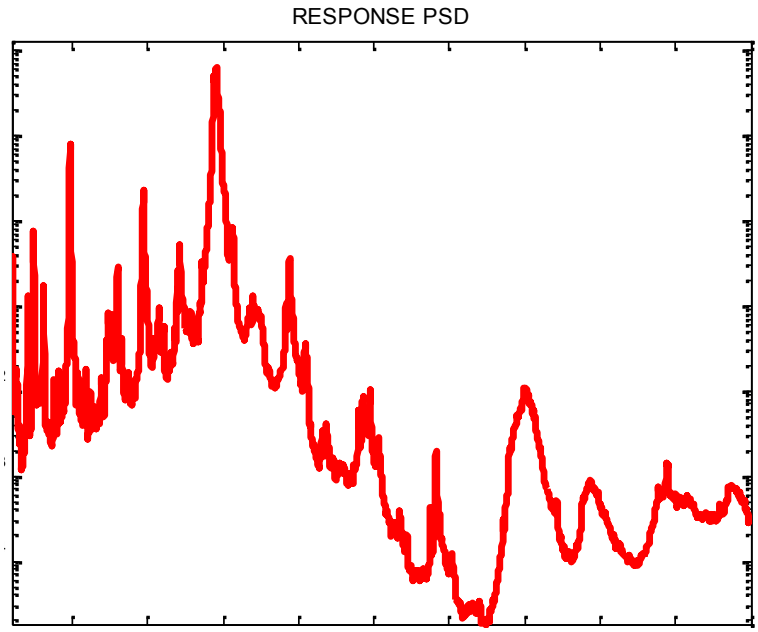

Figure 5.15 Stress PSD for Node 29217 (The Load Is Applied on the Direction of X Axis)

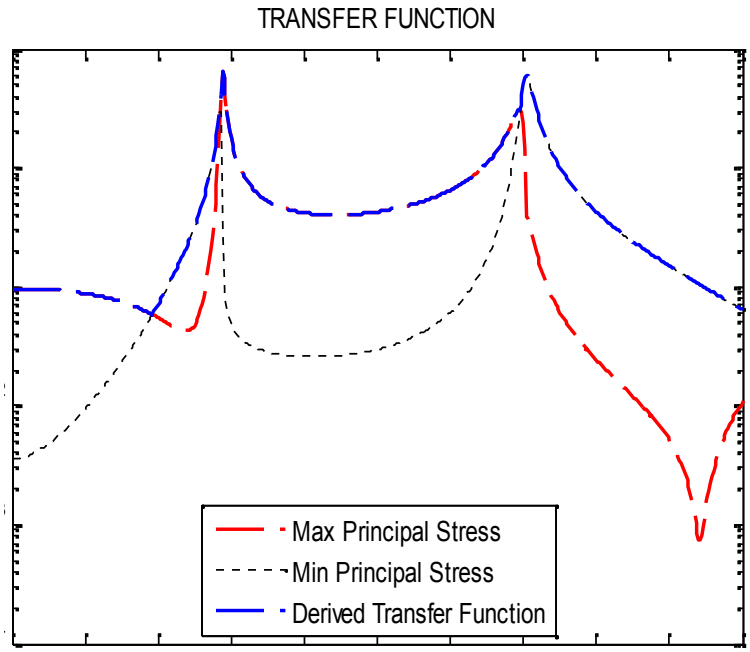

Figure 5.16 Comparison of the Maximum, Minimum Principal Stress Histories and Transfer Function for Node 23811 (The Load Is Applied on the Direction of *Y* Axis)

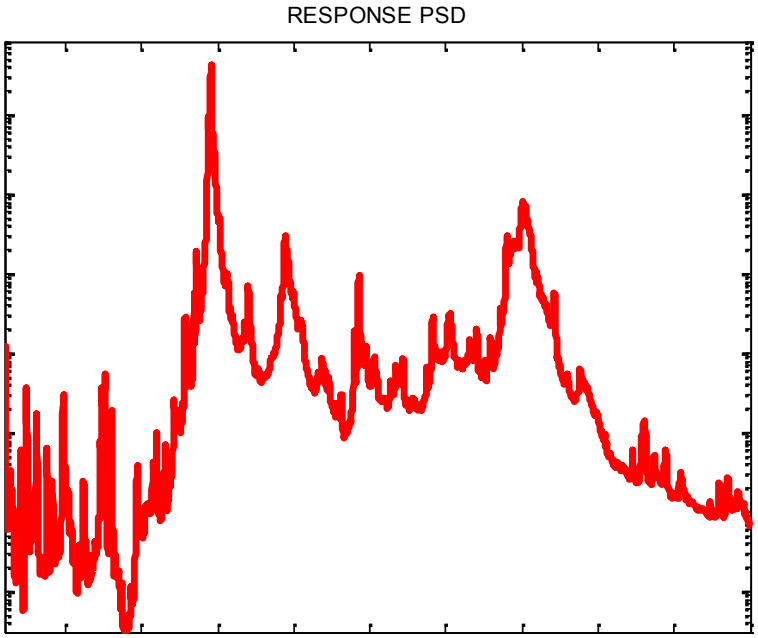

Figure 5.17 Stress PSD for Node 23811 (The Load Is Applied on the Direction of *Y* Axis)

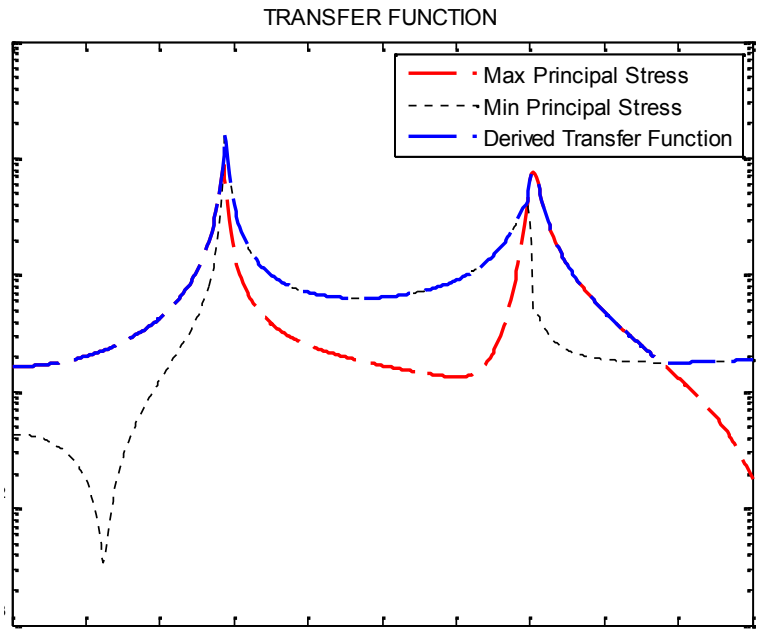

Figure 5.18 Comparison of the Maximum, Minimum Principal Stress Histories and Transfer Function for Node 29206 (The Load Is Applied on the Direction of *Y* Axis)

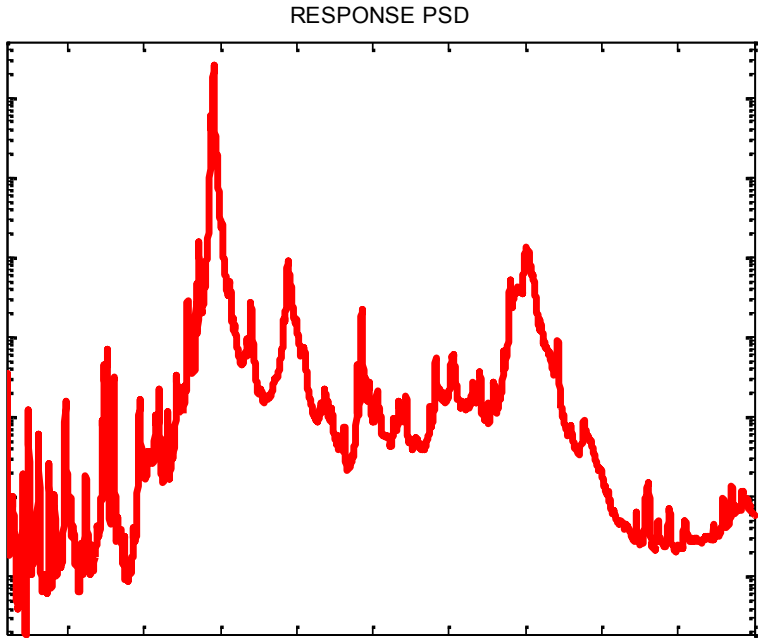

Figure 5.19 Stress PSD for Node 29206 (The Load Is Applied on the Direction of *Y* Axis)

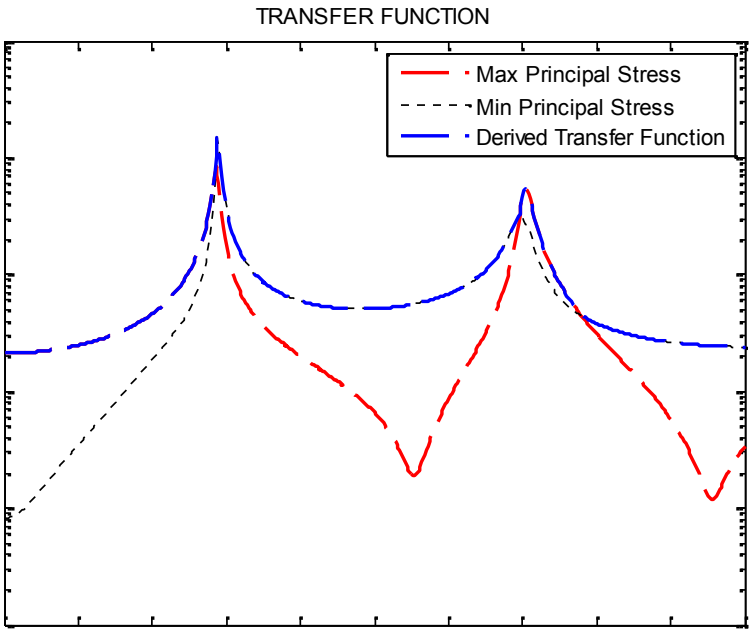

Figure 5.20 Comparison of the Maximum, Minimum Principal Stress Histories and Transfer Function for Node 29217 (The Load Is Applied on the Direction of Y Axis)

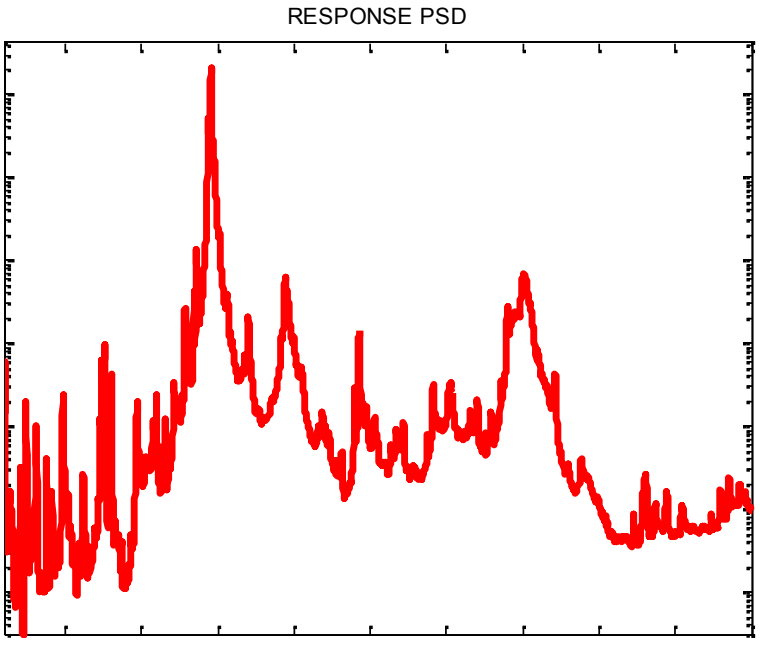

Figure 5.21 Stress PSD for Node 29217 (The Load Is Applied on the Direction of Y Axis)

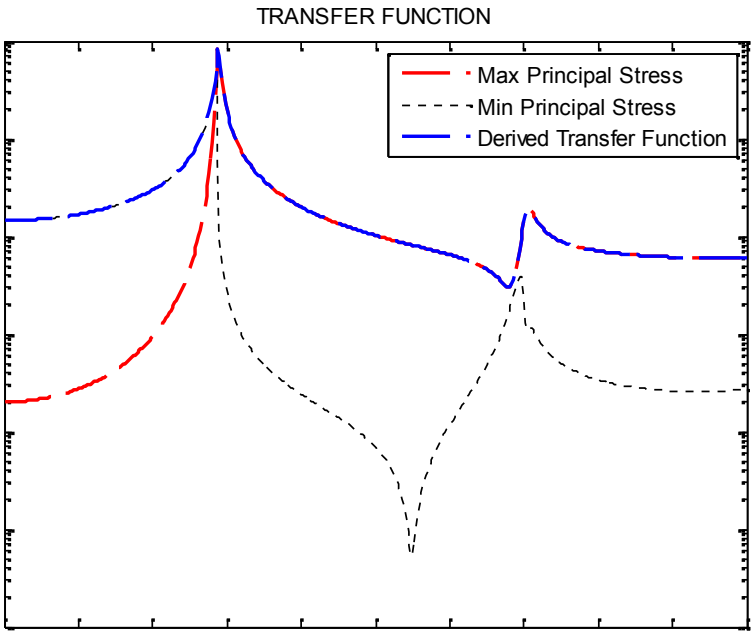

Figure 5.22 Comparison of the Maximum, Minimum Principal Stress Histories and Transfer Function for Node 23811 (The Load Is Applied on the Direction of Z Axis)

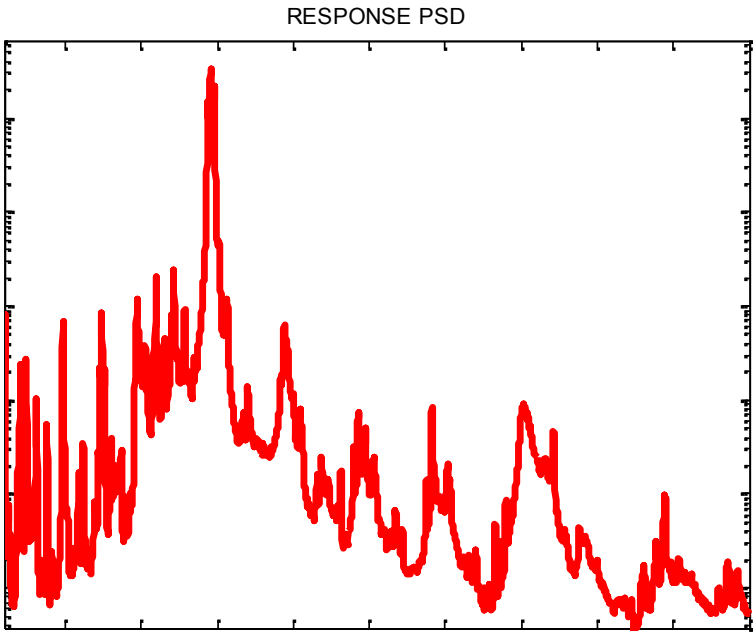

Figure 5.23 Stress PSD for Node 23811 (The Load Is Applied on the Direction of Z Axis)

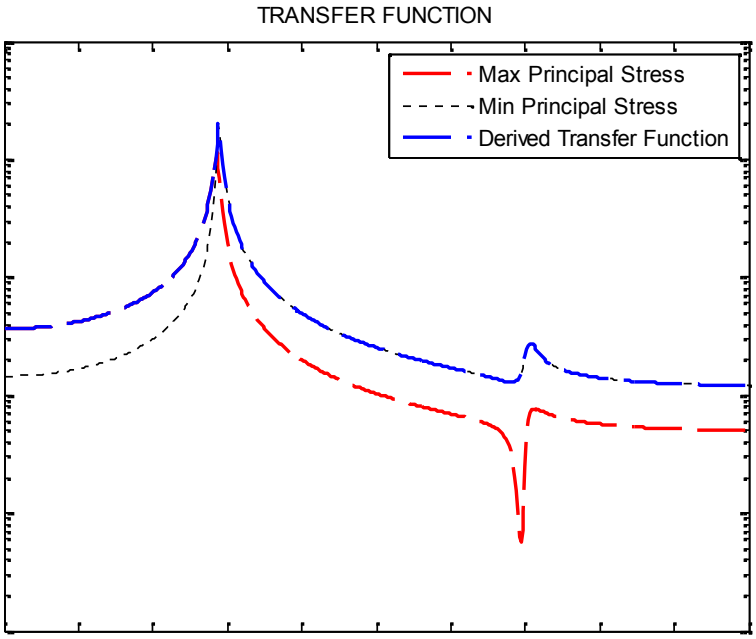

Figure 5.24 Comparison of the Maximum, Minimum Principal Stress Histories and Transfer Function for Node 29206 (The Load Is Applied on the Direction of Z Axis)

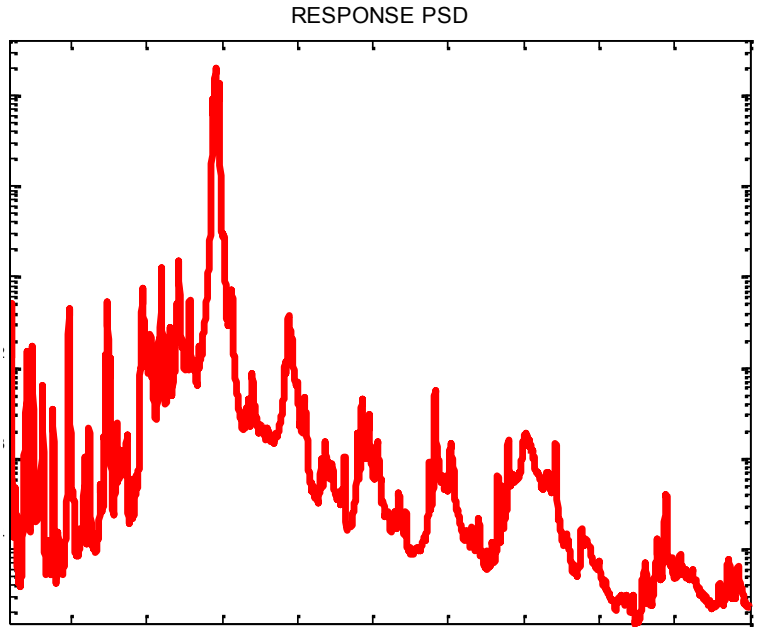

Figure 5.25 Stress PSD for Node 29206 (The Load Is Applied on the Direction of Z Axis)

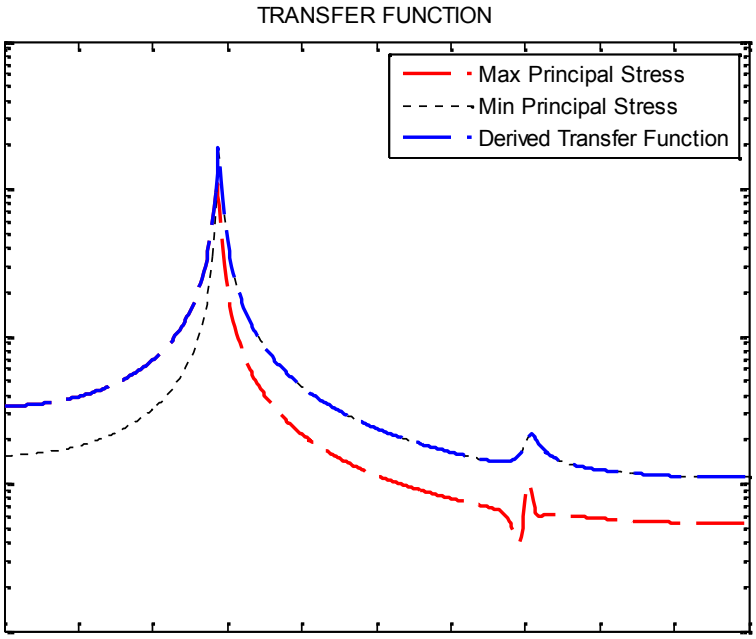

Figure 5.26 Comparison of the Maximum, Minimum Principal Stress Histories and Transfer Function for Node 29217 (The Load Is Applied on the Direction of Z Axis)

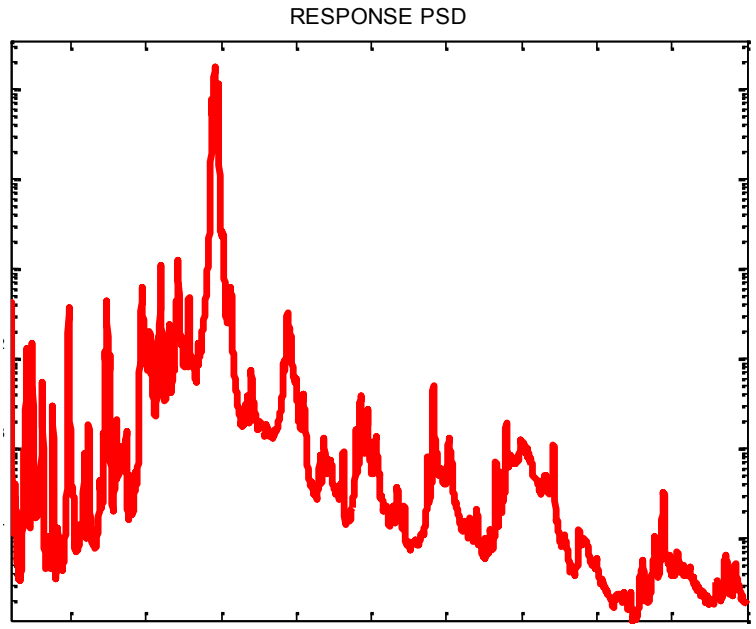

Figure 5.27 Stress PSD for Node 29217 (The Load Is Applied on the Direction of Z Axis)

Using obtained stress PSDs, stress RMS values of each critical node is calculated for each fatigue analysis. (Table 5.4)

Table 5.4 RMS Stress Values of Each Critical Node

Node Number	RMS STRESS (MPa)		
	X AXIS LOADING	Y AXIS LOADING	Z AXIS LOADING
23811	6.66	0.83	2.93
29206	16.51	1.92	7.26
29217	15.27	1.75	6.72

Finally, all stress levels are calculated in order to find the resultant damage on the Bracket by using stress PSDs. The calculated fatigue damage values of each critical node for each fatigue analyses are given in Table 5.5. In addition, by taking inverse of fatigue damage values fatigue life results are given in Table 5.6.

Table 5.5 Fatigue Damage Values of Each Critical Node

Node Number	FATIGUE DAMAGE ON EACH			TOTAL FATIGUE DAMAGE
	X AXIS LOADING	Y AXIS LOADING	Z AXIS LOADING	
23811	1.28E-20	3.69E-34	5.57E-26	1.28E-20
29206	1.14E-14	1.01E-28	4.87E-20	1.14E-14
29217	3.53E-15	2.55E-29	1.50E-20	3.53E-15

Table 5.6 Fatigue Life Values of Each Critical Node

Node Number	FATIGUE LIFE (s) ON EACH AXIS			FATIGUE LIFE (s)	FATIGUE LIFE (h)
	X AXIS LOADING	Y AXIS LOADING	Z AXIS LOADING		
23811	7.81E+19	2.71E+33	1.80E+25	7.81E+19	2.17E+16
29206	8.75E+13	9.86E+27	2.05E+19	8.75E+13	2.43E+10
29217	2.83E+14	3.92E+28	6.67E+19	2.83E+14	7.86E+10

When the fatigue damage results are analyzed, it can be easily observed that node 29206 is the most critical node. Also it is clear that the damage is caused by X axis loading and the fatigue damage contribution of loadings on the other axes can be neglected.

After the most critical node and the axis of the loading are obtained one more fatigue analysis is performed for the PSD input given in Figure 4.30 that will be used in accelerated test. The obtained fatigue analysis results and stress PSD are given in Table 5.7 and Figure 5.28, respectively.

Table 5.7 Fatigue Analysis Results for PSD Input Used in Accelerated Test

Node Number	**FATIGUE DAMAGE X AXIS LOADING**	**FATIGUE LIFE (s)**	**FATIGUE LIFE (h)**
29206	6.94E-05	1.44E+04	4.00E+00

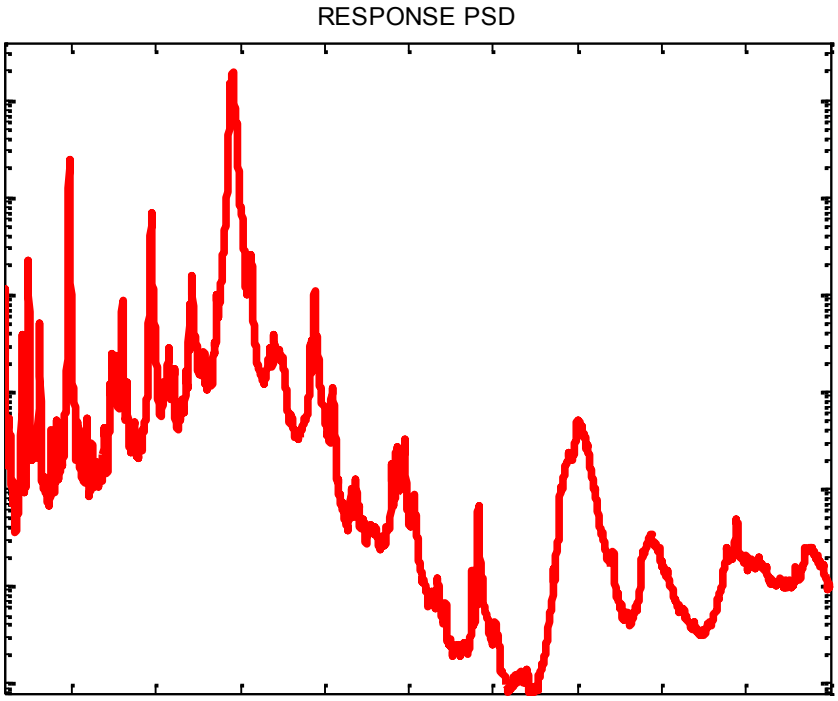

Figure 5.28 Stress PSD Obtained Using Scaled PSD Input

5.2.2 Fatigue Life Analysis of Bracket Using Commercial software

After harmonic analysis with unit load is performed, using the stress results and material information fatigue analyses are performed for real and accelerated loading. All needed parameters mentioned above are used for commercial software too.

As a result, the stress PSD's obtained using real and scaled PSD inputs are given in Figure 5.29 and Figure 5.30, respectively. In addition, the fatigue life results using real and scaled PSD inputs are listed in Table 5.8 and Table 5.9, respectively.

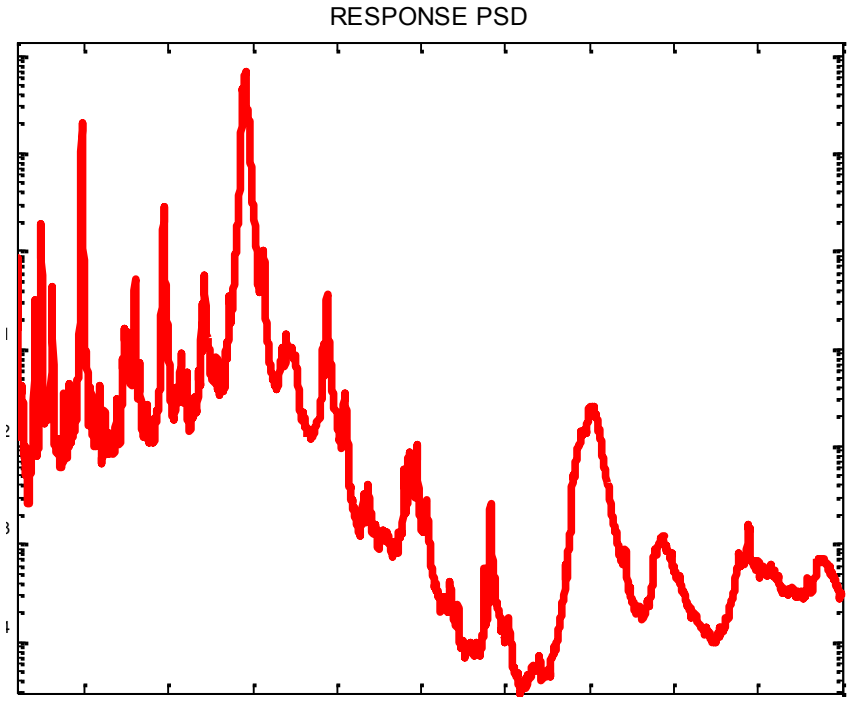

Figure 5.29 Stress PSD Obtained Using Real PSD Input (Commercial Software)

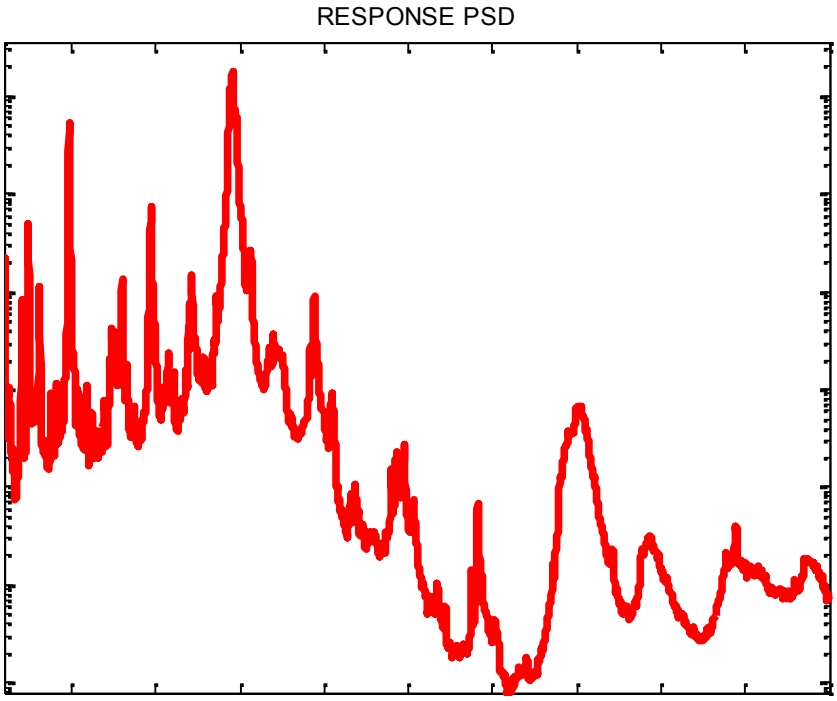

Figure 5.30 Stress PSD Obtained Using Scaled PSD Input (Commercial Software)

Table 5.8 Fatigue Analysis Results Obtained Using Real PSD Input

Node Number	FATIGUE DAMAGE X AXIS REAL LOADING	FATIGUE LIFE (s)	FATIGUE LIFE (h)
29206	8.63E-15	1.16E+14	3.22E+10

Table 5.9 Fatigue Analysis Results Obtained Using Scaled PSD Input

Node Number	FATIGUE DAMAGE X AXIS SCALED LOADING	FATIGUE LIFE (s)	FATIGUE LIFE (h)
29206	6.17E-05	1.62E+04	4.50E+00

5.2.3 Fatigue Life Testing of the Bracket

The fixture is fixed to vibration shaker as shown in Figure 5.6. The PSD profile shown in Figure 4.30 is the input.

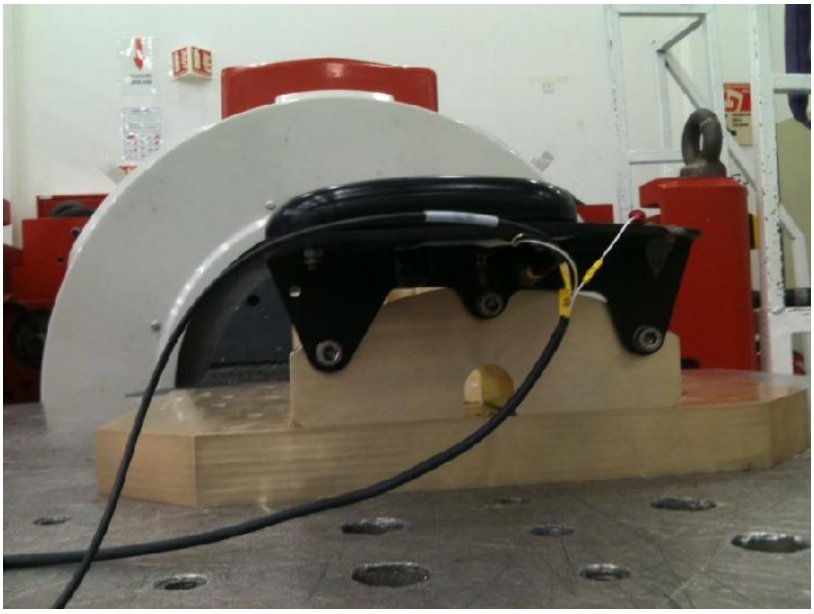

Figure 5.31 A View of the Cantilever Beam Fixture Fixed to Electromagnetic Vibration Test Equipment

As it is seen, the excitation direction of the shaker is normal to the gravity direction similar to cantilever beam fatigue test. Hence there is no mean stress correction for the numerical calculations too. When the crack is observed the test is stopped and the time from the beginning to the end of the test is accepted to be the fatigue life of the bracket. After 240 minutes, bracket is controlled in every 10 minutes and fatigue occurred in 317 minutes. The final view of the bracket that is subjected to fatigue test is given in Figure 5.32.

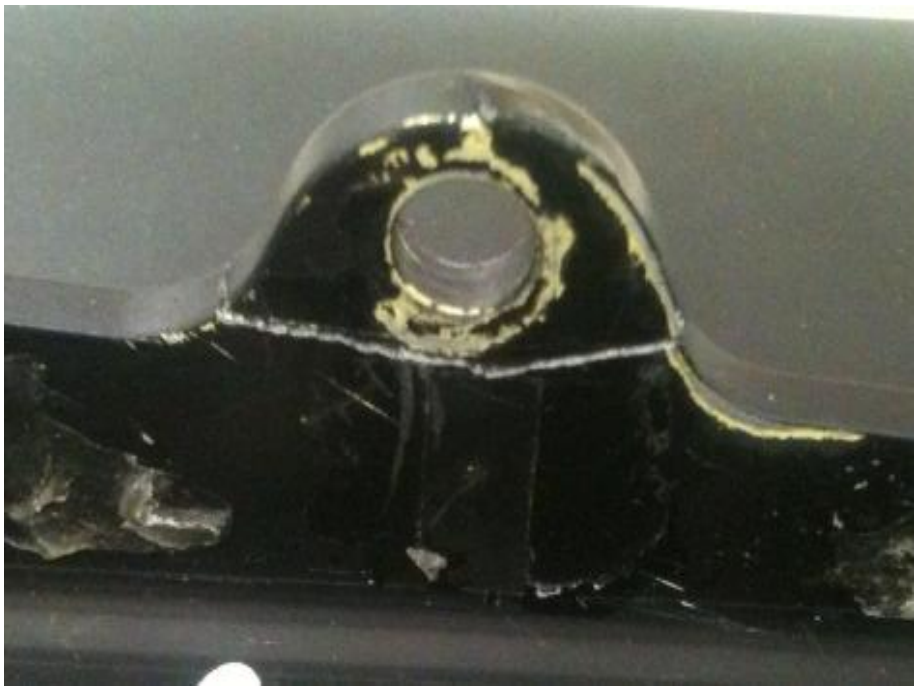

Figure 5.32 Final View of the Bracket that is subjected to Fatigue Test

5.2.4 Fatigue Life Results Comparison of the Bracket

As mentioned in the vibration fatigue theory section, PDF is calculated from stress PSD; hence the accuracy of obtained stress PSD is very important. Considering this effect, stress PSD's obtained from the numerical code and commercial software are compared which is given in Figure 5.33. Comparison of fatigue life results is performed and it is given in Table 5.10.

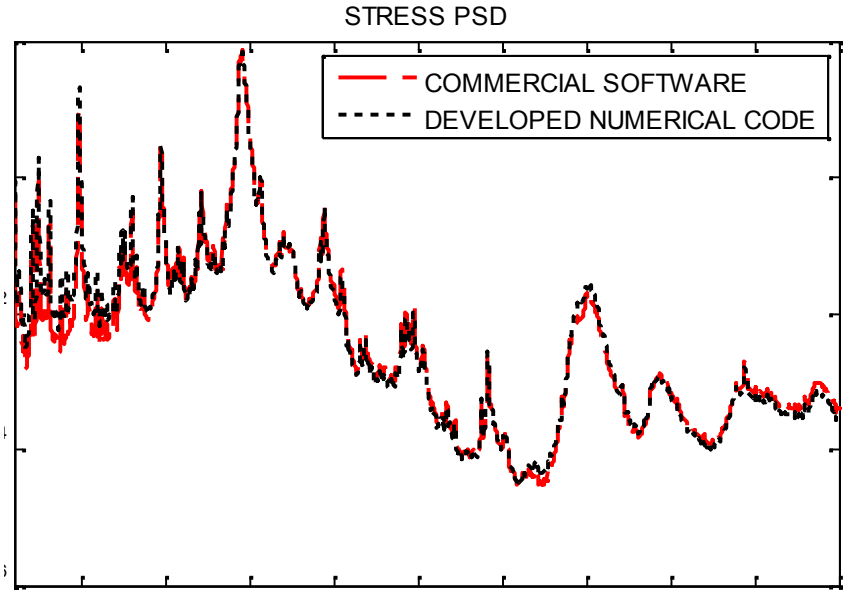

Figure 5.33 Comparison of PSD's Obtained from Numerical Code and Commercial software Using Scaled PSD Input

Table 5.10 Fatigue Life Result Comparison

	Numerical Code Result	**Commercial software Result**
Fatigue Life (s)	8.75E+13	1.16E+14

As mentioned for comparison of stress PSD's obtained from developed numerical code and commercial software for cantilever beam, commercial software uses its own algorithm while calculating stress PSD, hence the difference of the fatigue life results of the Bracket given in Table 5.10 is considerably enough to justify that developed numerical code gives accurate result according to commercial software.

Also comparison of accelerated fatigue life analyses and test results is performed and it is given in Table 5.11. In addition, comparison of the locations of the crack initiation for both finite element and manufactured models is given in Figure 5.34.

Table 5.11 Fatigue Life Result Comparison

	Numerical Code Result	**Commercial software Result**	**Fatigue Test Result**
Fatigue Life (m)	240	271	317

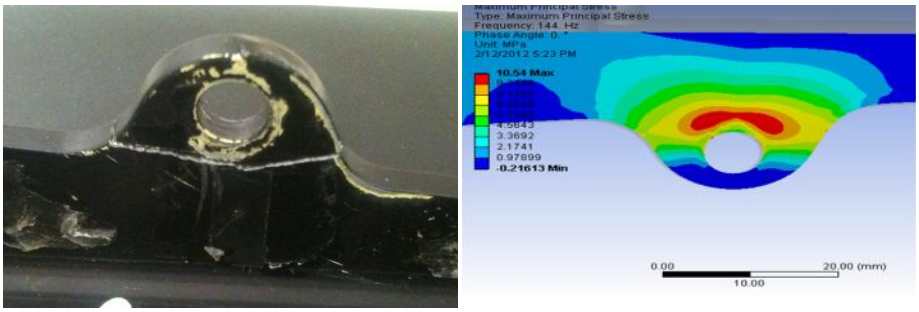

Figure 5.34 Final View of the Bracket that is subjected to Fatigue Test

5.3 Case Studies

After critical direction of the loading and the node on the finite element model are identified, fatigue life of Bracket is calculated using different vibration fatigue theories mentioned in Chapter 2. The obtained fatigue life results are given in Table 5.12. In addition, in order to see whether the PSD loading determined by MIL-STD-810F [28] is conservative or not, fatigue life results of Bracket are obtained using PSD input given in Figure 4.29 according to all vibration fatigue theories too. The identified critical node and direction of the loading are used for fatigue analyses. The fatigue life results obtained using MIL-STD-810F [28] PSD loading are given in Table 5.13.

Table 5.12 Fatigue Life Results of the bracket by Using Different Vibration Fatigue Theories for Node 29206 (The Real Load is Applied on the Direction of X Axis)

VIBRATION FATIGUE	FATIGUE LIFE (s)	FATIGUE LIFE (h)
NARROW-BAND	8.49E+13	2.36E+10
WIRCHING	1.98E+14	5.50E+10
TUNNA	8.49E+13	2.36E+10
HANCOCK	3.12E+11	8.68E+07
KAM and DOVER	4.10E+11	1.14E+08
STEINBERG	2.39E+11	6.63E+07
DIRLIK	8.75E+13	2.43E+10

Table 5.13 Fatigue Life Results of the bracket by Using Different Vibration Fatigue Theories for Node 29206 (The MIL-STD-810F [28] PSD Load is Applied on the Direction of X Axis)

VIBRATION FATIGUE	FATIGUE LIFE (s)	FATIGUE LIFE (h)
NARROW-BAND	9.65E+04	2.68E+01
WIRCHING	1.71E+05	4.75E+01
TUNNA	9.65E+04	2.68E+01
HANCOCK	2.49E+03	6.92E-01
KAM and DOVER	2.72E+03	7.55E-01
STEINBERG	2.31E+03	6.43E-01
DIRLIK	9.81E+04	2.72E+01

As expected, more conservative results are obtained from fatigue analyses performed using PSD input defined in MIL-STD-810F [28]. Generally, if there is no measured loading data, the loading data given in MIL-STD-810F [28] is used while performing analyses. However, it can be concluded that using PSD input MIL-STD-810F [28] can lead to overdesign of the structures due to very conservative results.

Fatigue life analyses using all vibration fatigue theories are also performed for the cantilever beam and the results are given in Table 5.14

Table 5.14 Fatigue Life Results of Cantilever Beam by Using Different Vibration Fatigue Theories

VIBRATION FATIGUE	FATIGUE LIFE (s)	FATIGUE LIFE (m)
NARROW-BAND	9.57E+01	1.59E+00
WIRCHING	1.59E+02	2.65E+00
TUNNA	6.05E+02	1.01E+01
HANCOCK	3.76E-03	6.27E-05
KAM and DOVER	3.76E-03	6.27E-05
STEINBERG	3.76E-03	6.27E-05
DIRLIK	9.84E+02	1.64E+01

Before performing fatigue tests, considering the studies in reference [10] and [29], although it depends on the characteristic of the loading, it is concluded that Dirlik [9] method generally gives the most accurate results of fatigue life. However, when the fatigue life results in Table 5.12 and Table 5.14 are analyzed, it can be easily observed that in Table 5.12, other methods like Tunna and Narrow-Band give also considerably similar results that of Dirlik and experiment while in Table 5.13 these indicated methods give considerably different results that of Dirlik and experiment.

In order to recognize the how such a situation occurs, irregularity factors are checked and given in Figure 5.35 and Figure 5.36 for the performed analyses of the Bracket and cantilever beam, respectively. As mentioned in Chapter 2 if the irregularity factor is closer to 1 process tends to be Narrow-Band and if it is closer to 0, process tends to be White Noise.

When the Figure 5.35 is checked carefully, it can be easily observed that irregularity factor is close to 1 and the process tends to be Narrow-Band. Since, naturally Narrow-Band and Tunna methods give considerably similar results to that of Dirlik and experiment.

However, when the the Figure 5.36 is checked carefully, it can be easily observed that irregularity factor is close to 0 and the process tends to be White-Noise. Since, naturally Narrow-Band and Tunna methods give more conservative results than that of Dirlik and experiments.

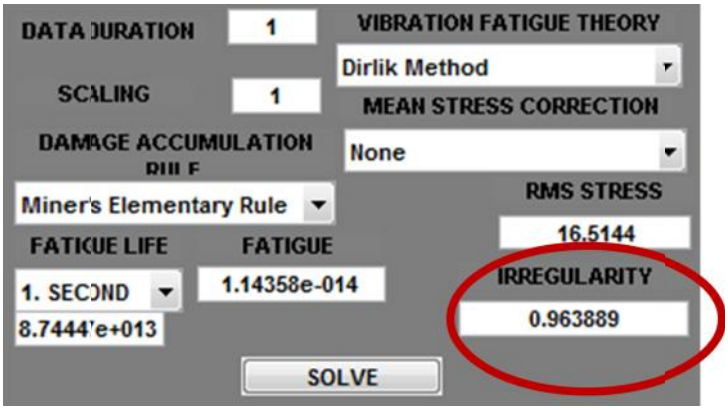

Figure 5.35 The Irregularity Factor Obtained from the Fatigue Life Analysis of the Bracket

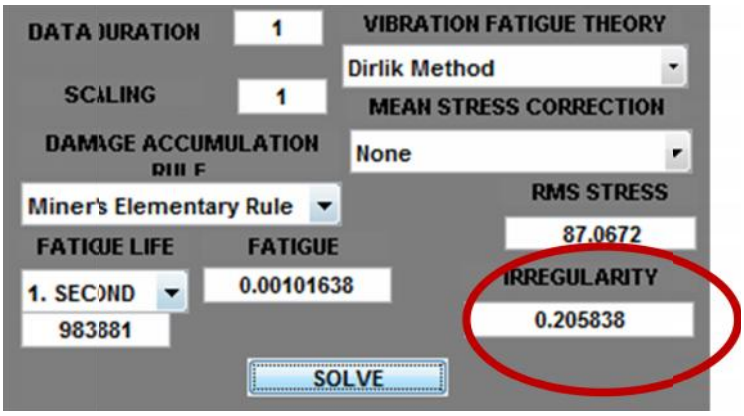

Figure 5.36 The Irregularity Factor Obtained from the Fatigue Life Analysis of the Cantilever Beam

In addition, in order to observe how the damping ratio affects the fatigue life results of the cantilever beam, four different fatigue life analyses are performed using 0.5%, 1%, 1.5% and 2% constant damping ratios and the results are given in Table 5.15.

Table 5.15 Fatigue Life Results of Cantilever Beam For Three Different Damping Ratios

FATIGUE THORIES	**FATIGUE LIFE (s)**			
FREQUENCY	**0.5%**	**1%**	**1.5%**	**2%**
NARROW-BAND	1.47E+02	2.58E+02	4.13E+02	6.73E+02
WIRCHING	2.45E+02	4.29E+02	6.87E+02	1.12E+03
TUNNA	1.22E+03	4.26E+03	1.08E+04	2.21E+04
HANCOCK	5.04E-03	5.25E-03	5.35E-03	6.60E+00
KAM and DOVER	5.04E-03	5.25E-03	5.35E-03	5.44E-03
STEINBERG	5.04E-03	5.25E-03	5.35E-03	5.44E-03
DIRLIK	1.41E+03	2.90E+03	5.00E+03	8.35E+03

Analyzing the results given in Table 5.15, it can be concluded that damping ratio of the structure affects the fatigue life significantly. Hence, accurate damping ratios should be used while performing fatigue analyses.

According to ASTM E 1048 85 [24], rainflow counting algorithm is developed and used in time domain fatigue life calculations. Detailed information about how rainflow counting algorithm is developed is given in Appendix B. This algorithm is also embedded in the developed numerical code.

In order to compare the fatigue life results obtained in time and frequency domains, stress history of the location where strain gage is glued on the Bracket is obtained in both time and frequency domains as mentioned in Chapter 4. It can be easily observed that strain gage is not on the most critical location; hence, the measured data will be used only for case study. Using developed rainflow algorithm, rainflow counting of the stress-time history (Figure 4.22) is performed and fatigue life is obtained. Then, using the stress PSD data (Figure 4.23), fatigue life is calculated for all vibration fatigue theories.

Similarly the strain gage on the cantilever beam couldn't be located on the most critical location due to geometric properties of notch and strain gage. However, since maximum and minimum principal stress values of the cantilever beam are close to normal stress values on the area of the most critical location, the strain gage data given in Figure 4.9 is scaled for the most critical location.

The scaled strain gage data in the time and frequency domains are given in Figure 5.37 and Figure 5.38, respectively.

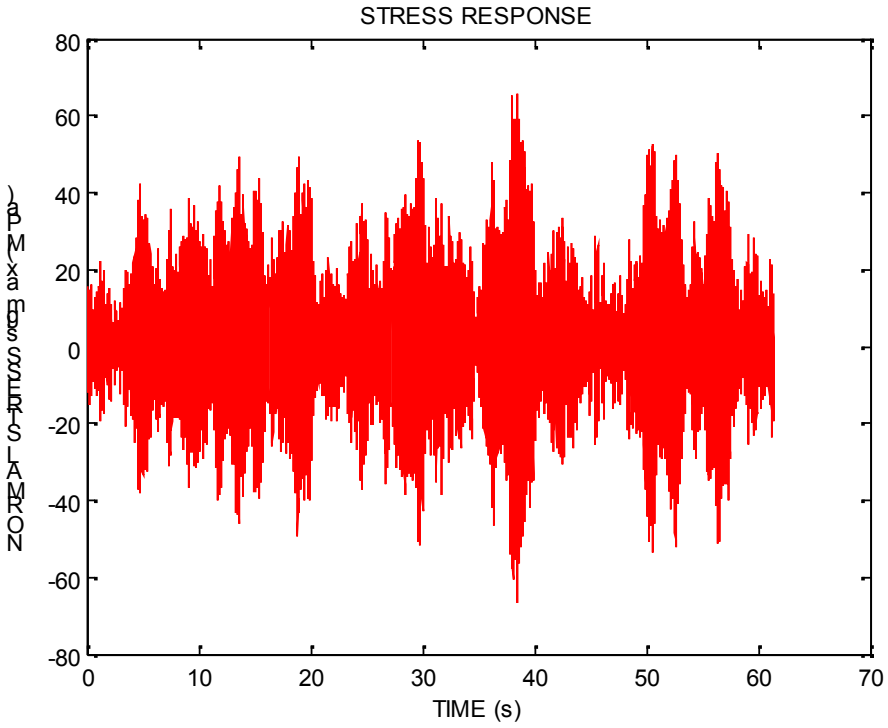

Figure 5.37 Scaled Stress Data for 0.001 g^2/Hz White Noise PSD Input for the Most Critical Location of Cantilever Beam

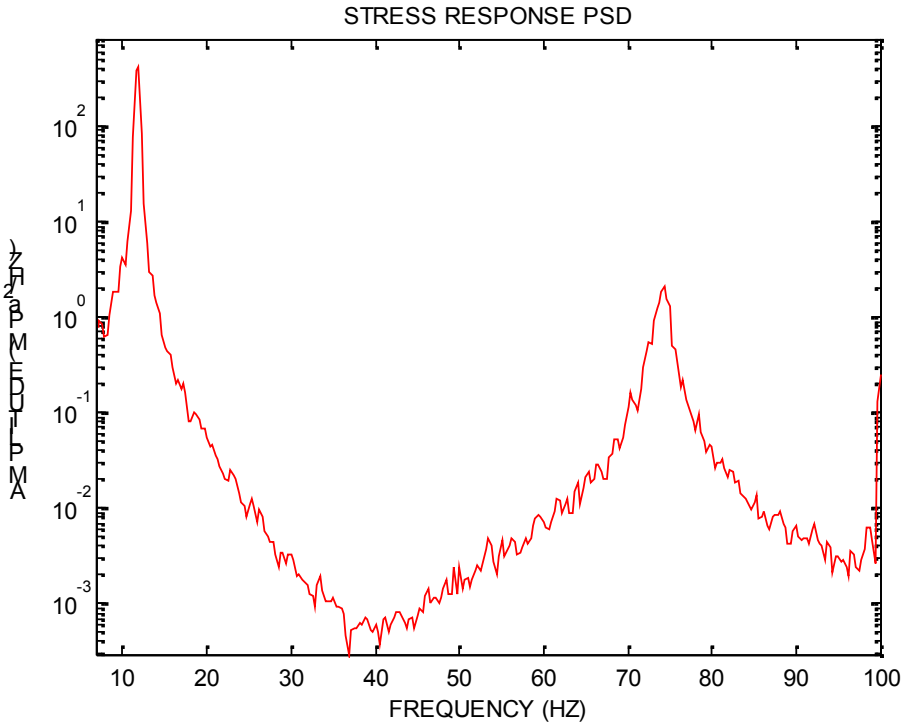

Figure 5.38 Scaled Stress PSD Data for 0.001 g^2/Hz White Noise PSD Input for the Most Critical Location of Cantilever Beam

The obtained data from this strain gage was used for verification of finite element model as mentioned above. In addition, the scaled data given in Figure 5.37 is used for case study in this section. In order to compare fatigue life results obtained in both time and frequency domains, the required calculations are carried out as follows:

Firstly, rainflow counting of the stress-time history Figure 5.37 is performed and using the results of the rainflow counting, fatigue life analysis is carried out by the developed numerical code. Then, using stress PSD data (Figure 5.38) fatigue life calculations are carried out for all vibration fatigue theories.

The comparisons of the results for the Bracket and the cantilever beam are given in Table 5.16 and Table 5.17 respectively.

Table 5.16 Comparison of Fatigue Life Results Calculated in Time and Frequency Domains (Bracket)

FATIGUE THORIES	FATIGUE LIFE (s)	FATIGUE LIFE (h)
FREQUENCY DOMAIN		
NARROW-BAND	2.26E+26	6.27E+22
WIRCHING	5.19E+26	1.44E+23
TUNNA	2.26E+26	6.27E+22
HANCOCK	7.84E+23	2.18E+20
KAM and DOVER	1.02E+24	2.83E+20
STEINBERG	6.35E+23	1.76E+20
DIRLIK	2.28E+26	6.35E+22
TIME DOMAIN		
RAINFLOW COUNTING	2.07E+26	5.74E+22

Table 5.17 Comparison of Fatigue Life Results Calculated in Time and Frequency Domains (Cantilever Beam)

FATIGUE THORIES	FATIGUE LIFE (s)	FATIGUE LIFE (h)
FREQUENCY DOMAIN		
NARROW-BAND	4.14E+09	1.15E+06
WIRCHING	6.89E+09	1.91E+06
TUNNA	9.95E+09	2.76E+06
HANCOCK	1.72E+07	4.78E+03
KAM and DOVER	1.93E+07	5.37E+03
STEINBERG	7.08E+06	1.97E+03
DIRLIK	1.40E+10	3.89E+06
TIME DOMAIN		
RAINFLOW COUNTING	1.43E+10	3.97E+06

The fatigue life results obtained using the same stress history expected to be the similar in time and frequency domains. When the results given in Table 5.16 are analyzed, it is seen that the fatigue life results that are obtained using Dirlik, Tunna and Narrow-Band solutions are considerably similar to that of Rainflow counting method in the time domain.

The reason of getting almost the same fatigue life results using Dirlik, Tunna and Narrow-Band methods is that irregularity factor is closer to 1 for the all obtained stress PSD's as indicated above.. However, when the results in Table 5.17 are analyzed, since irregularity factor is not closer to 1, Dirlik method gives the closest result to that of Rainflow counting.

CHAPTER 6

DISCUSSION AND CONCLUSION

In this study, a numerical code is developed in order to perform vibration induced fatigue calculations using vibration fatigue theories in the literature. The code is also capable of making fatigue life calculations in the time domain. Then by using this developed numerical code, fatigue life analyses of Bracket which is installed on an air platform together with a cantilever beam which is used for verification of the accuracy of the code are performed.

It is known that a slight increase of the stress causes considerable reduction in the fatigue life. Hence while performing fatigue analyses, the used finite element model has to be constructed precisely. However, complex structures, contacts, assemblies, complex boundary conditions or non linearity can cause unexpected stresses and this affects the accuracy of the fatigue life calculation. Hence, for verification of developed code, a simple cantilever beam is selected as a case study in order to avoid such a situation.

To begin with, finite element model of the cantilever beam is constructed and then vibration and strain gage experiments are performed for verification of finite element model. After the results are compared and finite element model is verified, fatigue analyses and tests are performed. While performing fatigue analysis of cantilever beam, damping ratios measured from FRF's are used.

Also fatigue analyses are repeated using different damping ratios and it is observed that damping ratio affects the fatigue life results considerably.

As indicated above there is small difference between commercial software and developed numerical code fatigue life results. The reason of this difference is due to the fact that while obtaining stress PSD's, commercial software determines the frequency resolution using its own algorithm which is different from harmonic analysis resolution. Hence, this different resolution of frequency causes small changes in RMS stress values. However, due to high sensitivity of fatigue life to stress, the indicated differences in fatigue life results are obtained. When the stress PSD obtained from commercial software is used by developed numerical code, it is observed that calculated fatigue life results are almost the same which points to the accuracy of the developed numerical code.

Fatigue tests are performed for 7 different beams. Beams are manufactured from standard sheet metal. In order to accelerate fatigue tests, two sided notches are placed close to the end of the cantilever beam from which it is fixed. Since notches cause stress concentrations, the notch areas were manufactured delicately. As mentioned above, stress life approach used in fatigue life calculations gives information about the structures until crack initiation starts. Hence, fatigue tests are ended when visible cracks occur. While performing fatigue tests, in order to check whether crack started to initiate or not, shaker is stopped periodically to observe the notch area. Periodic checking is started 3 minutes before the time indicated by fatigue life analysis result.

When fatigue test results are analyzed, it can be concluded that there are differences between fatigue life values. These differences occur due to errors in recognition of crack initiation times and although all beams are manufactured as delicately as possible to have the same dimensions and characteristics, there are small differences between beams due to manufacturing. The results obtained from fatigue tests are averaged before comparing the fatigue analysis and test results.

Moreover, when fatigue analysis and tests are compared, it can be observed that there are differences between them too. The reasons for these differences are predicted to be caused by differences between exact and measured values of the damping ratios, impossibility of exact manufacturing of the cantilever beam and unknown notch sensitivity of the material. In addition, as it is indicated above, the fatigue tests are stopped when visible cracks occur; hence, the differences between analyses and fatigue tests may also occur due to in recognition of crack initiation times

While measuring damping ratios, there are many factors that affect the accuracy of the damping ratio such as resolution of the frequency of FRF data (very effective when there is light damping). Considering the factors that affect the fatigue tests and analysis, the similarity of the results are acceptable and enough for verification of numerical code.

After the numerical code is verified, the same processes done for cantilever beam are performed for Bracket. First, finite element model is constructed and then it is verified with vibration and strain gage experiments. In addition, in order to obtain the real life loading that Bracket is subjected to, flight test is performed. First contents of flight are determined with pilots in accordance with real life use and then acceleration-time data is stored during whole flight. The contents of maneuvers during the flight are also important because the Bracket has to be exposed to real operational loading during flight test. In order to make vibration fatigue analysis, acceleration data is transformed from time domain to frequency domain. The accuracy of the loading is very important because the amplitude of the stress is very sensitive to frequency and amplitude of the loading. Hence, the flight test is mainly committed to obtaining accurate loading information.

Before fatigue analyses are carried out critical nodes are identified using the results of performed harmonic analyses on the each axis. Then, fatigue analyses are performed on the each axis of Bracket using measured loading and verified finite element model and fatigue life values of all the critical points are obtained.

When the results are analyzed, it is observed that fatigue damage occurs due to loading on the X axis of the Bracket as expected. It was expected because X axis loading has the largest RMS acceleration value and it is known that modes cannot be excited significantly by the loadings on other axes. It is assumed that the damage contribution of loadings on the other axes can be neglected. Then, in order to perform fatigue test the measured loading is scaled for obtaining feasible test duration and the fatigue analyses are repeated using the scaled PSD input.

The factors that affect the fatigue life of the structures are certainly valid for the bracket that is installed on air platform. Due to that fact that obtaining the exact damping ratio and perfectly manufactured structures is not practically possible addition to unknown notch sensitivity factor and impossibility of obtaining the exact crack initiation time, calculated fatigue life results are already expected to be slightly different from the fatigue life test result. However, the results obtained from the fatigue analysis and real life test are considerably close enough to justify that the analysis is significantly accurate. Also if the numbers of the fatigue tests are being increased, the absolute fatigue life of the bracket can be concluded as performed for cantilever beam.

REFERENCES

[1] "Fatigue (Material)," 2011. [Online]. Available: http://en.wikipedia.org/wiki/Fatigue_(material). Last accessed on 06/02/2012

[2] S. O. Rice, "Mathematical Analysis of Random Noise," *Selected Papers on Noise and Stochastic Processes, Dover, New York*, 1954.

[3] J. S. Bendat, "Probability functions for random responses," *NASA report on contract NAS-4590*, 1964.

[4] P.H. Wirsching and M. C. Light, "Fatigue under wide band random loading", Journal of Structural Division," pp. ASCE, pp. 1593-1607, 1980.

[5] G. K. Chaudhury and W. D. Dover, "Fatigue analysis of offshore platforms subject to sea w a v e loadings," *International Journal of Fatigue*, vol. 1, no. 1, pp. 13-19, 1985.

[6] J. M. Tunna, "Fatigue Life Prediction for Gaussian Random Loads at the Design Stage," *Fatigue Fact Engineering Mat. Struct*, vol. 9, no. 3, pp. 169-184, 1986.

[7] J. C. P. Kam and W. D. Dover, "Fast Fatigue Assessment Procedure for Offshore Structures under Random Stress History," *Proceedings of the Institution of Civil Engineers*, vol. 85, pp. 689-700, 1988.

[8] D. S. Steinberg, *Vibration Analysis for Electronic Equipment*, 3rd ed. John Wiley & Sons, 2000.

[9] T. Dirlik, "Application of computers in Fatigue Analysis," University of Warwick, 1985.

[10] N. W. M. Bishop and F. Sherratt, *Finite Element Based Fatigue Calculations*. NAFEMS, GERMANY, 2005.

[11] G. Petrucci and B. Zuccarello, "On the estimation of the fatigue cycle distribution from spectral density data," *Proceedings of the Institution of Mechanical Engineers, Part C: Journal of Mechanical Engineering Science*, vol. 213, no. 8, pp. 819-831, Aug. 1999.

[12] G. Petrucci and B. Zuccarello, “Fatigue life prediction under wide band random loading,” *Materials and Structures*, no. April, pp. 1183-1195, 2004.

[13] R. Tovo, “loading,” *International Journal of Fatigue*, vol. 24, pp. 1137-1147, 2002.

[14] D. Benasciutti and R. Tovo, “Spectral Methods for Lifetime Prediction under Wide-band,” *International Journal of Fatigue*, vol. 27, pp. 867-877, 2005.

[15] I. Rychlik, “On the ‘narrow-band’ approximation for expected fatigue damage,” *Probabilistic Engineering Mechanics*, vol. 8, no. 1, pp. 1-4, 1993.

[16] H. O. Madsen, S. Krenk, and N. C. Lind, *Methods of structural safety*, vol. 13, no. 3. 1986, p. 400.

[17] H. Y. Liou, W. F. Wu, and C. S. Shin, “A modified model for the estimation of fatigue life derived from random vibration theory,” *Probabilistic Engineering Mechanics*, vol. 14, pp. 281-288, 1999.

[18] W. F. Wu, H. Y. Liou, and H. C. Tse, “Estimation of fatigue damage and fatigue life of components under random loading,” vol. 161, no. 97, pp. 243-249, 1997.

[19] X. Pitoiset and A. Preumont, “Spectral methods for multiaxial random fatigue analysis of metallic structures,” *International Journal of Fatigue*, vol. 22, pp. 541-550, 2000.

[20] M. Aykan, “VIBRATION FATIGUE ANALYSIS OF EQUIPMENTS USED IN,” M.Sc. Thesis, Middle East Technical University, Ankara, 2005.

[21] Kocer B., “VIBRATION FATIGUE ANALYSIS OF STRUCTURES UNDER BROADBAND EXCITATION,” M.Sc. Thesis, Middle East Technical University, Ankara, 2010.

[22] J. Marin, *Mechanical Behavior of Engineering Materials*. Prentice-Hall, Englewood Cliffs, N.J., 1962, p. 224.

[23] A. Esin, “Properties of Materials for Mechanical Design,” Middle East Technical University, Gaziantep, 1981.

[24] “ASTM Designation E 1049-85: Standard Practices for Cycle Counting in Fatigue Analysis 1,” *Read*, vol. 85, no. Reapproved, pp. 1-10, 1997.

[25] M. Matsuishi and T. Endo, “Fatigue of metals subjected to varying stress,” *Japan Society of Mechanical Engineers Fukuoka Japan*, pp. 37–40, 1968.

[26] N. Bishop, “Fatigue Analysis of a Missile Shaker Table Mounting Bracket,” *Time*.

[27] “ANSYS Classic 11.0 and ANSYS Workbench 11.0 Help Manual.” .

[28] MIL-STD-810F, “Environmental Engineering Considerations and Laboratory Tests,” *Department of Defense Test Method Standard, USA*, 2000.

[29] V. K. Nagulapalli, A. Gupta, and S. Fan, “Estimation of Fatigue Life of Aluminum Beams subjected to Random Vibration Vinod Kumar Nagulapalli , Abhijit Gupta , and Shaofeng Fan Northern Illinois University,” *Mechanical Engineering*, no. 1.

[30] T. Irvine, “Vibration Response Spectrum.” pp. 1-20, 2009.

[31] Dr Neil Bishop, A. Caserio, and C. Mesa, “Vibration Fatigue Analysis in the Finite Element Environment,” *Americas User Conference, California*, pp. 1-15, 1998.

APPENDIX A

VERIFICATION OF THE METHOD USED TO OBTAIN STRESS PSD

In this study in order to obtain stress PSD of a base excited system, first harmonic analysis is performed with a unit global load instead of performing base excitation random vibration analysis. Because harmonic analysis results do not loose sign of stresses which allow calculating principal stresses. After harmonic analysis is performed, stress transfer function is obtained and multiplying square of obtained transfer function by PSD input, stress response PSD is obtained (Equation (A.1)).

$$PSD_{input} * Transfer\ Function^2 = \text{Response PSD} \tag{A.1}$$

According to unit of PSD input, unit of load used in harmonic analysis can be changed. Since in our case unit of the PSD input is g^2/Hz, 1 g load is selected as a unit load in order to perform harmonic analysis and for a general case units of PSD input, transfer function and response PSD should be as follow; (Equation(A.2))

$$\frac{g^2}{Hz} \cdot \left(\frac{MPa}{g}\right) = \frac{MPa^2}{Hz} \tag{A.2}$$

However, using obtained stress PSD, applying the formulation given in Equation (A.1) instead of that of base excitation random vibration analysis whether is accurate or not can be discussed.

In order to prove the method given Equation (A.1), an example in ANSYS Mechanical APDL VM68 is selected as a case study. This example includes a two degree of freedom system that is subjected to a base excitation PSD as shown in Figure A. 1. Mass and stiffness values are given in Figure A. 1 and damping is taken as 2% viscous damping ratio. This two degree of freedom system is also solved analytically using two different analytical solution methods. First solution is performed using base excitation random analysis and the second solution is carried out by multiplying square of transfer function with PSD input as indicated in Equation (A.1).

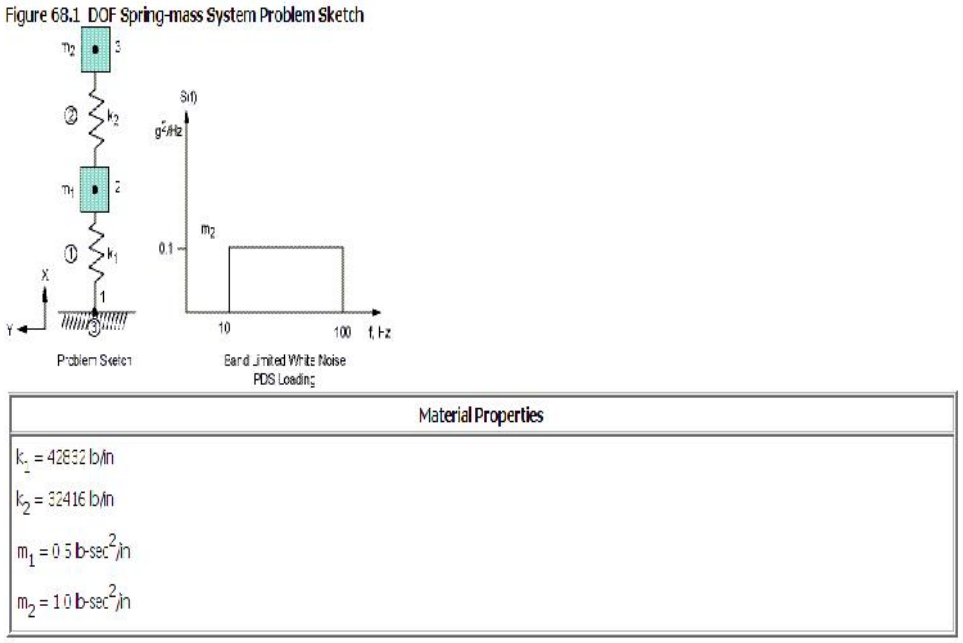

Figure A. 1 Two Degree of Freedom Example in ANSYS Mechanical APDL (VM 68) [27]

The two DOF system that has base acceleration excitation is given in Figure A. 2. The first solution is performed by using this system given in Figure A. 2 and formulations given as follows;

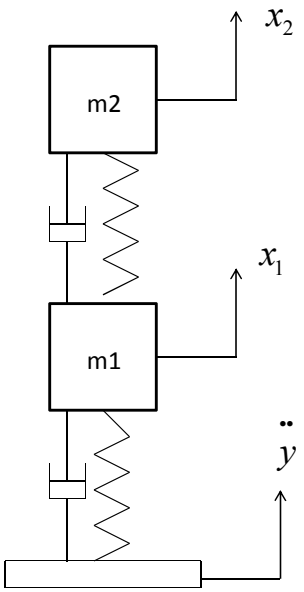

Figure A. 2 Two DOF system that has base acceleration excitation

Relative displacement according to base can be written as follow;

$$z_1 = x_1 - y \tag{A.3}$$

$$z_2 = x_2 - y \tag{A.4}$$

The equation of motion of the system can be formulated as given in Equation (A.5)

.

$$[M]\cdot\left\{\ddot{q}\right\}+[C]\cdot\left\{\dot{q}\right\}+[K]\cdot\left\{q\right\}=\{Q\} \tag{A.5}$$

where,

$$[M]=\begin{bmatrix} m_1 & 0 \\ 0 & m_2 \end{bmatrix} \tag{A.6}$$

$$[C]=\begin{bmatrix} c_1+c_2 & -c_1 \\ -c_1 & c_2 \end{bmatrix} \tag{A.7}$$

$$[K]=\begin{bmatrix} k_1+k_2 & -k_1 \\ -k_1 & k_2 \end{bmatrix} \tag{A.8}$$

$$\{q\}=\begin{Bmatrix} z_1 \\ z_2 \end{Bmatrix} \tag{A.9}$$

$$\{Q\}=\begin{Bmatrix} -m_1 \cdot \ddot{y} \\ -m_2 \cdot \ddot{y} \end{Bmatrix} \tag{A.10}$$

By substituting formulations between Equation (A.6) and Equation (A.10) into Equation (A.5), the Equation (A.11) can be obtained.

$$\begin{bmatrix} m_1 & 0 \\ 0 & m_2 \end{bmatrix} \cdot \begin{Bmatrix} \ddot{z}_1 \\ \ddot{z}_2 \end{Bmatrix} + \begin{bmatrix} c_1+c_2 & -c_1 \\ -c_1 & c_2 \end{bmatrix} \cdot \begin{Bmatrix} \dot{z}_1 \\ \dot{z}_2 \end{Bmatrix} + \begin{bmatrix} k_1+k_2 & -k_1 \\ -k_1 & k_2 \end{bmatrix} \cdot \begin{Bmatrix} z_1 \\ z_2 \end{Bmatrix} = \begin{Bmatrix} -m_1 \cdot \ddot{y} \\ -m_2 \cdot \ddot{y} \end{Bmatrix} \tag{A.11}$$

All equations indicated are above are in physical domain. In order to transform the equation into modal domain, the Equation (A.12) is used.

$$\{q\}=[\Phi]\cdot\{\eta\}, \tag{A.12}$$

where, $[\Phi]$ and $\{\eta\}=\begin{Bmatrix} \eta_1 \\ \eta_2 \end{Bmatrix}$ are eigenvectors and modal coordinates, respectively.

By substituting Equation (A.12) into Equation (A.11) and multiplying with $[\Phi]^T$, the Equation (A.13) can be obtained.

$$\begin{Bmatrix} \ddot{\eta} \\ \ddot{\eta} \end{Bmatrix} + \begin{bmatrix} 2\cdot\xi_1\cdot\omega_1 & 0 \\ 0 & 2\cdot\xi_1\cdot\omega_1 \end{bmatrix} \cdot \begin{Bmatrix} \dot{\eta} \\ \dot{\eta} \end{Bmatrix} + \begin{bmatrix} \omega^2{}_1 & 0 \\ 0 & \omega^2{}_2 \end{bmatrix} \cdot \begin{Bmatrix} \eta \\ \eta \end{Bmatrix} = [\Phi]^T \cdot \begin{Bmatrix} -m_1 \cdot \ddot{y} \\ -m_2 \cdot \ddot{y} \end{Bmatrix} \tag{A.13}$$

For the indicated two DOF system, eigenvectors are given in Equation (A.14).

$$[\Phi] = \begin{bmatrix} \Phi^1{}_1 & \Phi^2{}_1 \\ \Phi^1{}_2 & \Phi^2{}_2 \end{bmatrix} \tag{A.14}$$

By using the Equation (A.13) and Equation (A.14), the decoupled equations in modal coordinate can be written as follow;

$$\ddot{\eta}_1 + 2 \cdot \xi_1 \cdot \omega_1 \cdot \dot{\eta} + \omega^2{}_1 \cdot \eta = \Phi_1^1 \cdot (-m_1 \cdot \ddot{y}) + \Phi_2^1 \cdot (-m_2 \cdot \ddot{y}) \tag{A.15}$$

$$\ddot{\eta}_2 + 2 \cdot \xi_2 \cdot \omega_2 \cdot \dot{\eta} + \omega^2{}_2 \cdot \eta = \Phi_1^2 \cdot (-m_1 \cdot \ddot{y}) + \Phi_2^2 \cdot (-m_2 \cdot \ddot{y}) \tag{A.16}$$

By skipping the derivations, finally steady state solution for each modal coordinate can be written as follows;

$$\eta_1(\omega) = \frac{\Phi_1^1 \cdot (-m_1 \cdot \ddot{y}) + \Phi_2^1 \cdot (-m_2 \cdot \ddot{y})}{\omega^2{}_1 - \omega^2 + 2 \cdot \xi_1 \cdot \omega_1 \cdot \omega \cdot i} \cdot e^{(i \cdot \omega \cdot t)} \tag{A.17}$$

$$\eta_2(\omega) = \frac{\Phi_1^2 \cdot (-m_1 \cdot \ddot{y}) + \Phi_2^2 \cdot (-m_2 \cdot \ddot{y})}{\omega^2{}_2 - \omega^2 + 2 \cdot \xi_1 \cdot \omega_2 \cdot \omega \cdot i} \cdot e^{(i \cdot \omega \cdot t)} \tag{A.18}$$

Let's recall Equation (A.12) and transform the system from modal domain to physical domain as follows;

$$\{q\} = [\Phi] \cdot \{\eta\} \tag{A.19}$$

Finally, relative displacement FRF's can be obtained as given in Equation (A.20) and Equation (A.21).

$$z_1 = \left(\Phi_1^1 \cdot \left(\frac{\Phi_1^1 \cdot (-m_1 \cdot \ddot{y}) + \Phi_2^1 \cdot (-m_2 \cdot \ddot{y})}{\omega^2{}_1 - \omega^2 + 2 \cdot \xi_1 \cdot \omega_1 \cdot \omega \cdot i} \right) + \Phi_1^2 \cdot \left(\frac{\Phi_1^2 \cdot (-m_1 \cdot \ddot{y}) + \Phi_2^2 \cdot (-m_2 \cdot \ddot{y})}{\omega^2{}_2 - \omega^2 + 2 \cdot \xi_1 \cdot \omega_2 \cdot \omega \cdot i} \right) \right) \cdot e^{(i \cdot \omega \cdot t)} \tag{A.20}$$

$$z_2 = \left(\Phi_2^1 \cdot \left(\frac{\Phi_1^1 \cdot (-m_1 \cdot \ddot{y}) + \Phi_2^1 \cdot (-m_2 \cdot \ddot{y})}{\omega^2{}_1 - \omega^2 + 2 \cdot \xi_1 \cdot \omega_1 \cdot \omega \cdot i} \right) + \Phi_2^2 \cdot \left(\frac{\Phi_1^2 \cdot (-m_1 \cdot \ddot{y}) + \Phi_2^2 \cdot (-m_2 \cdot \ddot{y})}{\omega^2{}_2 - \omega^2 + 2 \cdot \xi_1 \cdot \omega_2 \cdot \omega \cdot i} \right) \right) \cdot e^{(i \cdot \omega t)} \tag{A.21}$$

The relative displacement can be re-written as follows;

$$z_1 = A_1 \cdot \ddot{y} \cdot e^{(i \cdot \omega \cdot t)}, \tag{A.22}$$

$$z_2 = A_2 \cdot \ddot{y} \cdot e^{(i \cdot \omega \cdot t)}, \tag{A.23}$$

where,

$$A_1 = \left(\Phi_1^1 \cdot \left(\frac{\Phi_1^1 \cdot (-m_1) + \Phi_2^1 \cdot (-m_2)}{\omega^2{}_1 - \omega^2 + 2 \cdot \xi_1 \cdot \omega_1 \cdot \omega \cdot i} \right) + \Phi_1^2 \cdot \left(\frac{\Phi_1^2 \cdot (-m_1) + \Phi_2^2 \cdot (-m_2)}{\omega^2{}_2 - \omega^2 + 2 \cdot \xi_1 \cdot \omega_2 \cdot \omega \cdot i} \right) \right) \tag{A.24}$$

$$A_2 = \left(\Phi_2^1 \cdot \left(\frac{\Phi_1^1 \cdot (-m_1) + \Phi_2^1 \cdot (-m_2)}{\omega^2{}_1 - \omega^2 + 2 \cdot \xi_1 \cdot \omega_1 \cdot \omega \cdot i} \right) + \Phi_2^2 \cdot \left(\frac{\Phi_1^2 \cdot (-m_1) + \Phi_2^2 \cdot (-m_2)}{\omega^2{}_2 - \omega^2 + 2 \cdot \xi_1 \cdot \omega_2 \cdot \omega \cdot i} \right) \right) \tag{A.25}$$

The Fourier transforms are converted to PSD by using the method given in Reference [30] as follows;

$$\lim_{T \to \infty} z_1(\omega) \cdot z_1{}^*(\omega) / T = z_{1\_PSD}(\omega) \tag{A.26}$$

$$\lim_{T \to \infty} z_2(\omega) \cdot z_2{}^*(\omega) / T = z_{2\_PSD}(\omega) \tag{A.27}$$

$$\lim_{T \to \infty} \ddot{y}(\omega) \cdot \ddot{y}^*(\omega) / T = \ddot{y}_{\_PSD}(\omega) \tag{A.28}$$

Finally, the relative displacement PSD's are given as follows;

$$z_{1\_PSD} = z_1 \cdot z_1{}^* = A_1 \cdot A^*{}_1 \cdot \ddot{y} \cdot \ddot{y}^* = A_1 \cdot A^*{}_1 \cdot \ddot{y}_{\_PSD} \tag{A.29}$$

$$z_{2\_PSD} = z_2 \cdot z_2{}^* = A_2 \cdot A^*{}_2 \cdot \ddot{y} \cdot \ddot{y}^* = A_2 \cdot A^*{}_2 \cdot \ddot{y}_{\_PSD} \tag{A.30}$$

where, * represents conjugate of the indicated term.

The two DOF system that has fixed base and unit g loading is given in Figure A. 3. The first solution is performed by using this system given in Figure A. 2 and formulations given as follows;

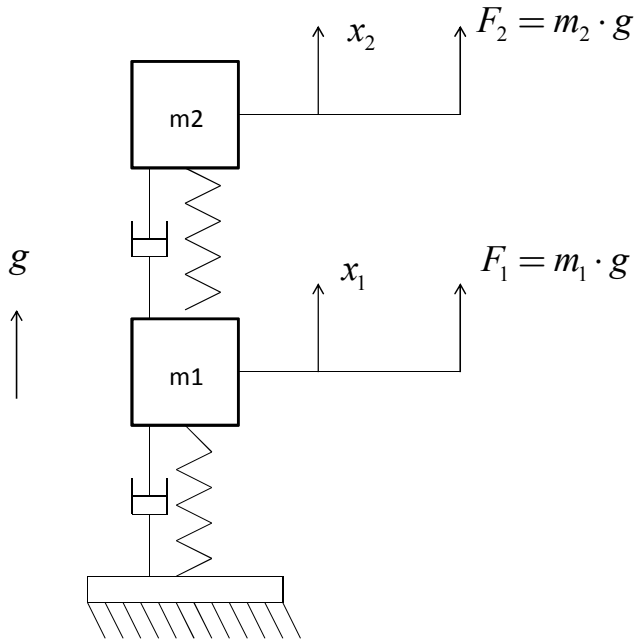

Figure A. 3 Two DOF system that has fixed base and unit g loading

The equation of motion of the system can be formulated as given in Equation (A.31).

$$[M]\cdot\left\{\ddot{q}\right\}+[C]\cdot\left\{\dot{q}\right\}+[K]\cdot\left\{q\right\}=\{Q\} \tag{A.31}$$

where,

$$[M]=\begin{bmatrix} m_1 & 0 \\ 0 & m_2 \end{bmatrix} \tag{A.32}$$

$$[C]=\begin{bmatrix} c_1+c_2 & -c_1 \\ -c_1 & c_2 \end{bmatrix} \tag{A.33}$$

$$[K]=\begin{bmatrix} k_1+k_2 & -k_1 \\ -k_1 & k_2 \end{bmatrix} \tag{A.34}$$

$$\{q\}=\begin{Bmatrix} x_1 \\ x_2 \end{Bmatrix} \tag{A.35}$$

$$\{Q\}=\begin{Bmatrix} m_1 \cdot g \\ m_2 \cdot g \end{Bmatrix} \tag{A.36}$$

By substituting formulations between Equation (A.32) and Equation (A.36) into Equation (A.31), the Equation (A.37) can be obtained.

$$\begin{bmatrix} m_1 & 0 \\ 0 & m_2 \end{bmatrix} \cdot \begin{Bmatrix} \ddot{x}_1 \\ \ddot{x}_2 \end{Bmatrix} + \begin{bmatrix} c_1+c_2 & -c_1 \\ -c_1 & c_2 \end{bmatrix} \cdot \begin{Bmatrix} \dot{x}_1 \\ \dot{x}_2 \end{Bmatrix} + \begin{bmatrix} k_1+k_2 & -k_1 \\ -k_1 & k_2 \end{bmatrix} \cdot \begin{Bmatrix} x_1 \\ x_2 \end{Bmatrix} = \begin{Bmatrix} m_1 \cdot g \\ m_2 \cdot g \end{Bmatrix} \tag{A.37}$$

All equations indicated are above are in physical domain. In order to transform the equation into modal domain, the Equation (A.38) is used.

$$\{q\}=[\Phi]\cdot\{\eta\} \tag{A.38}$$

where, $[\Phi]$ and $\{\eta\}=\begin{Bmatrix} \eta_1 \\ \eta_2 \end{Bmatrix}$ are eigenvectors and modal coordinates, respectively.

By substituting Equation (A.38) into Equation (A.37) and multiplying with $[\Phi]^T$, the Equation (A.39) can be obtained.

$$\begin{Bmatrix} \ddot{\eta} \\ \ddot{\eta} \end{Bmatrix} + \begin{bmatrix} 2\cdot\xi_1\cdot\omega_1 & 0 \\ 0 & 2\cdot\xi_1\cdot\omega_1 \end{bmatrix} \cdot \begin{Bmatrix} \dot{\eta} \\ \dot{\eta} \end{Bmatrix} + \begin{bmatrix} \omega^2{}_1 & 0 \\ 0 & \omega^2{}_2 \end{bmatrix} \cdot \begin{Bmatrix} \eta \\ \eta \end{Bmatrix} = [\Phi]^T \cdot \begin{Bmatrix} m_1 \cdot g \\ m_2 \cdot g \end{Bmatrix} \tag{A.39}$$

For the indicated two DOF system, eigenvectors are given in Equation (A.40).

$$[\Phi]=\begin{bmatrix} \Phi^1{}_1 & \Phi^2{}_1 \\ \Phi^1{}_2 & \Phi^2{}_2 \end{bmatrix} \tag{A.40}$$

By using the Equation (A.39) and Equation (A.40), the decoupled equations in modal coordinate can be written as follows;

$$\ddot{\eta}_1 + 2\cdot\xi_1\cdot\omega_1\cdot\dot{\eta} + \omega^2{}_1\cdot\eta = \Phi_1^1\cdot(-m_1\cdot g) + \Phi_2^1\cdot(-m_2\cdot g) \tag{A.41}$$

$$\ddot{\eta}_2 + 2\cdot\xi_2\cdot\omega_2\cdot\dot{\eta} + \omega^2{}_2\cdot\eta = \Phi_1^2\cdot(-m_1\cdot g) + \Phi_2^2\cdot(-m_2\cdot g) \tag{A.42}$$

By skipping the derivations, finally steady state solution for each modal coordinate can be written as follows;

$$\eta_1(\omega) = \frac{\Phi_1^1\cdot(-m_1\cdot g) + \Phi_2^1\cdot(-m_2\cdot g)}{\omega^2{}_1 - \omega^2 + 2\cdot\xi_1\cdot\omega_1\cdot\omega\cdot i}\cdot e^{(i\cdot\omega\cdot t)} \tag{A.43}$$

$$\eta_2(\omega) = \frac{\Phi_1^2\cdot(-m_1\cdot g) + \Phi_2^2\cdot(-m_2\cdot g)}{\omega^2{}_2 - \omega^2 + 2\cdot\xi_1\cdot\omega_2\cdot\omega\cdot i}\cdot e^{(i\cdot\omega\cdot t)} \tag{A.44}$$

Let's recall Equation (A.12) and transform the system from modal domain to physical domain as follows;

$$\{q\} = [\Phi]\cdot\{\eta\} \tag{A.45}$$

Finally, relative displacement FRF's can be obtained as given in Equation (A.46) and Equation (A.47).

$$x_1 = \left(\Phi_1^1\cdot\left(\frac{\Phi_1^1\cdot(-m_1\cdot g)+\Phi_2^1\cdot(-m_2\cdot g)}{\omega^2{}_1-\omega^2+2\cdot\xi_1\cdot\omega_1\cdot\omega\cdot i}\right)+\Phi_1^2\cdot\left(\frac{\Phi_1^2\cdot(-m_1\cdot g)+\Phi_2^2\cdot(-m_2\cdot g)}{\omega^2{}_2-\omega^2+2\cdot\xi_1\cdot\omega_2\cdot\omega\cdot i}\right)\right)\cdot e^{(i\cdot\omega t)} \tag{A.46}$$

$$x_2 = \left(\Phi_2^1\cdot\left(\frac{\Phi_1^1\cdot(-m_1\cdot g)+\Phi_2^1\cdot(-m_2\cdot g)}{\omega^2{}_1-\omega^2+2\cdot\xi_1\cdot\omega_1\cdot\omega\cdot i}\right)+\Phi_2^2\cdot\left(\frac{\Phi_1^2\cdot(-m_1\cdot g)+\Phi_2^2\cdot(-m_2\cdot g)}{\omega^2{}_2-\omega^2+2\cdot\xi_1\cdot\omega_2\cdot\omega\cdot i}\right)\right)\cdot e^{(i\cdot\omega t)} \tag{A.47}$$

The unit of the x_1 and x_2 is $\frac{m}{g}$. By using the Equation (A.1), displacement PSD can be obtained as follows;

$$x_{1\_PSD} = (x_1)^2 \cdot \ddot{y}_{\_PSD} \tag{A.48}$$

$$x_{2\_PSD} = (x_2)^2 \cdot \ddot{y}_{\_PSD} \tag{A.49}$$

The PSD results of relative displacement according to base are obtained and all results with comparison of them are given between Figure A. 4 and Figure A. 11.

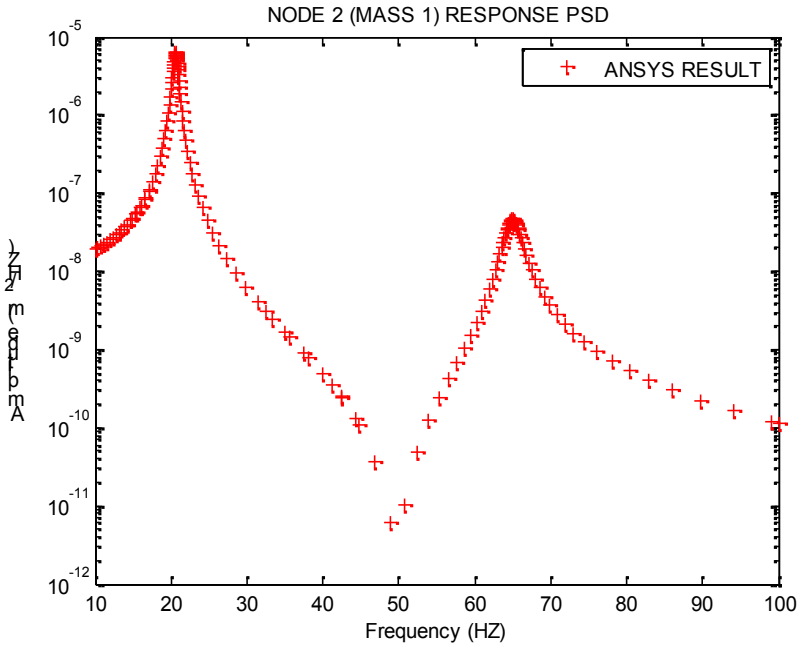

Figure A. 4 Displacement PSD of Mass 1, ANSYS

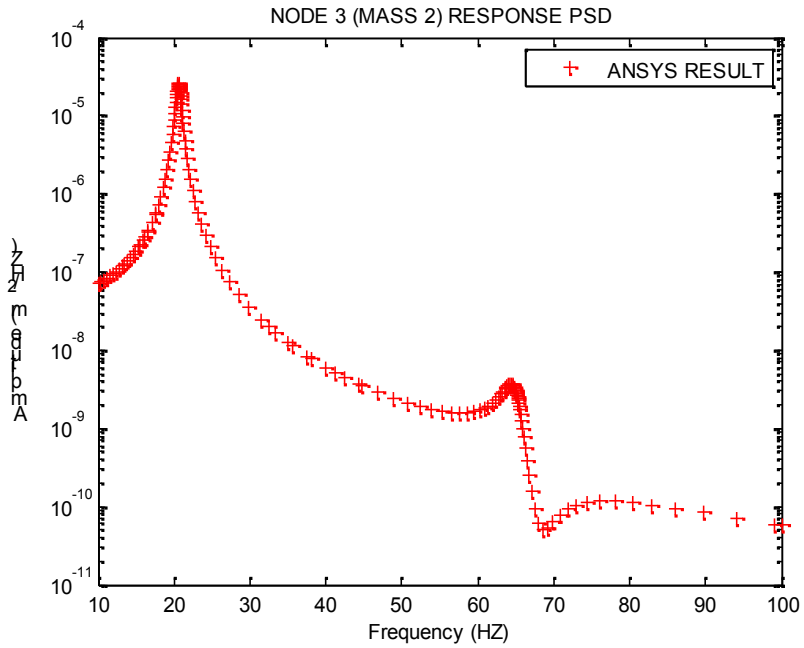

Figure A. 5 Displacement PSD of Mass 2, ANSYS

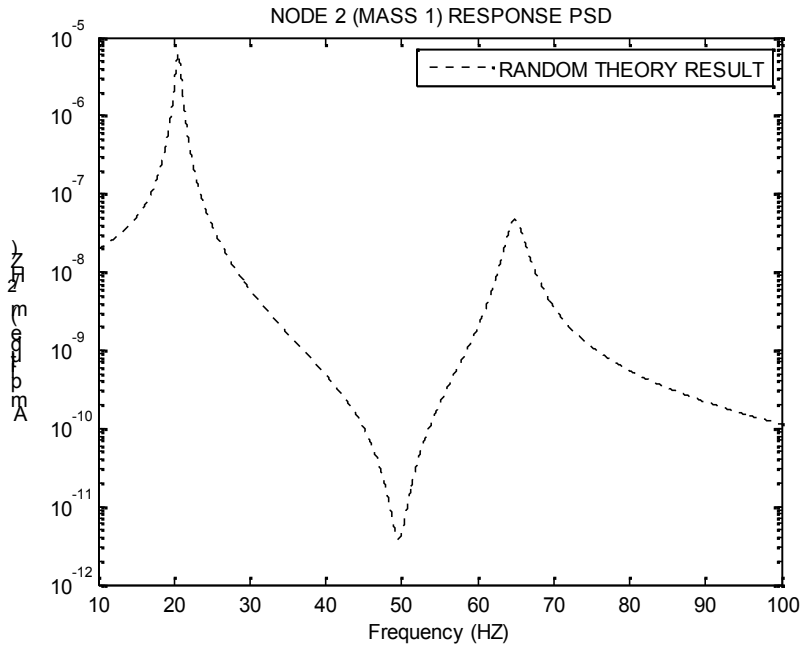

Figure A. 6 Displacement PSD of Mass 1, Random Theory

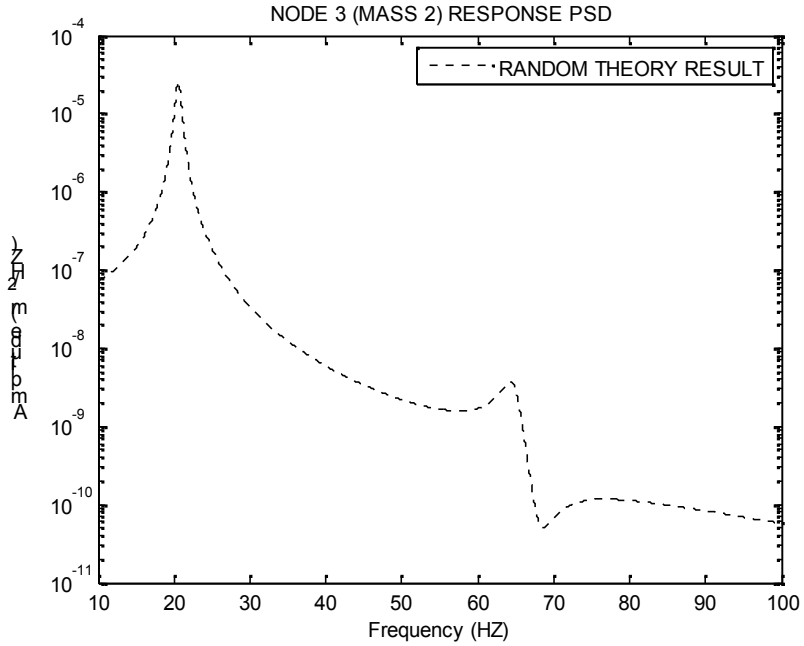

Figure A. 7 Displacement PSD of Mass 2, Random Theory

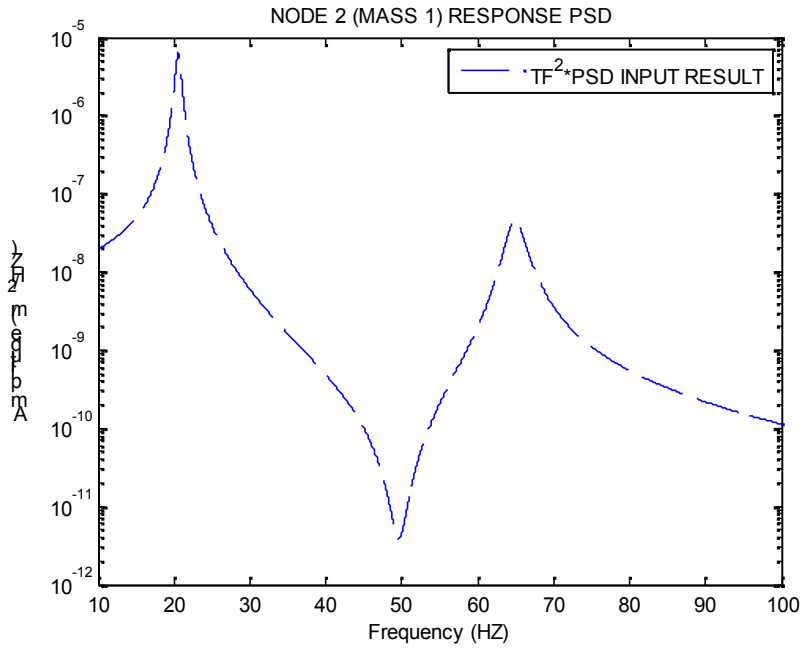

Figure A. 8 Displacement PSD of Mass 1, Transfer Function is Used

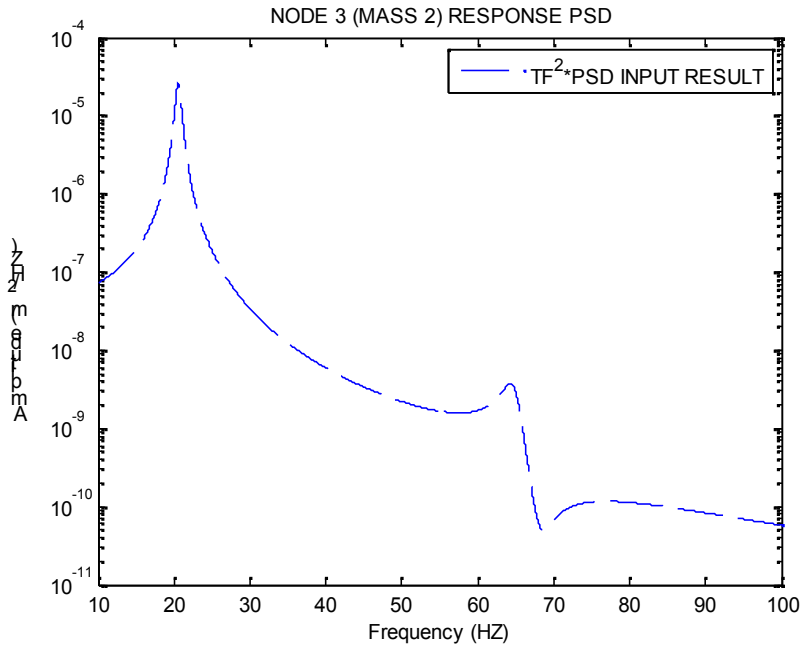

Figure A. 9 Displacement PSD of Mass 2, Transfer Function is Used

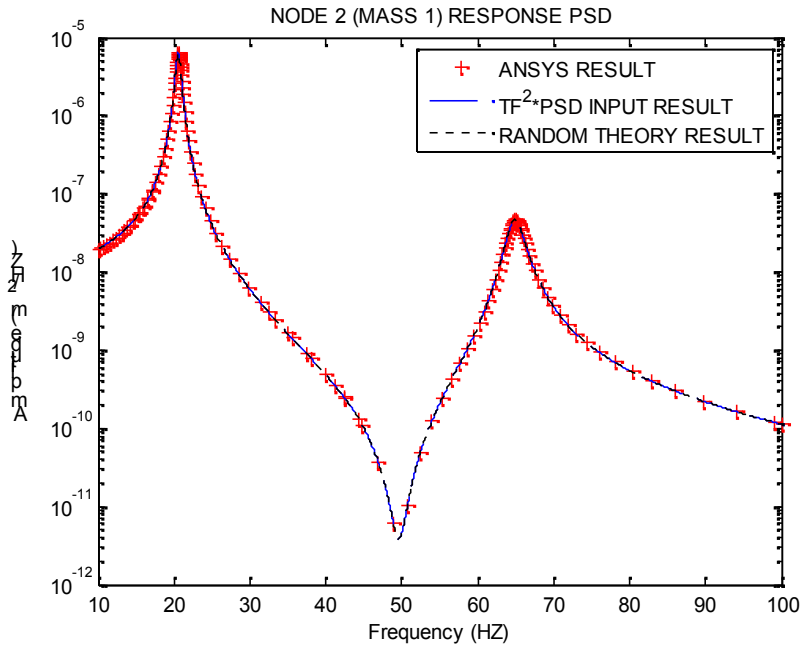

Figure A. 10 Displacement PSD of Mass 1, Comparison of Results

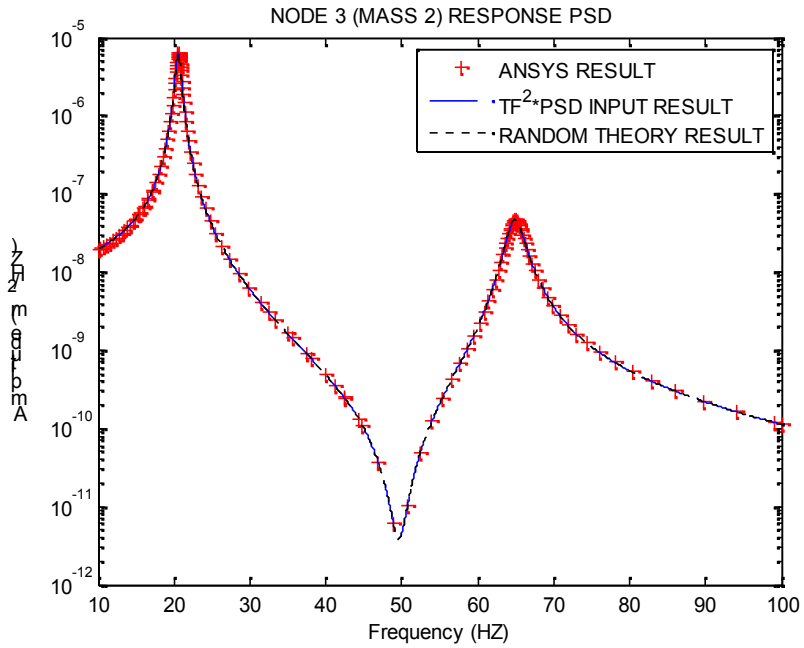

Figure A. 11 Displacement PSD of Mass 2, Comparison of Results

In addition, normal stress PSD's of the point shown in Figure 3.18 are obtained by performing random PSD analysis and applying formulation given in Equation (A.1) using transfer functions from unit g loading harmonic analysis and 0.01 g^2/Hz (0-250 Hz) PSD. The obtained stress PSD's and comparison of them are given in Figure A. 12, Figure A. 13 and Figure A. 14.

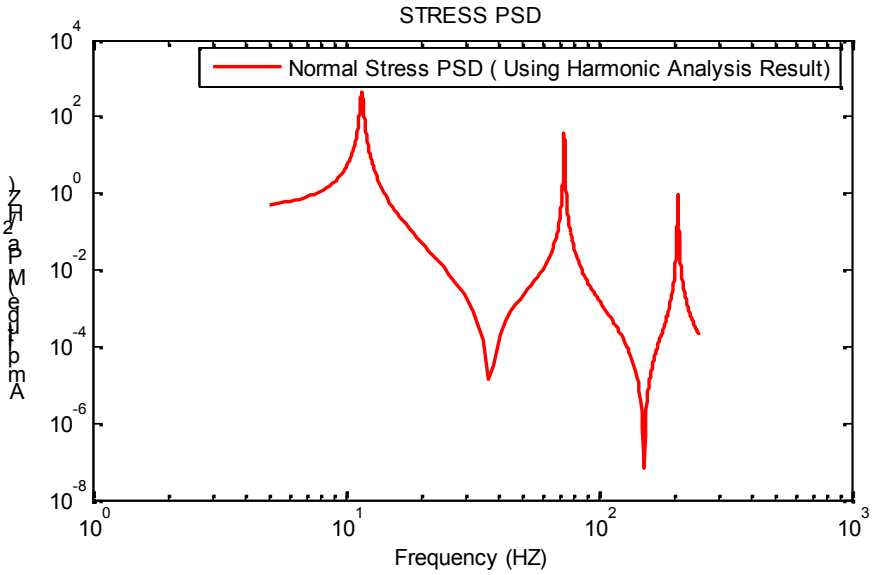

Figure A. 12 Normal Stress PSD (Using Harmonic Analysis Result)

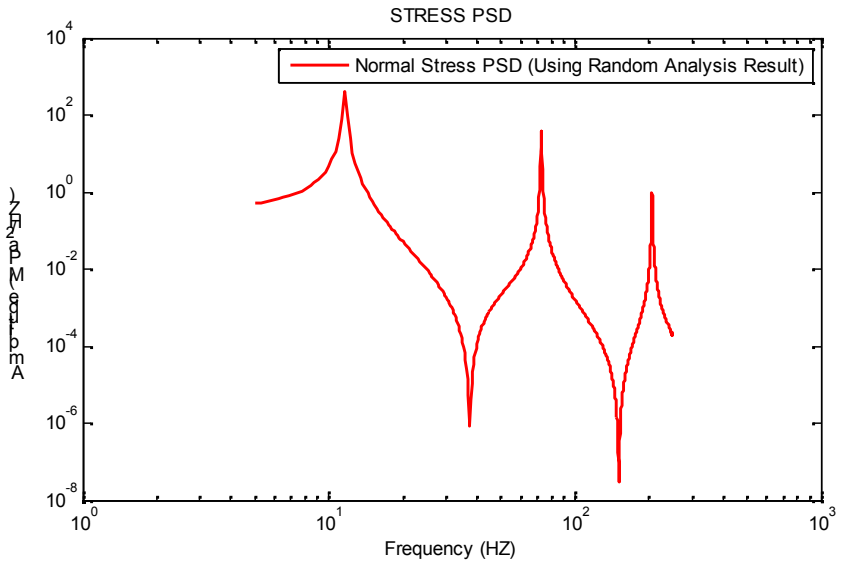

Figure A. 13 Normal Stress PSD (Using Random Analysis Result)

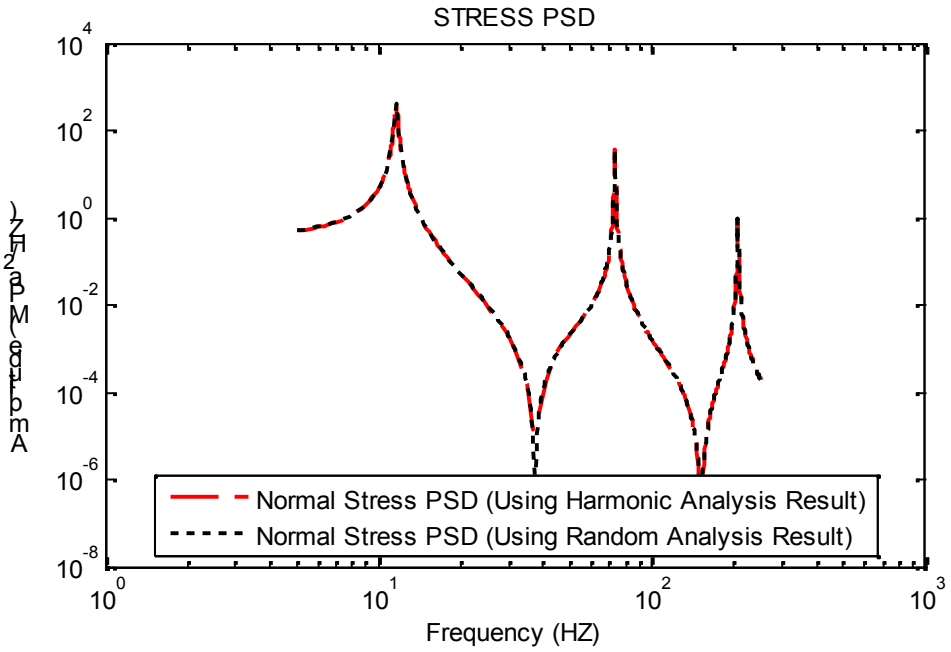

Figure A. 14 Comparison of Results

Comparison of the results show that response PSD obtained by multiplying square of transfer function with PSD input gives exactly the same result with response PSD obtained by using random vibration theory.

APPENDIX B

VERIFICATION OF RAINFLOW ALGORITHM

The rainflow algorithm is developed using ASTM E 1048 85 [24] standard guidelines. After algorithm is constructed, verification is performed using the data of examples given in Figure B. 1 and Figure B. 2.

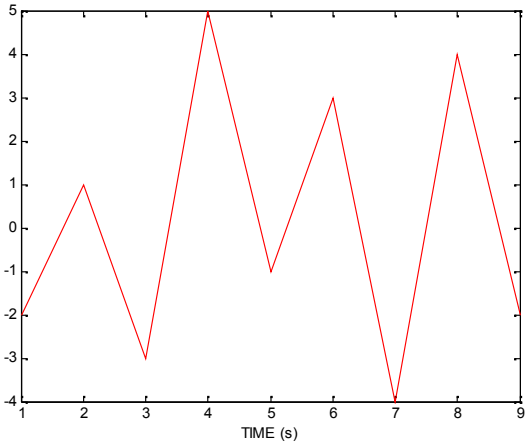

Figure B. 1 Example Used in ASTM E 1048 85 [24]

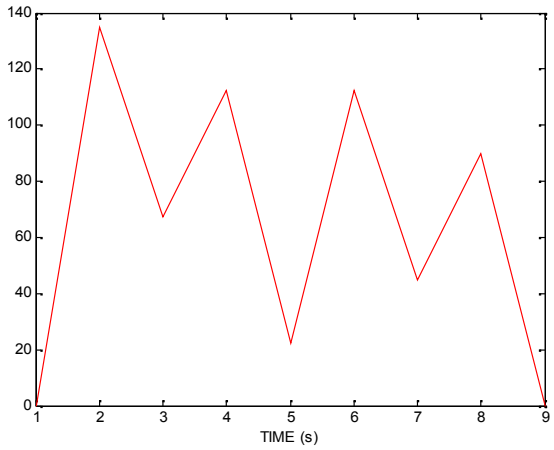

Figure B. 2 Example Given in Reference [31]

The points of the data of examples mentioned above are used to developed rainflow algorithm and the results are obtained for both example. (Table B. 1, Table B. 2)

Table B. 1 Rainflow Counting Result of the Example given in ASTM E 1048 85 [24]

RANGE UNITS	CYCLE
1	0
2	0
3	0.5
4	1.5
5	0
6	0.5
7	0
8	1
9	0.5
10	0

Table B. 2 Rainflow Counting Result of the Example Given in Reference [31]

RANGE	CYCLE COUNTS
45	2
90	1
135	1

The results calculated by developed rainflow algorithm are exactly same with the released results given in references.

APPENDIX C

USER MANUAL

As indicated above a numerical code is developed in this thesis. This numerical code, called Fatiguer, calculates the fatigue life of a structure in both frequency domain and time domain. In this appendix, user manual of the developed numerical code is given.

This numerical code is written in MATLAB and the general view of the GUI of the software is given in Figure C. 1.

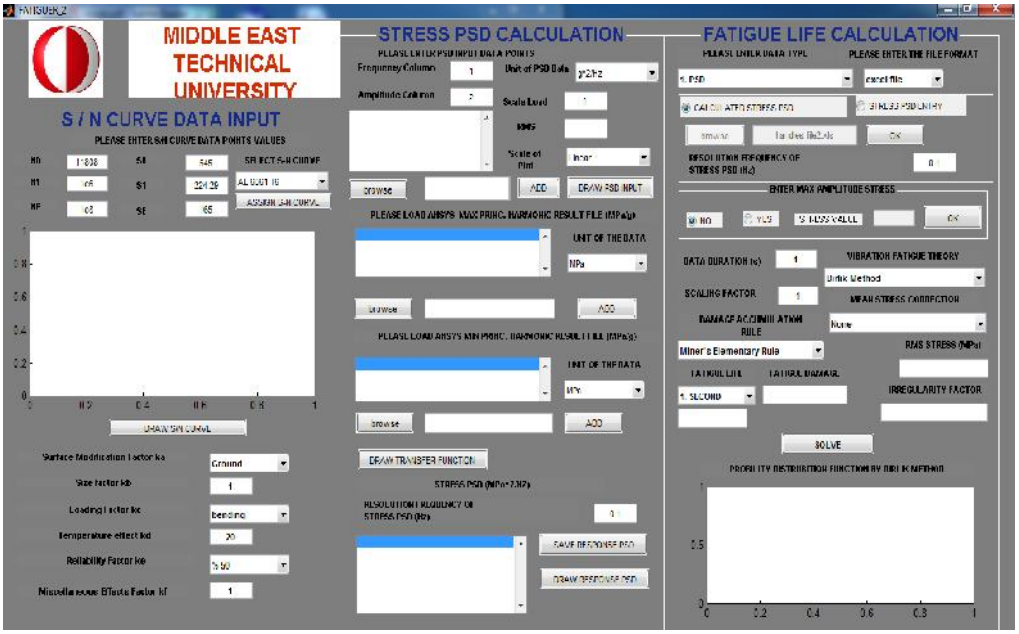

Figure C. 1 General View of GUI of Fatiguer

The software can be analyzed in three sections. In the first section of software, the required $S-N$ curve information should be entered. There are $S-N$ curve information of the AL 6061 T6, AL7075 T7651 and AL 7075 T7351 materials embedded in the software. If any other $S-N$ curve information is needed, it can be entered to software manually as indicated in Figure C. 2.

While entering the $S-N$ curve information, the points of $S-N$ curve should be used. If $S-N$ curve has one curve, S_1 should be entered as the same value with S_E and N_1 has to be entered as the same value with N_E. Before performing fatigue analysis, 'ASSIGN S/N CURVE' button should be clicked.

In order to check S/N curve, 'DRAW S/N CURVE' button shown in Figure C. 3 can be used. For editing endurance limit modifying factors, the boxes and drop down menu given in Figure C. 4 should be used.

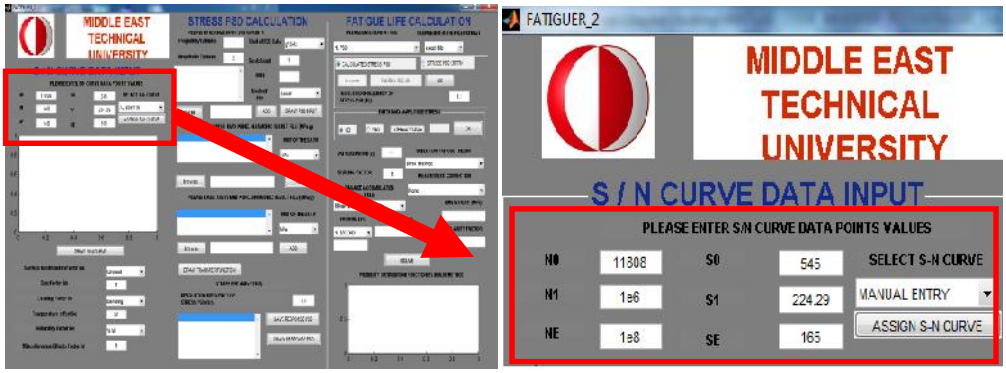

Figure C. 2 Manual Entry for $S-N$ Curve Information of Material

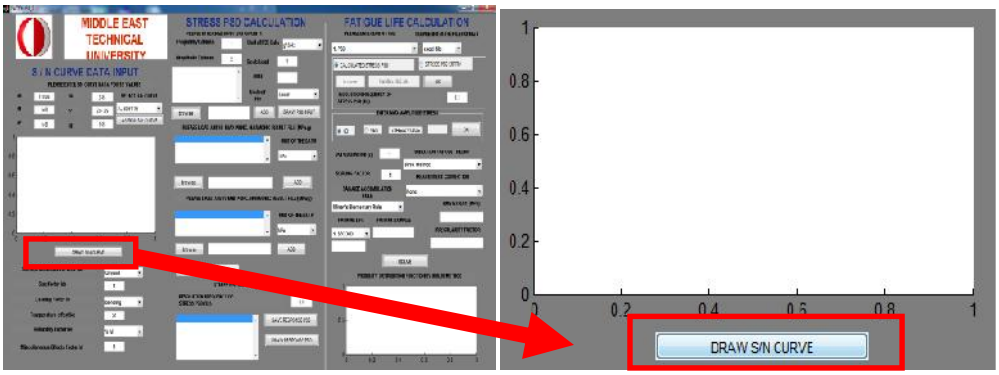

Figure C. 3 Draw $S-N$ Curve of Material

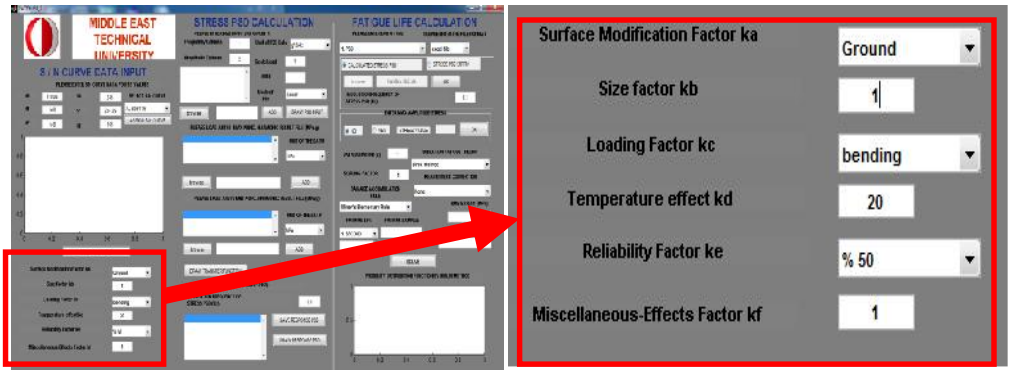

Figure C. 4 Endurance Limit Modifying Factors of $S-N$ Curve

In the second section, stress PSD is calculated. In fact, the second section can be analyzed in three parts. In the first part (Figure C. 5) PSD input should be entered to software. The format of the PSD input should be TEXT.

Before importing PSD input to software, using 'browse' button, the path of the file of the PSD input should be identified. Then the columns of frequency and amplitude and the unit of the PSD should be identified on the software menu given in Figure C. 5. Finally, using 'ADD' button, PSD input data can be imported. After, 'ADD' button is clicked, the RMS values of PSD can be obtained in the unit of input and the graph of the PSD can be carried out in linear, semi logarithmic and logarithmic scale separately. In addition, PSD input can be scaled using 'Scale Load' box on the GUI of the software. (Figure C. 5)

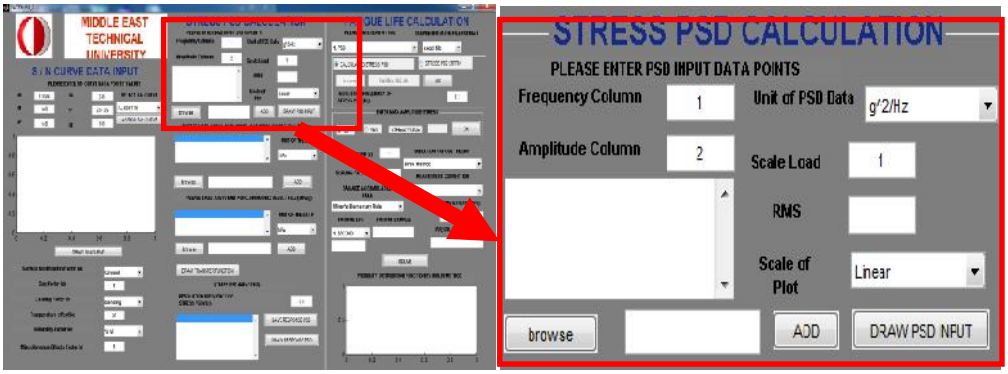

Figure C. 5 PSD Input Entrance for Stress PSD Calculation

In the second part of the second section of the GUI of the software, transfer function obtained from unit load harmonic analysis performed in ANSYS should be determined. Before explaining the second part of the second section, the way of the exporting the transfer functions from ANSYS will be expressed shortly.

If the harmonic analysis is performed in ANSYS Workbench, in the analysis settings, shown in Figure C. 6, 'Save MAPDL db' option should be clicked as 'Yes'. After harmonic analysis is performed, ANSYS Workbench should be terminated and ANSYS Classic should be opened using 'Mechanical APDL Product Launcher' shown in Figure C. 7. Then, the path of the result file should be identified using 'Browse' button and 'Run' button should be clicked in order to open ANSYS Classical. (Figure C. 8). When ANSYS Classic is opened 'RESUME DB' button should be clicked and 'General Postproc' link should be clicked. In order to define which node is the most critical, 'Read Results' link should be clicked and 'By Pick' should be selected. From the opening window, after choosing any set of result, 'Read' button should be clicked.(Figure C. 9)

Then, 'List Results' link should be clicked and 'Nodal Solution' should be selected. From the opening window the links in red rectangles shown in Figure C. 10 should be clicked. The opening window shows which node is the most critical given in Figure C. 11.

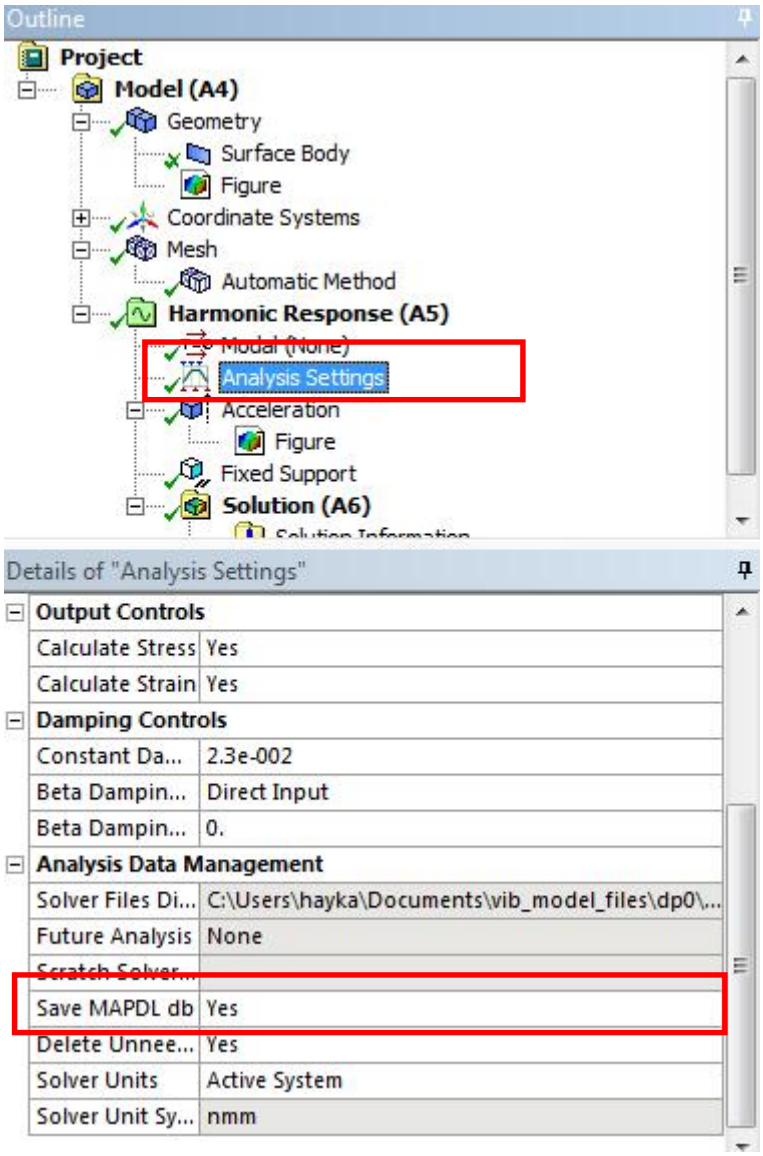

Figure C. 6 ANSYS Workbench Harmonic Analysis Settings

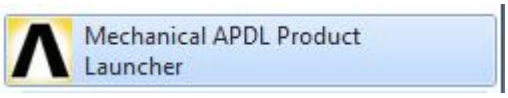

Figure C. 7 ANSYS Mechanical APDL Product Launcher Button

Figure C. 8 ANSYS Mechanical APDL Product Launcher Menu

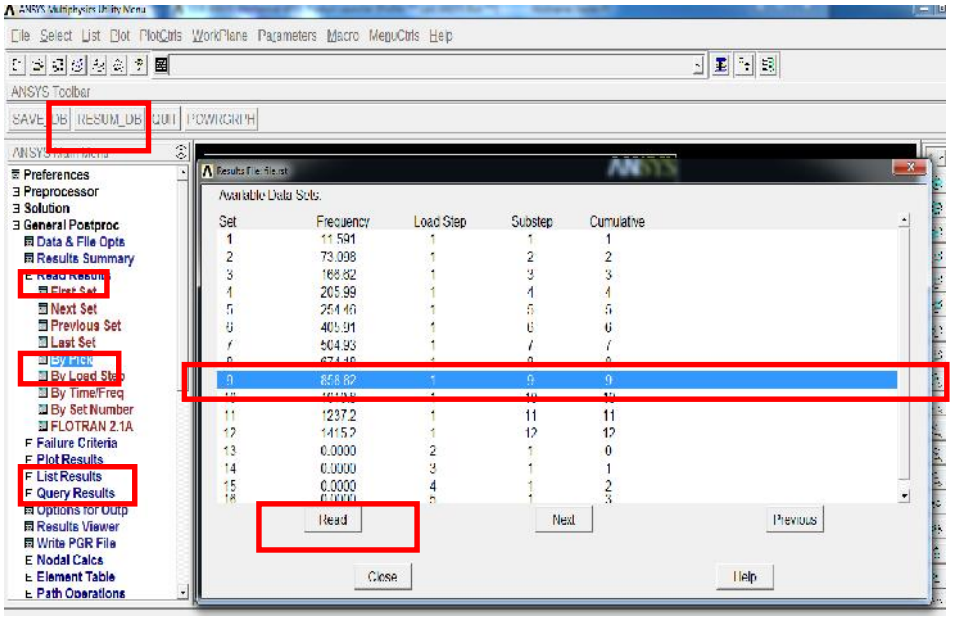

Figure C. 9 ANSYS Classical General Post processing

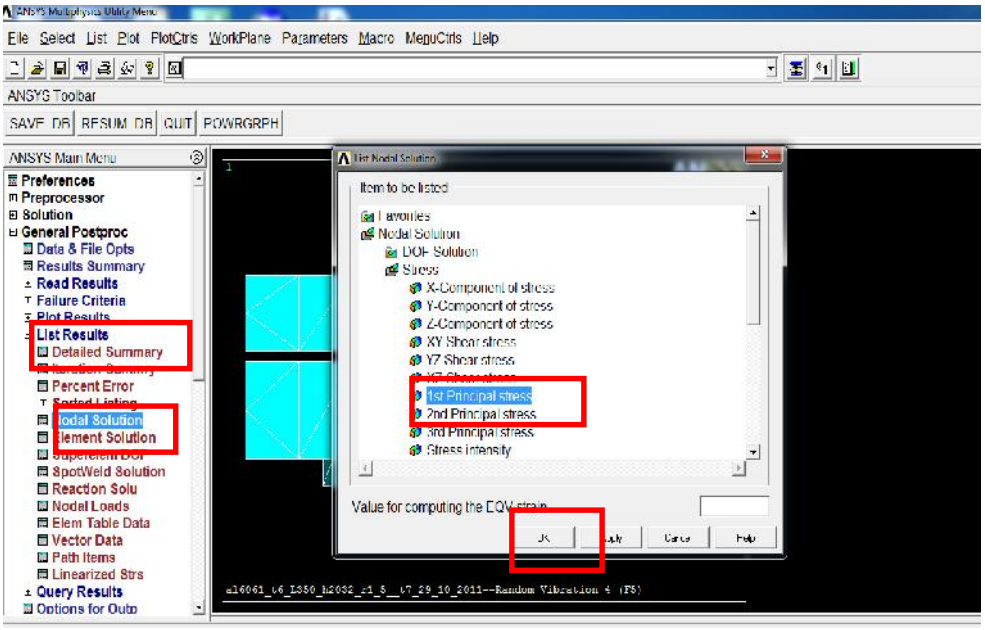

Figure C. 10 ANSYS Classical General Post processing, Listing Nodal Solutions

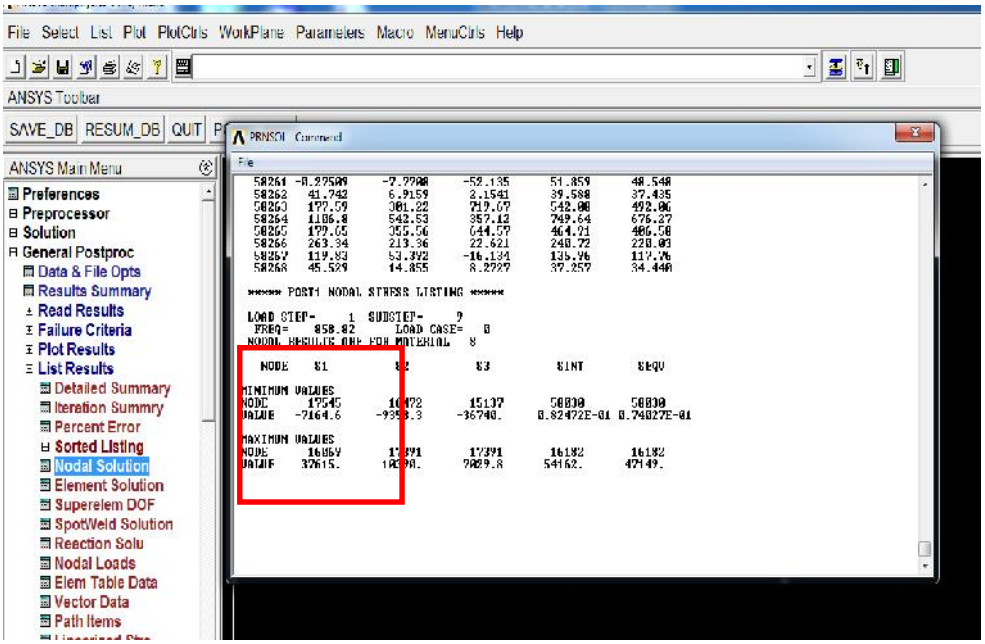

Figure C. 11 ANSYS Classical General Post processing, Finding the Most Critical Node

After the most critical node is obtained, by following the steps given in Figure C. 12, the window given in Figure C. 13 should be obtained and the most critical node number should be entered here.

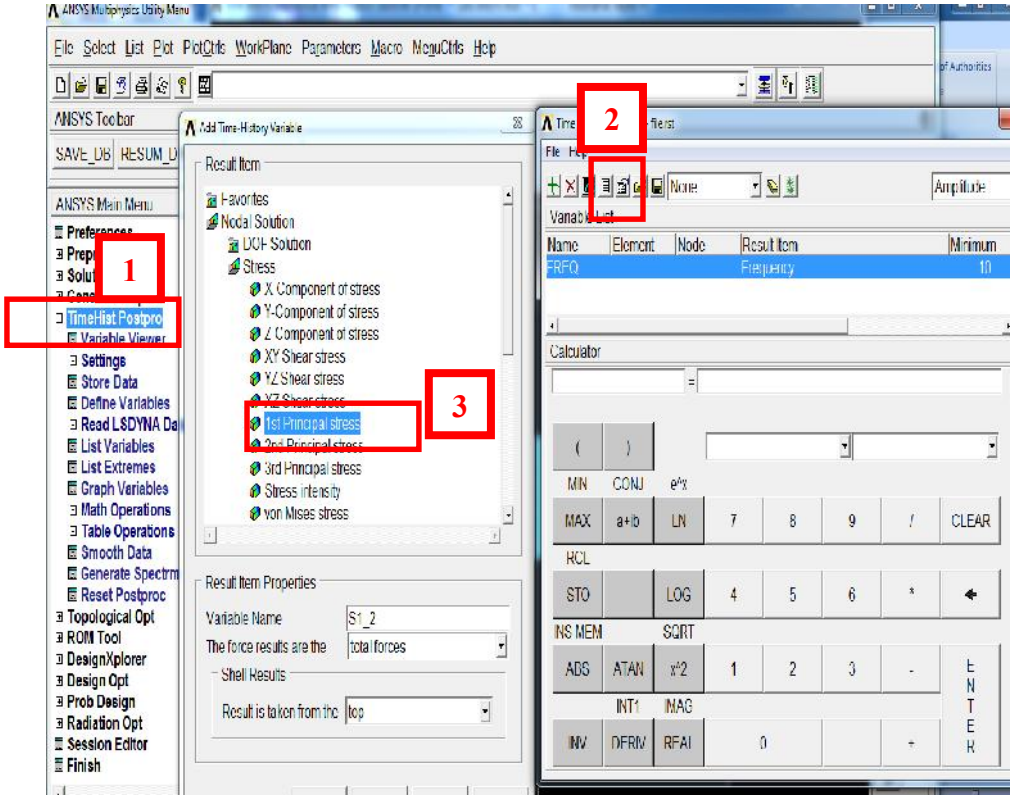

Figure C. 12 ANSYS Classical Time History Post processing, Obtaining Transfer Functions

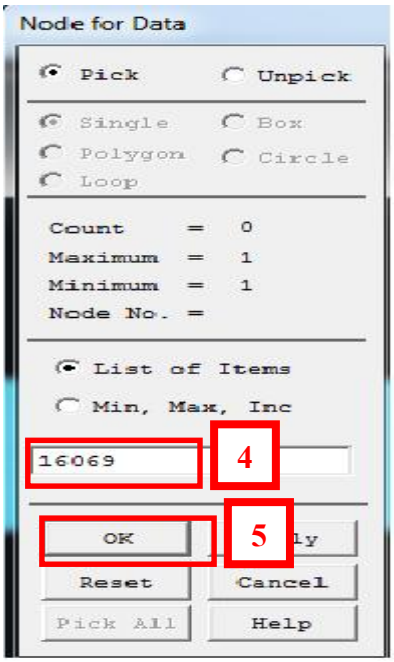

Figure C. 13 ANSYS Classical Time History Post processing, Node for Data Entrance

Then, following the steps given Figure C. 14 maximum and minimum principal stress transfer functions can be saved in TEXT format.

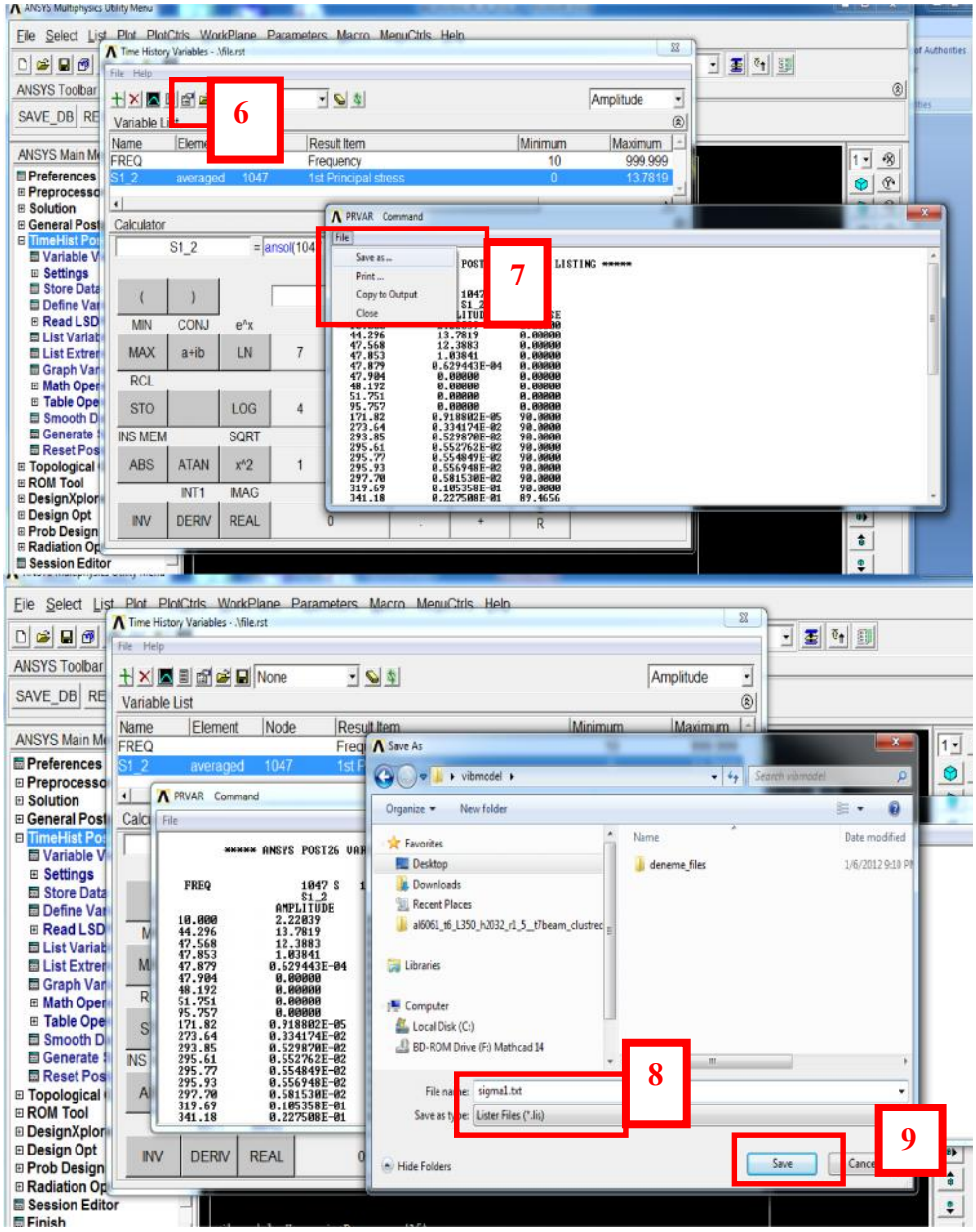

Figure C. 14 ANSYS Classical Time History Post processing, Saving Transfer Functions

After obtaining the transfer functions, importing to software can be accomplished by using the tools given in Figure C. 15. Before importing the transfer functions, using 'browse' buttons, the path of the files should be identified. Then, using 'ADD' button, PSD input data can be imported.

In the third part of the second section of the software, stress PSD is calculated using 'SAVE RESPONSE PSD' button and if the graph of the stress PSD is needed, 'DRAW RESPONSE PSD' can be used. In addition the frequency resolution of the stress PSD can be edited if needed. (Figure C. 16)

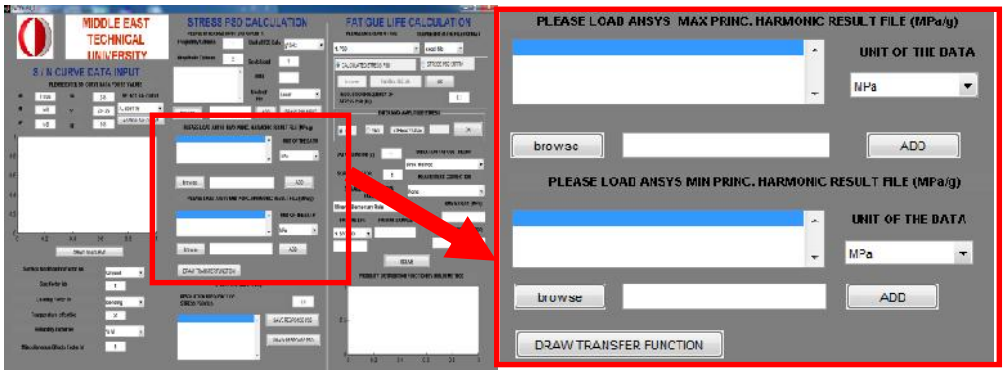

Figure C. 15 Importing Maximum and Minimum Principal Transfer Functions

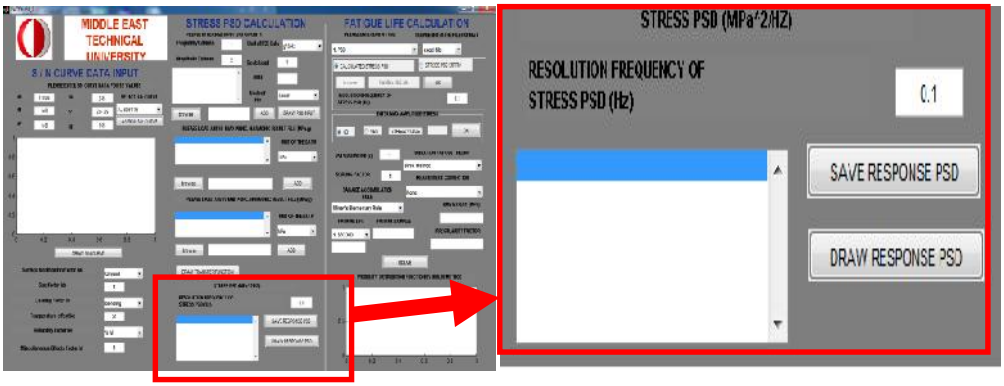

Figure C. 16 Stress PSD Calculation Using Fatiguer

The third section of the GUI of the software is used in order to calculate fatigue life of structures in frequency and time domains. For frequency domain calculations, PSD should be selected from drop down menu and 'OK' button should be clicked as illustrated in Figure C. 17. In this interface of the software, fatigue life calculations can be performed for a given stress PSD and $S-N$ curve using different vibration fatigue theories. Software calculates fatigue life for the stress PSD obtained from the second section as a default.

If there is an available stress PSD, there is no need to use second section of the software. In order to import stress PSD, 'STRESS PSD ENTRY' radiobutton should be clicked then 'OK' button should be used. Then, using 'browse' button, the path of the stress PSD file can be identified. The steps are illustrated in Figure C. 18. Then the format of the file should be selected using the drop down menu shown in Figure C. 19. The maximum amplitude of the stress is calculated as 3 times of the 1 sigma RMS value of the stress PSD to be on the safe side. However, if the real amplitude of the stress is known, it can be entered to empty box by using 'OK' button after 'YES' radiobutton is clicked as shown in Figure C. 20. Also stress PSD can be scaled and the duration can be determined. In addition, vibration fatigue theories, damage accumulation rule, mean stress correction method and fatigue life time options can be edited for the required calculations. When 'SOLVE' button is used, the software gives the results of fatigue life time, fatigue damage, 1 sigma RMS values of the stress PSD and irregularity factor of the stress PSD as a default. (Figure C. 21)

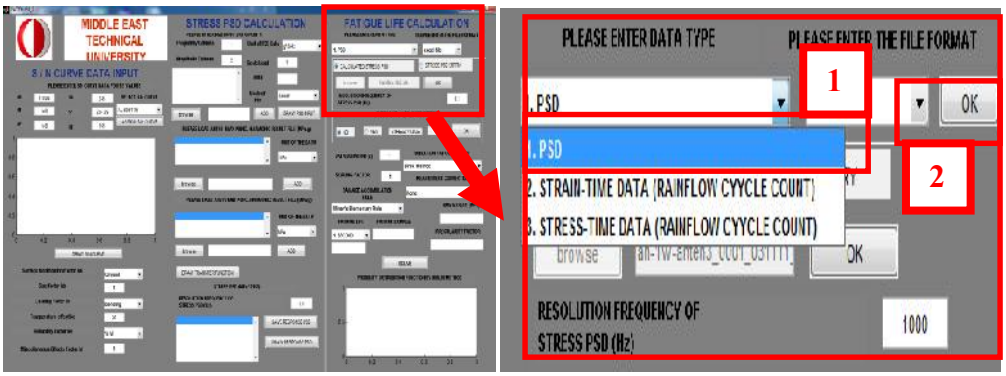

Figure C. 17 Selecting the Domain of the Calculations

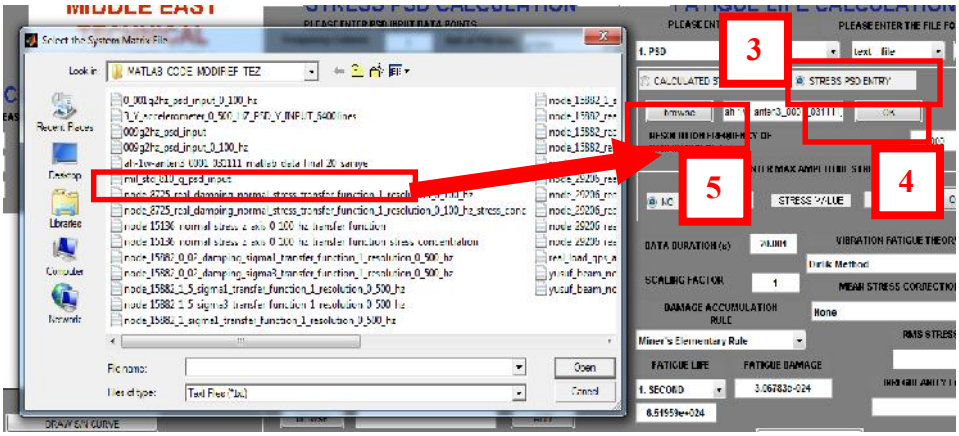

Figure C. 18 Manual Stress PSD Entrance to Software

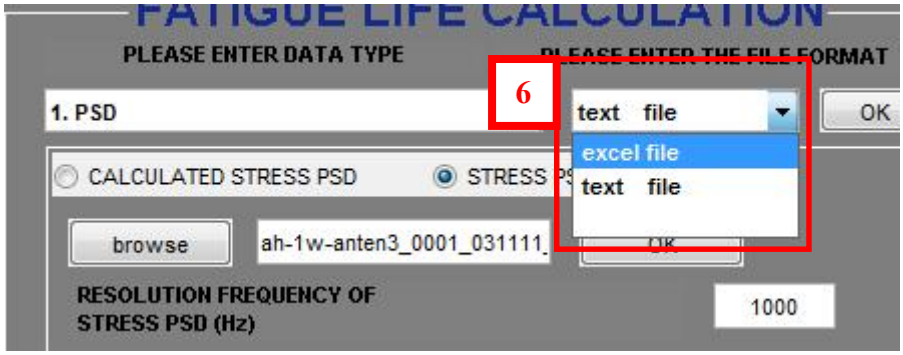

Figure C. 19 Selecting Format of the File That is Imported in the Frequency Domain

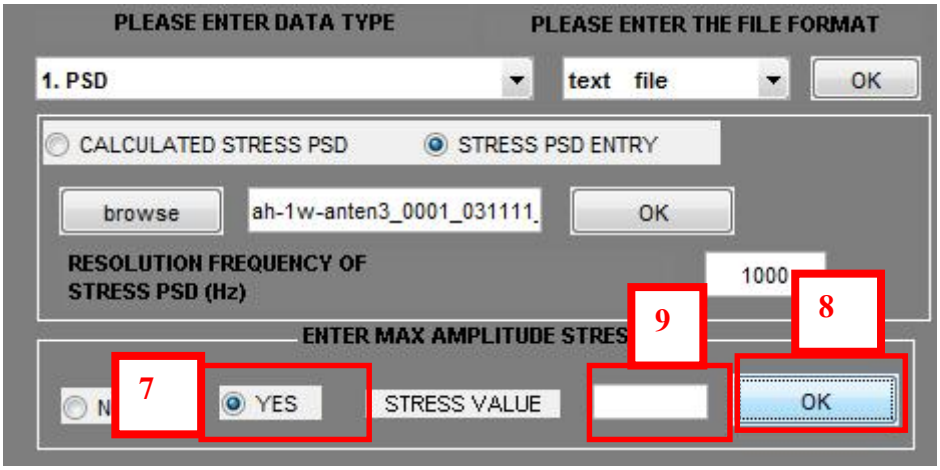

Figure C. 20 Maximum Amplitude of Stress Input Entrance for Stress PSD

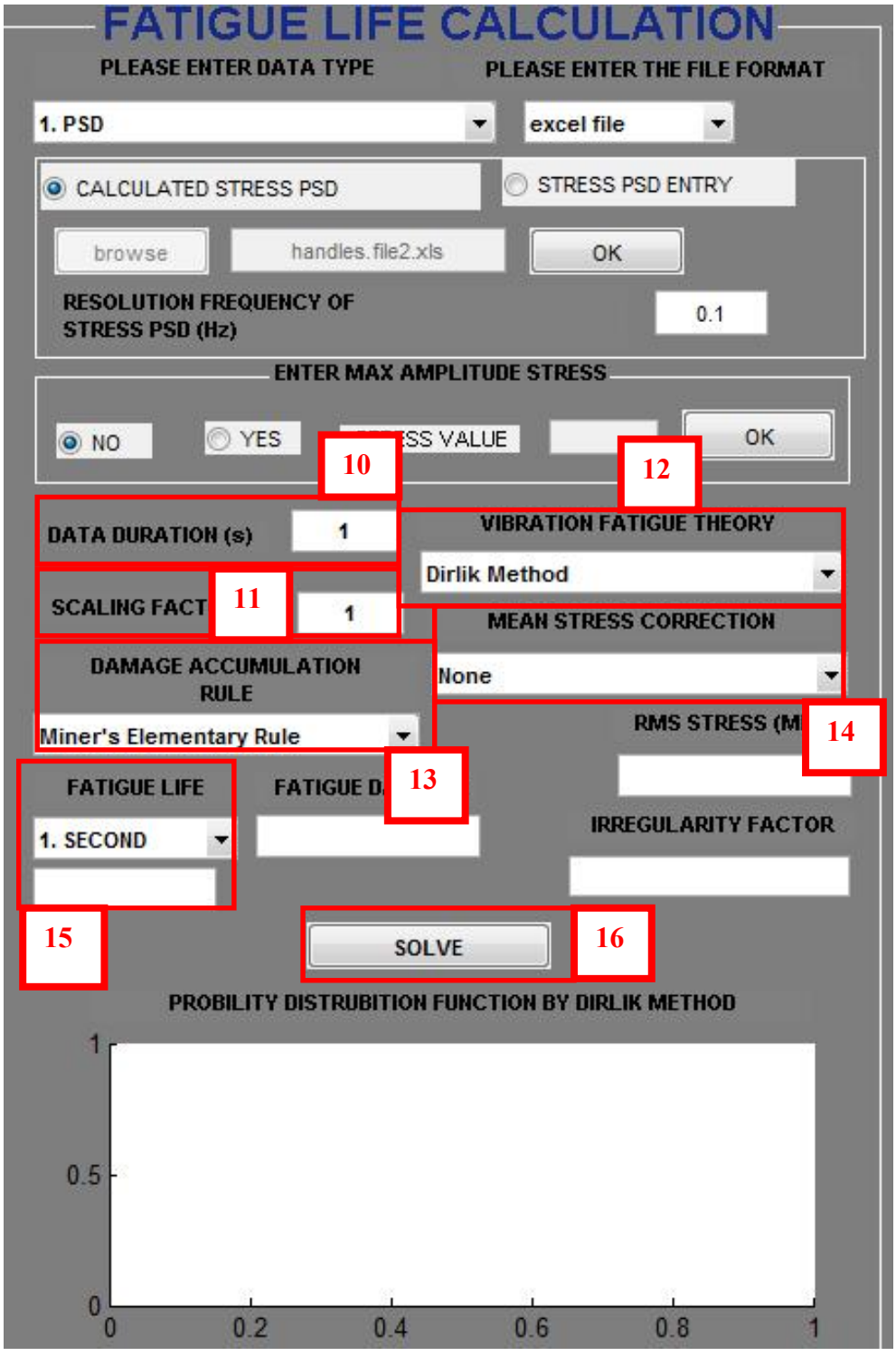

Figure C. 21 The Steps That are Followed to Perform Fatigue Analysis in the Frequency Domain

For time domain calculations, 'STRAIN TIME DATA (RAINFLOW COUNTING)' or 'STRESS TIME DATA (RAINFLOW COUNTING)' should be selected from drop down menu and 'OK' button should be used as illustrated in Figure C. 22. When the 'OK' button is clicked, interface of the third part of the software changes as illustrated in Figure C. 23.

In this interface of the software, fatigue life calculations can be performed for a given stress or strain time data using rainflow counting method. In order to import stress or strain time data 'browse' button should be used and the path of the stress PSD file should be identified. Then the format of the file should be selected using the drop down menu and 'ADD' button should be clicked in order to import data as shown in Figure C. 23. In addition, the sampling rate of the time data should be entered and if fatigue stress concentration is known, 'K_f' box should be used in order to modify the strain or stress-time data. If strain-time data is imported, Modulus of Elasticity of the material should be entered into software. After damage accumulation rule, mean stress correction method and fatigue life time options are edited for the required calculations, 'SOLVE' button should be used in order to obtain the results of fatigue life time, fatigue damage and the duration of the stress or strain time data. (Figure C. 23).As mentioned above, stress PSD, strain-time and stress–time data used in fatigue life calculations should be in the format of text and excel file. Both text and excel formats should be constructed as first column of the data includes time or frequency information and the second column includes the amplitude information of the data.

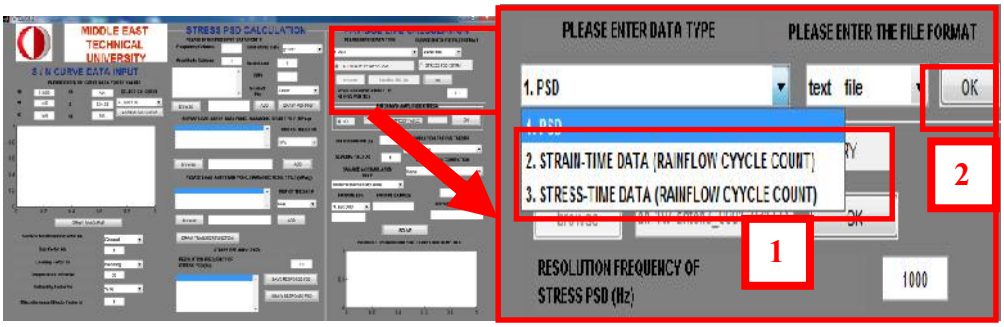

Figure C. 22 Selecting Format of the File That is Imported in the Time Domain

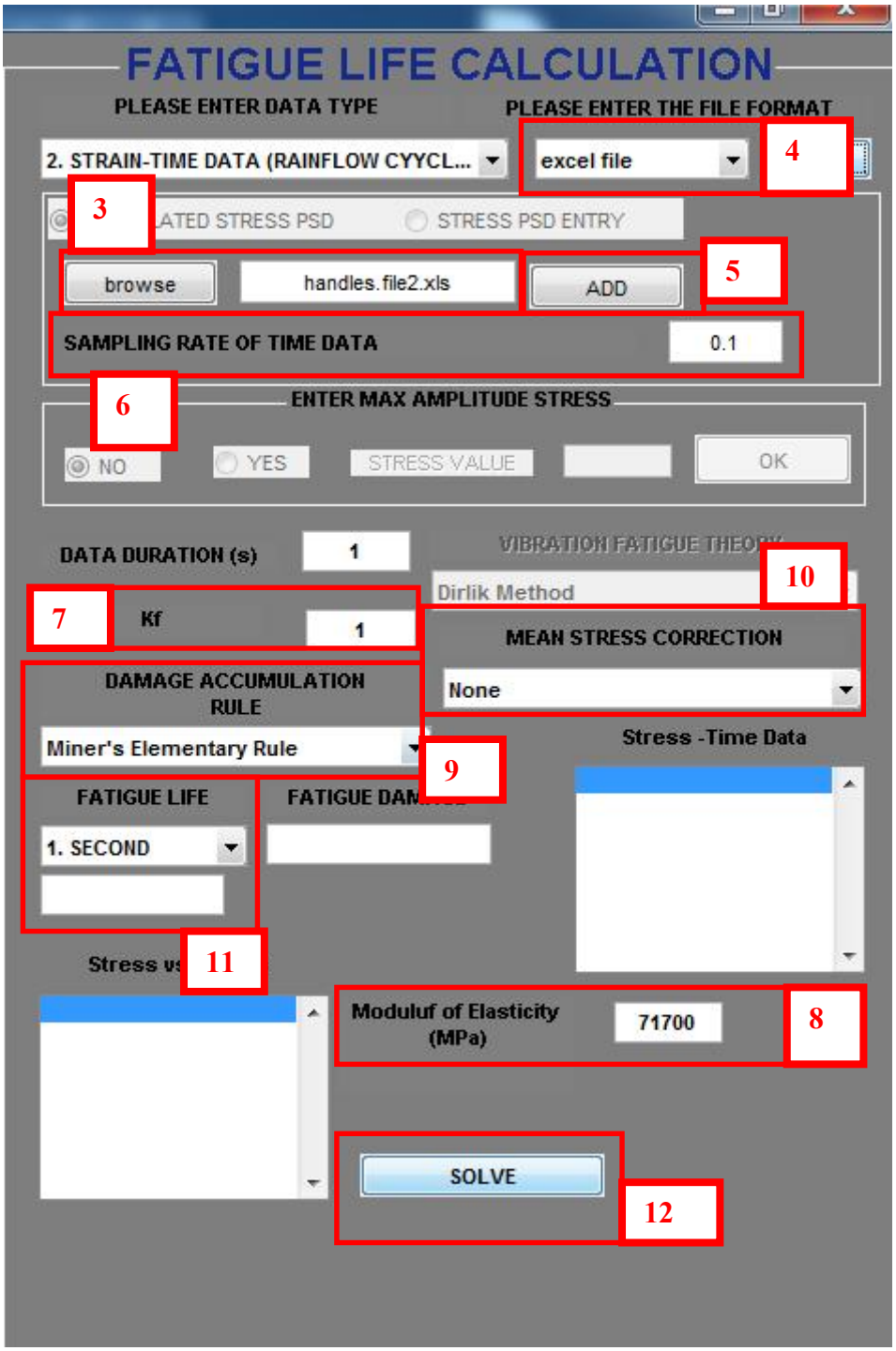

Figure C. 23 The Steps That are Followed to Perform Fatigue Analysis in the Time Domain